Testing Screened Fifth Forces: From Cosmological to Solar System Scales

by

Johannes David Dombrowski

Thesis submitted to
The University of Nottingham
for the degree of
Doctor of Philosophy

July 2021

Abstract

In this thesis we present three different approaches to testing screened fifth forces on scales ranging from the largest structures in the Universe to the Solar System.

Firstly, we study the cosmic matter bispectrum in a cubic Galileon model and find that the shape dependence of Vainshtein screening leaves a very intuitive signature on the bispectrum. A numerical analysis with `hi_class` demonstrates that the strength of the signal relative to the signal from general relativity alone is proportional to the fractional energy density of the Galileon at redshift $z = 0$ and evolves like $\propto a^{3/2}$. Since this shape dependence is very characteristic of Vainshtein screening, it may prove useful for differentiating between different models of fifth forces with data from future galaxy surveys.

Second, we determine the conditions under which the solar-system constraints on the time evolution of the gravitational constant may be extrapolated to cosmological scales. If these conditions are met for a specific fifth force model, strong constraints on the evolution of the cosmological gravitational constant are placed, which prohibit self acceleration as an explanation for the accelerated expansion of the late Universe. We find that the conditions hold for the most common screening mechanisms unless the screening is extreme in the sense that even the largest and least dense observable objects in the Universe are screened, in which case violations of the equivalence principle may prohibit the extrapolation of solar-system constraints to cosmological scales.

Lastly, we derive an analytic solution for the Galileon field in a hierarchical two-body system, where one mass greatly exceeds the other mass. We observe that the field around the smaller mass becomes elliptical outside the 'Vainshtein boundary'. We estimate that this ellipticity only has a small effect in the sun-earth system, but could be at the $\sim 4\,\%$ level on intergalactic scales and thus influence the dynamics of field galaxies moving through the field of a distant galaxy cluster in a manner significantly different from the predictions of pure general relativity.

Notation and conventions

In the following, we list several notations used throughout this work:

- We work in natural units, where the reduced Planck constant $\hbar$ and the speed of light c are equal to 1.
- The reduced Planck mass is denoted by $M_p = 1\sqrt{8\pi G_N} \approx 4.341 \times 10^{-9}\,\mathrm{kg}$.
- We choose the convention $\eta_{\mu\nu} = \mathrm{diag}\,(-1, 1, 1, 1)$ for the Minkowski metric.
- The components of space-time 4-vectors have Greek indices, the components of spatial 3-vectors are denoted with Latin indices. The Einstein sum convention is assumed: $A^\mu B_\mu = \sum_{\mu=0}^{3} A^\mu B_\mu$ and $a^i b_i = \sum_{i=1}^{3} a^i b_i$.
- An arrow signifies a spatial 3-vector: $\vec{a} = (a_1, a_2, a_3)^\top$.
- We write partial derivatives as ∂_μ and covariant derivatives as ∇_μ. However, $\vec{\nabla} = (\partial_1, \partial_2, \partial_3)^\top$ denotes the spatial gradient.
- The d'Alembert operator is defined as: $\Box \coloneqq \nabla^\mu \nabla_\mu$. Its spatial equivalent in flat space is the Laplace operator: $\Delta\phi \coloneqq \partial^i \partial_i \phi$. Some further short-hand notation: $(\nabla\phi)^2 \coloneqq \nabla^\mu\phi\nabla_\mu\phi$ and $(\nabla_\mu\nabla_\nu\phi)^2 \coloneqq (\nabla^\mu\nabla^\nu\phi)\,(\nabla_\mu\nabla_\nu\phi)$.
- The covariant derivative is defined as the Levi-Civita connection. The Christoffel symbols in terms of the metric g are given by:

  $$\Gamma^\sigma_{\mu\nu} = \frac{1}{2} g^{\sigma\rho}\left(\partial_\nu g_{\rho\mu} + \partial_\mu g_{\rho\nu} - \partial_\rho g_{\mu\nu}\right).$$

  In terms of the Christoffel symbols the Riemannian curvature tensor is given by:

  $$R^\rho{}_{\sigma\mu\nu} = \partial_\mu \Gamma^\rho_{\nu\sigma} - \partial_\nu \Gamma^\rho_{\mu\sigma} + \Gamma^\rho_{\mu\lambda}\Gamma^\lambda_{\nu\sigma} - \Gamma^\rho_{\nu\lambda}\Gamma^\lambda_{\mu\sigma}.$$

  The contractions of the curvature tensor are the Ricci tensor $R_{\mu\nu} = R^\lambda{}_{\mu\lambda\nu}$ and the Ricci scalar $R = g^{\mu\nu}R_{\mu\nu}$. The Einstein tensor is defined as $G_{\mu\nu} = R_{\mu\nu} - \frac{1}{2}Rg_{\mu\nu}$.
- The Fourier transform of a function $f(x)$ is denoted by a hat and we choose the normalisation: $\hat{f}(k) = \int \mathrm{d}x f(x) \mathrm{e}^{\mathrm{i}kx}$.

Acknowledgements

After three and a half years of PhD studies, it is time to thank a lot of wonderful people for supporting me during this exciting, but also stressful and emotionally challenging time.

First and foremost, I would like to express more sincerest thanks to my supervisor Clare Burrage. I could not have hoped for a better supervisor. Thank you for all your help and advice in my studies and for always being understanding and supportive when my personal life got difficult.

A big thanks also to everyone that is or has been a member of Clare's research group including Daniela Saadeh, Peter Millington, Ben Elder, Christian Käding, Ben Thrussel, Chad Briddon, Andrius Tamosiunas and Aneesh Naik. I learned a lot from our meetings and discussions and always felt welcome. The same is true for the rest of the members of the Particle Cosmology Group at the University of Nottingham. I especially enjoyed the banter with my office friends Will, Christian, Ben and Chad, which helped me through stressful times. A special thanks also to Daniela who helped me write the first paper of this project.

Furthermore, I would like to thank Matthias Bartelmann from Heidelberg University for keeping my scientific research interests diversified through frequent discussions about his kinetic field theory of cosmic structure formation and for general encouragement.

Outside the University, my life in Nottingham was greatly enriched by the Choir of St. Mary's Church in Nottingham lead by the delightful John Keys.

To my family I would like to say: I have missed you during my time in Nottingham! I am all the more grateful to my mother and my brothers Thomas and Andreas for visiting me in Nottingham; I will always remember these visits. An important thanks also goes to my grandmother, who awoke my interest in cosmology at an early age, and my father who always supported my scientific career.

Finally and most importantly, I would like to thank my beloved Odila for coming with me to Nottingham and making these years far away from my family much more enjoyable. Thank you for comforting me in the most difficult times and for bringing light into everyday life through your creative ideas.

This thesis was financially supported by the Research Leadership Award RL-2016-028 from the Leverhulme Trust.

Contents

1. Introduction

The quest for understanding the nature of gravity is a daunting one and an old one. Gravity has seen two paradigm shifts over the course of history. In 1686 Sir Isaac Newton formulated gravity as a force with inverse-square law sourced by matter in his principia mathematica, see Ref. [1]. This hypothesis was uncontested until Albert Einstein formulated his general relativity (GR) in 1916, see Ref. [2], which describes gravity as a geometric effect rather than a force, with freely-falling objects following geodesics of a space-time metric curved by matter sources, see Secion 2.1 for details. The Newtonian inverse-square law is obtained from GR through a consistent non-relativistic limit. Like Newtonian gravity before, GR remained uncontested for over a century and to date no significant deviations from GR predictions have been observed.

However, there exist a number of reasons to repeatedly put GR to the test. A plethora of unresolved questions and some tensions with data plague the cosmological standard model as derived from GR, see Chapter 2. Among these challenges are the famous cosmological constant problem, the mysteries of dark energy and dark matter, and the H_0 tension, only to mention a few, see Section 2.5 for a detailed discussion. Furthermore, GR lacks a unification with the other fundamental forces. Aside from these well established reasons to test GR with ever increasing rigour, we are further motivated by pure curiosity to explore the boundaries of a theory which has stood the test of time almost like no other.

A vast jungle of alternative gravitational theories trying to contest GR has grown over the last few decades, see Chapter 3. Due to a lack of a consistent framework combining all known modified gravity theories, every study of modified gravity has to focus on a subset of theories which may be handled within a single framework. In this thesis we decided to focus on the popular scalar-tensor theories of gravity, which add a scalar field as an additional fundamental field to the metric of GR. Scalar-tensor theories often arise naturally from higher dimensional theories of gravity and may be formulated in the framework of Horndeski gravity.

Horndeski gravity contains in general non-minimal couplings of the scalar field to gravity which lead to fifth forces sourced by matter and mediated by the scalar field. Such fifth forces are strongly constrained within the Solar System and thus must be equipped with a screening mechanism suppressing the strength of the force on solar-system scales compared to the strength of gravity. We discuss the most common screening mechanisms, the Vainshtein, Chameleon and Symmetron mechanisms, in Section 3.4.

The premise of this thesis was to find new ways of testing screened fifth forces on cosmological and solar-system scales. To this end we first examined the effects of Vainshtein screening on the cosmic matter bispectrum using a conformally coupled cubic Galileon model as a toy model, see Chapter 4 and Ref. [3]. Vainshtein screening is shape dependent in the sense that its effectiveness around a matter source depends on the geometry of the matter distribution. We found that this shape dependence leaves a very intuitive signature on the cosmic bispectrum. The bispectrum depends on three wavenumbers forming a closed triangle $\vec{k}_1 + \vec{k}_2 + \vec{k}_3 = 0$. We observe that the strength of the Vainshtein-screening signal in the bispectrum depends on the shape of the bispectrum triangle in a way which closely resembles the real-space shape dependence.

Scalar-tensor theories offer an explanation for the late-time accelerated expansion of the Universe alternative to the cosmological constant and quintessence scenario. Since scalar-tensor theories may be formulated in either the Einstein or the Jordan frame, see Section 3.3, the Universe could be accelerated in the Jordan frame, but seem not accelerated in the Einstein frame[1]. This approach to explaining the accelerated expansion is called 'self-acceleration' and is possible if the gravitational constant evolves in time. On small scales such a time-evolving gravitational constant is constrained by lunar-laser ranging experiments. In a second study, see Chapter 5 and Ref. [5], we examined under which circumstances the solar-system constraints may be extrapolated to cosmological scales. We found that it is challenging for screening mechanisms to suppress the time evolution of the gravitational constant in the Solar System. Only Chameleon or Symmetron mechanisms can evade the lunar-laser ranging constraints through violations of the equivalence principle if they have a large conformal coupling.

[1] Since all observables like the redshift are frame-independent, see Ref. [4], the apparent frame-dependence is only present in the unobserved scale factor. The redshift would indicate an accelerating Universe in the scenario of self-acceleration.

It is generally very difficult to obtain analytic solutions of screening models in the non-linear regime. In the Chapter 6 we present an unpublished, analytic calculation of the cubic Galileon field in a hierarchical two-body system, where one mass greatly exceeds the other mass. Our analytic calculation is valid close to the smaller of the two masses and reveals some remarkable phenomenology. At an intermediate distance from the small mass, outside its Vainshtein boundary but close enough to the mass that our calculations are still valid, the field becomes ellipsoidal rather than spherically symmetric. This result may be applied for the earth-sun system where the ellipsoidal field in principle affects the motion of test masses moving through the field of the earth at a sufficient distance. However, these effects are strongly suppressed in the Solar System due to the Vainshtein screening. The ellipticity might be relevant on intergalactic scales. As an example we take the system of the Virgo cluster and the local group and determine that the fifth force effects could be as large as $\sim 4\,\%$ of gravity. Galaxies in the vicinity of the local group would experience an asymmetric pull towards the local group due to the elliptic field profile.

We summarise all our findings in Chapter 7.

2. The Cosmological Standard Model

Over the last decades a widely accepted standard model of cosmology has been established, which relies on general relativity (GR) and the cosmological principle. In this Chapter we summarise the most important aspects of the cosmological standard model, reference the observational evidence for it as well as its shortcomings and challenges.

2.1. General Relativity

One of the most important pillars of the cosmological standard model is general relativity. First introduced by Albert Einstein in 1915, see Ref. [2], GR has stood the test of time and no significant deviation from GR has been observed so far despite being repeatedly put under scrutiny on laboratory, solar-system, astrophysical and cosmological scales, see Refs. [6–10].

The central assumption of general relativity is Einstein's equivalence principle (EEP):[1]

- **Einstein's Equivalence Principle:** In an arbitrary gravitational field no local non-gravitational experiment can distinguish a freely falling, non-rotating system from a uniformly moving system in the absence of a gravitational field.

A weaker version of the equivalence principle (WEP) simply states that the motion of a test body is independent of its mass and composition, while a stronger version of the equivalence principle (SEP) assumes the universality of free fall even for massive, self-gravitating objects in addition to the EEP, which then also contains

[1] Various equivalent variants of this principle exist in the literature. Here we use the formulation from Ref. [11]

gravitational experiments. As we will discuss later, see Section 5.3.2, gravitational theories with screened fifth forces violate the strong equivalence principle since objects with large masses can shield themselves from parts of the fifth force due to their self-field.

The EEP implies that the gravitational field in an infinitesimal region of space-time can always be 'transformed away' with a suitable coordinate transformation such that the metric becomes Minkowski: $\mathrm{diag}(-1, 1, 1, 1)$. In the language of differential geometry this implies that the space time is described by a pseudo-Riemannian manifold whose metric g has the signature of a Minkowski metric. The phenomenon of gravitation is thus directly related to the curvature of the space-time manifold and the fundamental field of gravity is the symmetric rank 2 metric tensor $g_{\mu\nu}$. From a field-theory perspective gravity is the theory of a massless spin-2 field, which is unique in a sense described by Lovelock's theorem below.

It remains to determine the field equations for the metric tensor, for which we make use of Lovelock's theorem, see Refs. [12, 13]:

- **Lovelock's Theorem:** In a four dimensional space-time the only second-order equations of motion obtained from an action principle with action $S = \int \mathrm{d}^4x \mathcal{L}(g_{\mu\nu})$ is of form:

$$\alpha\sqrt{-g}\left(R^{\mu\nu} - \frac{1}{2}g^{\mu\nu}R\right) + \lambda\sqrt{-g}g^{\mu\nu} = 0, \tag{2.1}$$

  where α and λ are constants, and $R^{\mu\nu}$ and R are the Ricci tensor and Ricci scalar respectively.

The simplest though not the only choice[2] of an action leading to these equations of motion is the Hilbert action:

$$S = \int \mathrm{d}^4x\sqrt{-g}\left(\alpha\frac{R}{2} - \lambda\right). \tag{2.2}$$

If we include additional (matter) field content to the action, this has to be done in a covariant, i.e. coordinate independent, way to satisfy the EEP. Therefore, the

[2]It is possible to add boundary terms to the action, however, these will not contribute to the equations of motion, see e.g. Ref. [14]

Lagrangian of the matter fields ψ_i has to depend on the metric g:

$$S = \int \mathrm{d}^4x \left(\sqrt{-g} \left(\alpha \frac{R}{2} - \lambda \right) + \mathcal{L}_m \left(g_{\mu\nu}, \psi_i \right) \right). \tag{2.3}$$

Variation of this action with respect to $g_{\mu\nu}$ results in the Einstein equations in the presence of matter:

$$G_{\mu\nu} - \Lambda g_{\mu\nu} = M_p^{-2} T_{\mu\nu}, \tag{2.4}$$

where we have fixed the constant $\alpha = M_p^2 = 1/(8\pi G_N)$ such that the correct coupling strength of gravity is recovered in the weak field limit (G_N is the Newtonian gravitational constant), and we rescaled $\lambda = M_p^2 \Lambda$ to obtain the conventional normalisation of the cosmological constant (CC) Λ, which is not fixed at this point. Furthermore, we introduced the Einstein tensor $G_{\mu\nu} = R_{\mu\nu} - 1/2 R g_{\mu\nu}$ and defined the energy-momentum tensor of the matter fields as:

$$T_{\mu\nu} = -\frac{2}{\sqrt{-g}} \frac{\delta \mathcal{L}_m}{\delta g^{\mu\nu}}. \tag{2.5}$$

The contracted Bianchi-identities $\nabla_\mu G^{\mu\nu} = 0$ (∇ is a covariant derivative), result in the energy-momentum continuity equation:

$$\nabla_\mu T^{\mu\nu} = 0. \tag{2.6}$$

2.2. The Friedmann Universe

The standard model of cosmology relies on two central assumptions:

- **Isotropy:** When averaged over large scales, any observable properties of the Universe are independent of the spatial direction.[3]
- **Cosmological Principle:** Our position in the Universe is in no aspect preferred compared to any other position.[4]

[3] This assumption can be demonstrated by examining the matter distribution on large scales. In this way, this assumption has repeatedly been put under scrutiny by observations and its validity is actively discussed, see Refs. [15, 16]

[4] Large-scale inhomogeneities, i.e. violations of the cosmological principle, have been discussed in the past as alternatives to dark energy or as solution to the H_0-tension, however, strong bounds exist for these models, see Refs. [17–19].

When combined these two assumptions lead to the conclusion that the Universe is statistically isotropic and homogeneous. If we are only interested in the properties of the Universe on the largest scales, we can therefore treat it as homogeneous[5]. On smaller scales, local inhomogeneities have to be taken into account perturbatively, see Section 2.3, or with numerical simulations, but we will ignore them in this Section.

The standard model of cosmology furthermore assumes that the dynamics of the Universe are described by general relativity. The assumptions of statistical, spatial homogeneity and isotropy then demand at the background level, where local inhomogeneities are ignored, that the space-time manifold M is a warped product $I \times \Sigma$ with $I \subset \mathbb{R}$ and a three-dimensional Riemannian space Σ of constant curvature k. The averaged or 'background' metric of the space-time thus has the form of a Friedmann metric:

$$g = -\mathrm{d}t^2 + a^2(t)\gamma, \tag{2.7}$$

where $a(t)$ is the scale factor and γ is the metric of the manifold Σ:

$$\gamma = \frac{\mathrm{d}r^2}{1 - kr^2} + r^2 \mathrm{d}\Omega^2. \tag{2.8}$$

Current observations seem to suggest that the curvature is zero or very close to it, see Ref. [21]. For reasons of simplicity, we will set $k = 0$ for the rest of this thesis. It is often times convenient to introduce a conformal time-coordinate τ, such that the Friedmann metric becomes:

$$g = a^2(\tau)\left(-\mathrm{d}\tau^2 + \gamma\right). \tag{2.9}$$

By examining the metric in Eq. (2.7), we observe that the scale factor $a(t)$ describes the expansion (or contraction) of the spatial dimensions with time. A consequence of an expansion of the Universe is a decay of the three-momentum $p \propto 1/a$ of freely moving particles. For photons the momentum is inversely proportional to the wavelength and therefore light emitted at time t_1 with wavelength λ_1 will be observed at time t_0 (today) with a redshifted wavelength $\lambda_0 = \lambda_1 a(t_0)/a(t_1)$. We say the observed object has redshift $z = a(t_0)/a(t_1) - 1$.

[5] It is however an actively debated question whether local inhomogeneities could have a back-reaction effect on the dynamics of the Universe as a whole, see Ref. [20].

In order to satisfy the Einstein equations, Eq. (2.4), the symmetries of $g_{\mu\nu}$ demand that the background energy-momentum tensor has perfect fluid form with pressure p and density ρ:

$$T^{\mu\nu} = (p+\rho)u^\mu u^\nu + pg^{\mu\nu}, \tag{2.10}$$

where u^μ is the velocity of a comoving observer: $u^\mu = \delta^\mu_0$ (or $u^\mu = \frac{1}{a}\delta^\mu_0$ for the conformal time-coordinate).

Assuming the Friedmann metric, Eq. (2.9), and the energy-momentum tensor, Eq. (2.10), the $(0,0)$ and (i,i) components of the Einstein equations become the Friedmann equations:

$$\frac{\mathcal{H}^2}{a^2} = \frac{\rho}{3M_p^2} + \frac{\Lambda}{3}, \tag{2.11}$$

$$\frac{1}{a^2}\left(\mathcal{H}^2 + 2\mathcal{H}'\right) = -\frac{p}{3M_p^2} + \frac{\Lambda}{3}, \tag{2.12}$$

where the conformal Hubble function $\mathcal{H}$ is defined through a'/a with primes denoting derivatives with respect to conformal time. The conformal Hubble function is related to the Hubble function H by $\mathcal{H} = aH$. The continuity equation, Eq. (2.6), becomes:

$$\rho' + 3\mathcal{H}(\rho + p) = 0. \tag{2.13}$$

In order to solve this system of equations an equation of state for the cosmological fluid is required. The equation of state of a single fluid can often be written as $p = w\rho$. The equation of state parameter w takes on the value of $1/3$ for radiation, 0 for matter and -1 for the cosmological constant 'fluid' (the density of the cosmological constant 'fluid' is defined as $\rho_\Lambda = M_p^2\Lambda$). If the fluids $\{i\}$ are independent of each other, the continuity equation holds for them individually and can be solved:

$$\rho_i = \rho_{i,0}a^{-3(1+w_i)}. \tag{2.14}$$

We have scaled our spatial coordinates such that $a = 1$ at the present time and defined $\rho_{i,0}$ as the density of fluid i today. It is convenient to rescale the densities relative to the critical density $\rho_{\rm cr} = 3M_p^2H^2$: $\Omega_i = \rho_i/\rho_{\rm cr}$. In a Universe without spatial curvature ($k = 0$) as we have assumed for simplicity, the critical density is

equal to the total density of all fluids and thus:

$$1 = \sum_i \Omega_i(t). \tag{2.15}$$

If the relative abundance of all fluids today $\{\Omega_{i,0}\}$ is known together with their equations of state, the expansion history $a(t)$ of the Universe is determined by the first Friedmann equation, Eq. (2.11). Alternatively, one can use observations of the expansion history to determine the consituents of the Universe and their properties. Past observations have presented us with the following picture of the history of the Universe:[6]

- **Inflation:** Inflation is a postulated era during the earliest stages of the Universe, where the Universe expanded (almost) exponentially or in other words: $H(t) \approx$ const. This requires a fluid with an equation of state $w \approx -1$, which is usually assumed to be a scalar field (inflaton) whose potential is significantly larger than its kinetic energy. This era is postulated as a natural explanation of the low spatial curvature k of the Universe and the 'horizon problem', i.e. the question why patches of the Universe seem to be correlated despite there being no explanation for this correlation. Furthermore, quantum fluctuations of the inflaton field give rise to tiny inhomogeneities, which are observable in the cosmic microwave background and which are the seeds of all structure in the Universe.

- **Radiation Domination ($z > 3387 \pm 21$):** In the early Universe the radiation density dominated the expansion history and the scale factor evolved like $a \propto \sqrt{t}$. During this era, several events happened (or are postulated to have happened) which are extremely relevant for particle physics, but are only mentioned here briefly for reasons of completeness: baryogenesis, dark matter freeze-out, electroweak phase transition and big-bang nucleosynthesis.

- **Matter Domination ($3387 \pm 21 > z \gtrsim 0.3$):** During this era, the expansion of the Universe is mostly influenced by non-relativistic matter ($a \propto t^{2/3}$), although only part of this matter is given by the 'ordinary', baryonic matter

[6] Observational data in the rest of this section are taken from the final data release of the Planck mission, see Ref. [21].

$(\Omega_{b,0}h^2 = 0.022\,42 \pm 0.000\,14)$[7]. The rest of the matter content is usually assumed to be cold dark matter ($\Omega_{\mathrm{cdm},0}h^2 = 0.119\,33 \pm 0.000\,91$), i.e. a mysterious type of matter, which is not interacting with the electromagnetic force and which is non-relativistic.[8]

During matter domination, at $z = 1089.80 \pm 0.21$, protons and electrons combined to form atoms for the first time, dubbed 'recombination', making the Universe transparent. The light emitted at recombination is visible today as the cosmic microwave background (CMB). During the later stages of matter domination the density fluctuations grow and form stars, galaxies and galaxy clusters. The first stars reionise large parts of the Universe at $z = 7.82 \pm 0.71$.

- **CC/Dark Energy domination ($z \lesssim 0.3$):** During the late Universe, the expansion of the Universe accelerates, see Refs. [25, 26]. This is either due to the presence of a cosmological constant or any of the many proposed alternatives to the CC, usually dubbed 'dark energy'. The scale factor currently seems to evolve towards an exponential expansion: $a \propto \exp\left(\sqrt{\Omega_{\Lambda,0}H_0}t\right)$. Retrieving more precise observations of this era is of immense interest to differentiate between the plethora of models which are proposed as explanation for the accelerated expansion of the Universe.

2.3. Structure Formation

Having discussed the evolution of the homogeneous Universe, we now discuss the evolution of inhomogeneities which are small enough to be treated perturbatively. For this thesis it will be important to discuss cosmological perturbation theory up to second order in the perturbative quantities.

Due to the symmetries of the metric, the metric perturbations have 10 degrees of freedom. We can write:

$$\mathrm{d}s^2 = a^2\left[-(1+2\Psi)\mathrm{d}\tau^2 + 2\omega_i \mathrm{d}x^i \mathrm{d}\tau + \left((1-2\Phi)\delta_{ij} + \chi_{ij}\right)\mathrm{d}x^i \mathrm{d}x^j\right], \tag{2.16}$$

where χ_{ij} is trace-free and symmetric and Ψ, Φ, ω_i and χ_{ij} are functions of time

[7] h is a dimensionless constant describing the Hubble parameter $H_0 = 100h\mathrm{km/s/Mpc}$.

[8] Alternative explanations for the phenomenon of dark matter in terms of modifications of gravity are actively discussed, see Refs. [22–24].

and space. It is very useful to decompose the metric perturbations (Ψ, Φ, ω_i, χ_{ij}) in terms of scalars, vectors and tensors,[9] because the resulting 4 scalar, 4 vector and 2 tensor degrees of freedom turn out to be completely independent on the linear level. We define:

$$\begin{aligned} \omega_i &= \partial_i \omega + \hat{\omega}_i, \\ \chi_{ij} &= \hat{\chi}_{ij} + \partial_i \hat{\chi}_j + \partial_j \hat{\chi}_i + \left(\partial_i \partial_j - \frac{1}{3} \delta_{ij} \Delta \right) \chi, \end{aligned} \tag{2.17}$$

where hatted quantities are divergenceless, e.g. $\partial^i \hat{\omega}_i = 0$ and $\partial^i \hat{\chi}_{ij} = 0$, and $\hat{\chi}_{ij}$ is symmetric and traceless. It is possible to remove 2 scalar and 2 vector degrees of freedom through coordinate (or gauge) transformations. Various gauge choices are possible; in the following, we will choose the Newtonian gauge, where $\omega = \chi = 0$. It turns out that vector perturbations decay like $1/a$, and thus, we will neglect them in the following. Tensor perturbations might become instrumental in determining the nature of inflation through observations of the cosmic microwave background, however, they are not particularly important to the evolution of the large-scale structures in the matter and dark energy dominated Universe, which will be the main focus of this section and Chapter 4. Thus, only 2 scalar perturbations are relevant for our discussion here:[10]

$$\mathrm{d}s^2 = a^2 \left[-(1+2\Psi)\mathrm{d}\tau^2 + (1-2\Phi)\delta_{ij}\mathrm{d}x^i \mathrm{d}x^j \right]. \tag{2.18}$$

As a next step we examine the perturbed energy-momentum tensor. In general the energy-momentum tensor will take the form of a real fluid:

$$T_{\mu\nu} = (p+\rho) u_\mu u_\nu + p g_{\mu\nu} + \Pi_{\mu\nu}. \tag{2.19}$$

The anisotropic stress-tensor $\Pi_{\mu\nu}$ describes any deviations from the ideal fluid case, i.e. deviations of particle motion from a coherent flow or single stream. Assuming matter perturbations only, anisotropic stress only becomes relevant on smaller scales, where structures virialise and multi-streaming occurs. On the scales relevant for linear perturbations we can neglect $\Pi_{\mu\nu}$. Furthermore, for this thesis only the evolution of matter perturbations will be relevant. For this reason we

[9] The nomenclature of scalar, vector and tensor refers to the transformation properties under spatial rotations.

[10] For more details on vector and tensor modes, see standard textbooks like Ref. [27]

may neglect pressure.

We write the perturbed density and velocity as $\rho = \bar{\rho}(1+\delta)$ and $u^\mu = a^{-1}(\delta^\mu_0 + v^\mu)$ with $v^\mu = (v^0, \vec{v})^\top$. The relative matter perturbation δ is also called density contrast. It turns out that any vorticity $\nabla \times \vec{v}$ decays like a^{-1} on linear scales and can be ignored. Therefore, we can write $\vec{v} = \nabla v$.

All perturbative quantities (δ, v, v^0, Φ and Ψ) may be expanded into first-order, second-order, etc. perturbations:

$$\delta = \delta^{(1)} + \frac{\delta^{(2)}}{2} + \dots \tag{2.20}$$

In the following, bracketed superscripts denote the order in perturbation theory of physical quantities. Since the normalisation of the velocity field is fixed $u^\mu u_\mu = -1$, we can relate v^0 order by order with the other perturbative quantities. At first order ($v^0 \approx v^{0,(1)}$) we have:

$$v^{0,(1)} = -\Psi^{(1)}. \tag{2.21}$$

We are now ready to examine the evolution equations for the linear perturbations. At first order in the perturbative quantities, the 0 and i components of the energy-momentum continuity equation, Eq. (2.6), are respectively:

$$\delta^{(1)\prime} = -\Delta v^{(1)} + 3\Phi^{(1)\prime} \tag{2.22}$$

$$v^{(1)\prime} + \mathcal{H} v^{(1)} = -\Psi^{(1)}. \tag{2.23}$$

The first equation is also called (matter) continuity equation, while the second equation is the Euler equation.

We now consider the Einstein equations, Eq. (2.4). In order to simplify the Einstein equations we employ the quasi-static approximation (QSA) which states that time derivatives of the perturbative quantities can be ignored compared to the spatial derivatives, i.e. $|\delta'| \sim \mathcal{H}|\delta| \ll k|\delta| \sim |\partial_i \delta|$. This assumption is well justified if we are interested in sub-horizon modes ($k^2 \gg \mathcal{H}^2$) only and its validity in the context of a large range of gravitational theories was considered in Refs. [28, 29]. Using the QSA, the $(0,0)$ and (i,i) components of the Einstein equations, Eq. (2.4), become the Poisson equation and the gravitational slip equation:

$$2M_p^2 \Delta\Phi^{(1)} = a^2 \bar{\rho} \delta^{(1)} \tag{2.24}$$

$$\Phi^{(1)} - \Psi^{(1)} = 0. \tag{2.25}$$

As a next step we combine the continuity and Euler equations by applying a derivative with respect to conformal time to the continuity equation, Eq. (2.22), and a Laplace-operator to the Euler equation, Eq. (2.23). This enables us to eliminate $\Delta v^{(1)\prime}$ and we obtain:

$$\delta^{(1)\prime\prime} + \mathcal{H}\delta^{(1)\prime} = \Delta\Psi^{(1)}. \tag{2.26}$$

We have used here the gravitational slip equation, $\Phi^{(1)} = \Psi^{(1)}$, together with the QSA to eliminate the expressions $\Phi^{(1)\prime\prime}$ and $\mathcal{H}\Phi^{(1)\prime}$, which can be neglected in comparison with $\Delta\Psi^{(1)}$. Finally, we use the Poisson equation, Eq. (2.24), and obtain:

$$\delta^{(1)\prime\prime} + \mathcal{H}\delta^{(1)\prime} = \frac{a^2\bar{\rho}}{2M_p^2}\delta^{(1)}. \tag{2.27}$$

Being an equation of motion of second order, two independent solutions exist, the growing and the decaying mode: depending on the initial conditions for the matter perturbations ($\delta_i^{(1)}$ and $\delta_i^{(1)\prime}$), the density contrast can either decay or grow in time. Since the decaying mode is very quickly subdominant compared to the growing mode, we will ignore it for now. Introducing the linear growth factor $D_+(a)$ through $\delta^{(1)}(a) = D_+(a)\delta_i^{(1)}$, we obtain the linear growth equation:

$$D_+'' + \mathcal{H}D_+' = \frac{a^2\bar{\rho}}{2M_p^2}D_+. \tag{2.28}$$

In a matter dominated era where $a \propto t^{2/3} \propto \tau^2$ the linear growth factor is proportional to the scale factor: $D_+ \propto a$. The decaying mode on the other side is proportional to $a^{-3/2}$.

At some point during the cosmic evolution this perturbative treatment of structure formation will break down on small scales. A good indicator for this is the magnitude of the density contrast. On scales where the density contrast is of order 1:

$$|\delta| \sim 1, \tag{2.29}$$

non-linear methods like N-body simulations are required to model structure growth.

In the regime where $|\delta|$ is still significantly smaller than 1, it may still be important to model the small non-linearities. In this case, second order perturbation theory applies. For the second order perturbations it becomes extremely useful to study the equations of motion in Fourier space. In the following, hatted quan-

tities are Fourier transformed with the conventions: $\hat{f}(k) = \int \mathrm{d}x\, f(x)\mathrm{e}^{\mathrm{i}kx}$. The continuity and Euler equations now become:

$$\hat{\delta}^{(2)\prime}(\vec{k}) - k^2\hat{v}^{(2)}(\vec{k}) = S^{(6)} \coloneqq 2\int \frac{\mathrm{d}^2k_1\mathrm{d}^3k_2}{(2\pi)^3}\delta_D(\vec{k}-\vec{k}_1-\vec{k}_2) \times \alpha(\vec{k}_1,\vec{k}_2)\frac{D_+'}{D_+}\hat{\delta}^{(1)}(\vec{k}_1)\hat{\delta}^{(1)}(\vec{k}_2), \tag{2.30}$$

$$-k^2\hat{v}^{(2)\prime}(\vec{k}) - k^2\mathcal{H}\hat{v}^{(2)}(\vec{k}) + \frac{a^2\bar{\rho}}{2M_p^2}\hat{\delta}^{(2)}(\vec{k}) = S^{(7)} \coloneqq -2\int \frac{\mathrm{d}^2k_1\mathrm{d}^3k_2}{(2\pi)^3}\delta_D(\vec{k}-\vec{k}_1-\vec{k}_2) \times \beta(\vec{k}_1,\vec{k}_2)\left(\frac{D_+'}{D_+}\right)^2\hat{\delta}^{(1)}(\vec{k}_1)\hat{\delta}^{(1)}(\vec{k}_2), \tag{2.31}$$

where we used the Poisson equation to eliminate the gravitational potential in the Euler equation and made use of the first order relation $\delta^{(1)\prime} = -\Delta v^{(1)}$ such that $\delta^{(1)}$ is the only first order quantity appearing. The nomenclature $S^{(6)}$ and $S^{(7)}$ was chosen for consistency with our calculations in Chapter 4.3.5. Furthermore, we introduced the form factors:

$$\alpha(\vec{k}_1,\vec{k}_2) = 1 + \frac{\vec{k}_1\cdot\vec{k}_2}{2k_1^2k_2^2}\left(k_1^2+k_2^2\right), \tag{2.32}$$

$$\beta(\vec{k}_1,\vec{k}_2) = \frac{\vec{k}_1\cdot\vec{k}_2\left(\vec{k}_1+\vec{k}_2\right)^2}{2k_1^2k_2^2}. \tag{2.33}$$

Combining the continuity and Euler equations gives the second order analogue to Eq. (2.27):

$$\hat{\delta}^{(2)\prime\prime} + \mathcal{H}\hat{\delta}^{(2)\prime} - \frac{a^2\bar{\rho}}{2M_p^2}\hat{\delta}^{(2)} = S^{(\delta)} \coloneqq S^{(6)\prime} + \mathcal{H}S^{(6)} - S^{(7)} = \int \frac{\mathrm{d}^2k_1\mathrm{d}^3k_2}{(2\pi)^3}\delta_D(\vec{k}-\vec{k}_1-\vec{k}_2)\mathcal{K}(\vec{k}_1,\vec{k}_2,\tau)\hat{\delta}^{(1)}(\vec{k}_1)\hat{\delta}^{(1)}(\vec{k}_2), \tag{2.34}$$

where the kernel $\mathcal{K}$ is given by:

$$\begin{aligned}\mathcal{K}(\vec{k}_1,\vec{k}_2,\tau) &= 2\left(\frac{(D_+'D_+)'}{D_+^2} + \frac{D_+'}{D_+}\mathcal{H}\right)\alpha(\vec{k}_1,\vec{k}_2) + 2\left(\frac{D_+'}{D_+}\right)^2\beta(\vec{k}_1,\vec{k}_2) \\ &= 2\left(f^2\mathcal{H}^2 + \frac{a^2\bar{\rho}}{2M_p^2}\right)\alpha(\vec{k}_1,\vec{k}_2) + 2f^2\mathcal{H}^2\beta(\vec{k}_1,\vec{k}_2).\end{aligned} \tag{2.35}$$

In the last expression we introduced the linear growth rate $f \coloneqq \mathrm{d}\log D_+/\mathrm{d}\log a$

and used the linear growth equation, Eq. (2.28).

The solution for the second order density contrast takes the form:

$$\hat{\delta}^{(2)}(\vec{k}) = \int \frac{\mathrm{d}^2 k_1 \mathrm{d}^3 k_2}{(2\pi)^3} \delta_D(\vec{k} - \vec{k}_1 - \vec{k}_2) F_2(\vec{k}_1, \vec{k}_2, \tau) \hat{\delta}^{(1)}(\vec{k}_1) \hat{\delta}^{(1)}(\vec{k}_2), \tag{2.36}$$

if the function F_2 solves the differential equation:

$$F_2'' + \mathcal{H} F_2' - \frac{a^2 \bar{\rho}}{2 M_p^2} F_2 = \mathcal{K}. \tag{2.37}$$

During matter domination this differential equation is solved by:

$$F_2(\vec{k}_1, \vec{k}_2) = 2 + \frac{\mu}{k_1 k_2} \left(k_1^2 + k_2^2\right) - \frac{4}{7}(1 - \mu^2), \tag{2.38}$$

where $\mu = \vec{k}_1 \cdot \vec{k}_2 / k_1 k_2$ is the cosine of the angle between $\vec{k}_1$ and $\vec{k}_2$.

2.4. Statistics of Cosmological Structures

Different cosmological models, e.g. alternative theories of gravity, will leave an imprint on cosmic structures by, among other things, modifying the linear growth equation, Eq. (2.28). Therefore, observing cosmic structures is crucial for testing alternative cosmological models. However, a conceptual problem arises here. The timescales for the evolution of cosmic structures is significantly longer than the timescales of any observations, i.e. we can not follow the evolution of a single structure over time. Instead we have to look at other structures in different stages of their evolution and at different times of the cosmic history. We then have to assume that statistically the evolution of structure will be independent of the structure's position in the Universe (cosmological principle). A statistical analysis of cosmic structures is therefore inevitable.

Observations of the CMB suggest that the initial density fluctuations are Gaussian to a high degree. This will remain true even at later times if the structures are growing linearly. Therefore, all information on the statistics of large-scale cosmic structures is contained in the power spectrum $P(k)$ defined through:

$$(2\pi)^3 \delta_D \left(\vec{k}_1 + \vec{k}_2\right) P(k) = \langle \hat{\delta}(k_1) \hat{\delta}(k_2) \rangle, \tag{2.39}$$

where δ_D is a Dirac delta-distribution and $\hat{\delta}(k)$ is the Fourier transform of the density contrast. The brackets $\langle \dots \rangle$ represent an ensemble average, which in practice is usually replaced by a spatial average.

The power spectrum is directly related to the correlation function $\xi(y) = \langle \delta(\vec{x})\delta(\vec{x}+\vec{y})\rangle$:

$$\xi(y) = \int \frac{k^2 \mathrm{d}k}{2\pi^2} P(k) \frac{\sin(ky)}{ky}. \tag{2.40}$$

For $y = 0$ the correlation function becomes the variance σ of the density contrast δ. If we are interested in the variance of the density contrast smoothed at some scale R by some window function W_R ($\delta_R(\vec{x}) \coloneqq \int \mathrm{d}^3\vec{x}' W_R(\vec{x}-\vec{x}')\delta(\vec{x}')$), we obtain:

$$\sigma_R = \int \frac{k^2 \mathrm{d}k}{2\pi^2} \hat{W}_R^2(k) P(k). \tag{2.41}$$

We are now in a position to make our statement in Eq. (2.29), that linear structure growth breaks down on scales where $\delta \sim 1$, more precise. We define the non-linearity scale r_{nl} such that:

$$\sigma_{r_{\mathrm{nl}}} = 1. \tag{2.42}$$

At scales smaller than r_{nl} structure growth is highly non-linear.

On scales significantly larger than r_{nl} the growth of structure is given by the linear growth $\delta = D_+ \delta_i$. Hence the power spectrum evolves as $P(k,\tau) = D_+^2(\tau) P_i(k)$, where P_i is the initial power spectrum. In this thesis we are mostly interested in the evolution of structures during the matter and dark energy dominated eras. The initial power spectrum at the beginning of the matter dominated era is given by the power spectrum generated from the quantum fluctuations during inflation ($P(k) \propto k^{n_s}$ with $n_s = 0.9665 \pm 0.0038$, see Ref. [21]) times the square of the transfer function $T(k)$, which describes the complicated dynamics of structures prior to recombination where matter and radiation perturbations interacted. The result is a power spectrum which is roughly proportional to k on scales larger than k_{eq}^{-1}, the horizon scale at matter radiation equality, and falls off like k^{-3} at smaller scales since radiation pressure suppresses the growth of structure during radiation domination on sub-horizon scales.

Regardless of whether small non-Gaussianities are present in the initial density fluctuations, the fluctuations will not remain perfectly Gaussian once the evolution of structures deviates slightly from the linear growth. A good measure for these

non-Gaussianities is the bispectrum $B(\vec{k}_1, \vec{k}_2, \vec{k}_3)$ which is defined through:

$$\langle \hat{\delta}(\vec{k}_1)\hat{\delta}(\vec{k}_2)\hat{\delta}(\vec{k}_3)\rangle = (2\pi)^3 \delta_D(\vec{k}_1 + \vec{k}_2 + \vec{k}_3) B(\vec{k}_1, \vec{k}_2, \vec{k}_3). \tag{2.43}$$

To compute the bispectrum we have to go to second order in perturbation theory, because if we substitute the density contrast δ by just the linear density contrast, the bispectrum will be proportional to $\langle \delta_i \delta_i \delta_i \rangle$, which vanishes for Gaussian initial conditions. Using the solution in Eq. (2.36) for the second order density contrast, we can compute the lowest order contributions to the bispectrum:[11]

$$\begin{aligned}\langle \delta(\vec{k}_1)\delta(\vec{k}_2)\delta(\vec{k}_3)\rangle &\approx \frac{1}{2}\langle \delta^{(2)}(\vec{k}_1)\delta^{(1)}(\vec{k}_2)\delta^{(1)}(\vec{k}_3)\rangle + \text{perm.} \\ &= \frac{1}{2}\int \frac{\mathrm{d}^3 q_1 \mathrm{d}^3 q_2}{(2\pi)^3} F_2(\vec{q}_1, \vec{q}_2, \tau) D_+^4 \\ &\quad \times \left[\delta_D(\vec{k}_1 - \vec{q}_1 - \vec{q}_2)\langle \delta_i(\vec{q}_1)\delta_i(\vec{q}_2)\delta_i(\vec{k}_2)\delta_i(\vec{k}_3)\rangle + \text{perm.}\right]\end{aligned} \tag{2.44}$$

The expression perm. implies summation over cyclic permutations of the wavenumbers $\vec{k}_1$, $\vec{k}_2$ and $\vec{k}_3$. Assuming that the initial density fluctuations are Gaussian, we may use Wick's theorem to write:

$$\begin{aligned}\langle \delta_i(\vec{q}_1)\delta_i(\vec{q}_2)\delta_i(\vec{k}_2)\delta_i(\vec{k}_3)\rangle = (2\pi)^3 \Big[& P_i(q_1)P_i(k_2)\delta_D(\vec{q}_1 + \vec{q}_2)\delta_D(\vec{k}_2 + \vec{k}_3) \\ & + P_i(q_1)P_i(q_2)\delta_D(\vec{q}_1 + \vec{k}_2)\delta_D(\vec{q}_2 + \vec{k}_3) \\ & + P_i(q_1)P_i(q_2)\delta_D(\vec{q}_1 + \vec{k}_3)\delta_D(\vec{q}_2 + \vec{k}_2)\Big].\end{aligned} \tag{2.45}$$

The first term in the brackets is proportional to $\delta_D(\vec{k}_1)$ when putting in the constraint $\vec{k}_1 = \vec{q}_1 + \vec{q}_2$ from Eq. (2.44). We will drop this term since $\vec{k}_1 = 0$ corresponds to an unobservable, infinite scale. Combining Eqs. (2.44) and (2.45) gives:

$$\langle \delta(\vec{k}_1)\delta(\vec{k}_2)\delta(\vec{k}_3)\rangle \approx (2\pi)^3 \delta_D(\vec{k}_1 + \vec{k}_2 + \vec{k}_3)\left[F_2(\vec{k}_1, \vec{k}_2)P(k_1)P(k_2) + \text{perm.}\right]. \tag{2.46}$$

It is convenient to introduce the reduced bispectrum $Q(\vec{k}_1, \vec{k}_2, \vec{k}_3)$, which has the advantage of being mostly scale-independent:

$$Q(\vec{k}_1, \vec{k}_2, \vec{k}_3) = \frac{B(\vec{k}_1, \vec{k}_2, \vec{k}_3)}{P(k_1)P(k_2) + \text{perm.}} = \frac{F_2(\vec{k}_1, \vec{k}_2)P(k_1)P(k_2) + \text{perm.}}{P(k_1)P(k_2) + \text{perm.}}. \tag{2.47}$$

[11] From now on we drop the hats on Fourier-transformed quantities. It will always be apparent from the context whether a quantity is Fourier transformed or not.

2.5. Challenges for the ΛCDM model

The widely accepted concordance or ΛCDM cosmological model makes two important assumptions. First, ΛCDM posits that baryonic matter makes up only a small fraction of the matter content of the Universe with the large remaining part of the matter being cold dark matter. Second, ΛCDM assumes that the accelerated expansion of the Universe is caused by a cosmological constant. The evidence for this ΛCDM model is remarkable, but it leaves some questions unanswered and is in some rare cases in tension with observational data. In this section we summarise some of the evidence for ΛCDM and its challenges. This list is by no means complete, we try to give a concise overview here.

The amount of evidence for dark matter is remarkable (see Ref. [30] for a historic overview), especially because it appears on a large range of scales. The dynamics inside of galaxies and galaxy clusters can not be explained with just the baryonic mass and the laws of general relativity. This was already noted by Fritz Zwicky in 1933, see Refs. [31, 32]. If the galaxy lies inside of a halo of dark matter as predicted by N-body simulations, the dynamics are easily explained. Furthermore, the mass of the clusters estimated from X-ray observations or gravitational lensing, see Ref. [33], exceeds the baryonic mass significantly, see Ref. [34]. The most spectacular evidence for dark matter on galaxy cluster scales comes from the displacement of the center of mass of colliding clusters like the Bullet Cluster compared to the location of visible matter, see Ref. [35]. Furthermore, the existence of small scale structures implies that dark matter is non-relativistic or 'cold', because 'hot' dark matter would wash out small scale structures through free streaming.[12]

Evidence for dark matter also exists on even larger scales through observations of the CMB, see Ref. [21]. While matter perturbations mix with radiation perturbations prior to recombination and thus get wiped out on small scales by diffusion, dark matter can sustain small-scale perturbations and seed the formation of galaxies. Furthermore, the distribution of the acoustic peaks in the CMB is sensitive to the presence of dark matter.

However, the dark matter paradigm is not without issues, especially on galactic scales. Simulations of CDM suggest that the density profile of galaxies is cuspy at the centre. However, observations seem to indicate a flattening of the density profile towards the centre. This discrepancy is dubbed the cusp-core problem,

[12] An intermediate 'warm' state for dark matter is also discussed as possibility, see e.g. Ref. [36].

see Ref. [37]. Furthermore, simulations of CDM predict a much larger amount of substructure inside the halos of galaxies than observed, see Ref. [38]. Another famous discrepancy between the CDM paradigm and galaxy-scale observations is the apparent tight relation between baryons and the dark matter in galaxies, also known as the Tully-Fisher relation, see Ref. [39], which is unexpected since dark matter and baryons do not interact other than gravitationally.

Observational evidence for the late-time accelerated expansion of the Universe comes from two very different approaches. Late Universe probes measuring the luminosity distance of Type Ia supernovae using a distance ladder technique were the first to give conclusive prove of the accelerated expansion, see Refs. [25, 26]. A second 'early Universe' method uses measurements of the baryon-acoustic oscillations in both the CMB and the galaxy clustering to constrain the late-Universe expansion, see Refs. [21, 40]. It is however an open question whether the observed accelerated expansion of the Universe is caused by a cosmological constant, which is assumed in the ΛCDM model and which has a constant equation of state parameter w of -1, or a dynamical dark energy with varying equation of state. Current bounds from the DES survey[13], Ref. [41], indicate $w_p = -1.01^{+0.04}_{-0.04}$ and $w_a = -0.28^{+0.37}_{-0.48}$ for a parametrisation $w = w_p + w_a\,(a_p - a)$ with the pivot redshift $z_p = 1/a_p - 1 = 0.2$. Determining the nature of dark energy through more precise measurements of the equation of state is perhaps the most important challenge of present day cosmology.

While both the early and late-Universe method conclude that the expansion of the late Universe is accelerated, they disagree on a different observable: the value of the Hubble constant H_0. This problem is also known as the Hubble-tension and is probably the biggest obstacle for the cosmological standard model as the tension seems to grow. Depending on which data are combined the tension has $4 - 6\sigma$ significance, see Ref. [42].

Since the ΛCDM model attributes the accelerated expansion of the Universe to a cosmological constant with value $\Lambda \sim (1 \times 10^{-3}\,\mathrm{eV})^4 \sim (1 \times 10^{-30} M_p)^4$ it is in strong conflict with the cosmological constant expected from the quantum-mechanical zero-point energy of the particles in the standard model of particle physics (SM). Naively, the zero point energy of the standard model particles is

[13] This analysis combines DES data with external data including Planck, SDSS, 6dF, BOSS and SNIa data.

given by:

$$\langle \rho \rangle \sim \sum_{SM} \int_0^{\Lambda_{\mathrm{UV}}} \frac{\mathrm{d}^3 k}{(2\pi)^3} \frac{1}{2} \hbar \omega(k) \sim \int_0^{\Lambda_{\mathrm{UV}}} \mathrm{d}k \, k^2 \sqrt{k^2 + m^2} \sim \Lambda_{\mathrm{UV}}^4. \tag{2.48}$$

In this heuristic calculation we treated all modes of the standard model fields as quantum mechanical, harmonic oscillators and summed over their ground state energies $\hbar\omega(k)/2$. Λ_{UV} is the cut-off of the standard model which has to be of order $\Lambda_{\mathrm{UV}} \gtrsim 1\,\mathrm{TeV}$ or higher.[14] Therefore, the zero-point energy of the standard model is at least 60 orders of magnitude larger than the observed cosmological constant. If the total cosmological constant is given by a bare constant Λ_0 plus the zero-point energy of the standard model particles, the bare constant must be fine-tuned to at least the 60th decimal point such that the total cosmological constant is consistent with the cosmological observations. This is the famous cosmological constant problem.

A secondary problem arises with the value of the cosmological constant problem: Its value is such that its energy density is very similar to the matter density at the present time. This seems like a remarkable coincidence given that the two quantities scale very differently with the size of the scale factor. Thus, this problem is called the 'coincidence problem'.

So far no convincing solution to both the cosmological constant and coincidence problem have been found. Together with the other observational challenges for ΛCDM mentioned in this section, they motivate us to look beyond ΛCDM. In this thesis we are particularly interested in investigating alternative models of gravity as possible extensions of the ΛCDM paradigm.

[14] For a more detailed analysis of the cosmological constant problem see Ref. [43].

3. Modified Gravity and Screening

We have demonstrated in the previous Chapter that there exists a well established cosmological concordance model which explains most of the observed phenomena in the Universe very well. However, we also showed that some conceptual and observational issues remain like the cosmological constant problem or the H_0-tension. This motivates us to investigate one of the key assumptions of the cosmological standard model more carefully, the validity of general relativity. To this end we consider possible extensions and modifications of general relativity in this Chapter, focusing in particular on screening models, which play an important role for the rest of this thesis.

Besides the cosmological motivations, there are more general reasons to look at modified gravity models. It is well known that general relativity lacks a unification with the other fundamental forces. Therefore, we expect general relativity to be modified at some scale and it is paramount to repeatedly put general relativity to the test as any observed modifications might give clues to the nature of a unified theory. In fact, we will see that many modified gravity theories, especially the higher-dimensional approaches, are inspired by string theory.

In the past most modified gravity models have been proposed as a solution to one of the previously mentioned problems in the concordance model, in particular the cosmological constant problem. Despite these efforts no convincing solution to the CC problem has been found through the analysis of modified gravity models. In this thesis we will thus take a more general approach to modifications of gravity. We ask the simple question what modifications of GR could look like and how they could be detected on any scale, independent of whether they are capable of explaining the accelerated expansion of the Universe.

3.1. Lovelock's Theorem and Modified Gravity

In Chapter 2.1 we saw that, according to Lovelock's theorem, the Einstein field equations are unique under a set of assumptions. Therefore, modifications of the field equations can only be formulated by breaking one or more of the assumptions in Lovelock's theorem. In this section we will give an overview of the most relevant modified theories of gravity using Lovelock's theorem as a guiding principle. This list of models is by no means complete and for further reading we refer the reader to the reviews in Refs. [14, 44].

According to Lovelock's theorem the Einstein field equations are unique if the following assumptions are met:

1. gravity is a metric theory with a single metric and no other field content,
2. the equations of motion are second order in the derivatives of the metric,
3. the space-time is four dimensional,
4. the equations of motion can be derived from an action principle and
5. locality holds.

Therefore, any modification of general relativity has to give up on at least one of these assumptions.

Since many of the modified gravity models mentioned in the following predict that the speed of gravitational waves differs from the speed of light, they have been put under severe pressure by the simultaneous measurement of gravitational and electromagnetic waves radiated during a binary neutron star merger, Refs. [9, 45], which constrains the speed of the gravitational waves to be very close to the speed of light.[1] We will mention the influence of these constraints on the different modified gravity models, where known.

Perhaps the most straightforward approach to modified gravity is to add additional fields to the theory thus violating the first assumption of Lovelock's theorem.[2] The simplest examples are scalar-tensor theories of gravity where a scalar

[1] We note that the authors of Ref. [46] argue that the energy scale of these observations is close to the cutoff scale of some modified gravity models, specifically models with cutoff scale $M \sim \left(M_p H_0^2\right)^{1/3} \sim 260\,\mathrm{Hz}$. Therefore, the effective field theory breaks down and the speed of the gravitational waves might not be modified in this regime.

[2] Another option violating the first assumption of Loveclock's theorem is a non-metric approach to gravity as in Ref. [47].

field is added to the metric. If we restrict ourselves to second-order equations of motion to avoid Ostrogradsky instabilities, see Ref. [48], the most general action of a scalar-tensor theory is given by the Horndeski action, which was first discovered in 1974 in Ref. [49] and then rediscovered in Ref. [50] as generalisation of the Galileon gravity of Ref. [51]. The Horndeski action may be written as:

$$S[g_{\mu\nu},\phi] = \int \mathrm{d}^4x \left[\sqrt{-g}\sum_{i=2}^{5}\mathcal{L}_i + \mathcal{L}_m[g_{\mu\nu},\psi_m]\right], \tag{3.1}$$

with

$$\begin{aligned}
\mathcal{L}_2 &\coloneqq K(\phi,X), && (3.2)\\
\mathcal{L}_3 &\coloneqq -G_3(\phi,X)\Box\phi, && (3.3)\\
\mathcal{L}_4 &\coloneqq G_4(\phi,X)R + G_{4,X}\left[(\Box\phi)^2 - (\nabla_\mu\nabla_\nu\phi)^2\right], && (3.4)\\
\mathcal{L}_5 &\coloneqq G_5(\phi,X)G_{\mu\nu}\nabla^\mu\nabla^\nu\phi - \frac{1}{6}G_{5,X}(\pi,X)\left[(\Box\phi)^3 - 3(\Box\phi)(\nabla_\mu\nabla_\nu\phi)^2\right.\\
&\quad \left.+2\nabla^\mu\nabla_\alpha\phi\nabla^\alpha\nabla_\beta\phi\nabla^\beta\nabla_\mu\phi\right]. && (3.5)
\end{aligned}$$

X is an abbreviation of the standard kinetic term $X \coloneqq -(\nabla\phi)^2/2$ and the G_i are arbitrary functions of ϕ and X. $G_{i,X}$ is the derivative of G_i with respect to X, ψ_m represents matter fields which are coupled to the Jordan-frame metric $g_{\mu\nu}$. The standard Einstein-Hilbert term is recovered for $G_4 = M_p^2/2$ and $G_5 = 0$. The Horndeski model is a unified framework for a plethora of modified gravity models like Brans-Dicke gravity, Ref. [52], and the covariant Galileon, Refs. [53, 54], which plays an integral part for this thesis and will be further discussed in Section 3.2.

The constraints on the speed of gravitational waves demand $G_{4,X} \approx 0$ and $G_5 \approx$ const on the cosmological background, see Refs. [55–58]. This means that Horndeski theories with non-zero $G_{4,X}$ and non constant G_5 are only valid if the scalar field on the cosmological background is negligible, which means that the field can not explain the accelerated expansion of the late Universe. Since scalar-tensor theories will be the main focus of this thesis, we will discuss them in much greater detail in the following sections.

Besides scalar fields, vector fields and tensor fields have been considered as additional field content. Analogous to scalar-tensor theory, where the most general action leading to second-order equations of motion is given by the Horndeski action, the generalised Proca theory, Ref. [59], is the most general vector-tensor

theory with second-order equations of motion. The speed of gravitational waves in generalised Proca theory is modified in a very similar way as in Horndeski gravity, see Ref. [60], and thus very similar constraints apply. Considering a second rank-2 tensor, which is non-dynamical, leads to massive gravity theories, see Ref. [61] for a review. Massive gravity is not affected by the neutron star merger results since the wavelengths observed at the LIGO detector are much lower than the cosmologically relevant graviton mass scale $m_g \sim H_0 \sim 10^{-33}\,\mathrm{eV}$.

It is also possible to add more than one field to the field content, the most prominent example being TeVeS, Ref. [62], the relativistic version of MOND (Modified Newtonian Dynamics), Ref. [22], which is designed to explain the rotation curves in galaxies without the need for dark matter. TeVeS adds two scalar and one vector field to the metric. However, TeVeS seems to be ruled out by the neutron star merger observations, see Ref. [63].

We now turn to a different class of modified gravity theories, which violate the second assumption of Lovelock's theorem, i.e. introduce higher-order derivatives in the equations of motion. It is usually very challenging to construct consistent theories with higher derivatives in the equations of motion since the Hamiltonian is in general not bounded from below and the ground state may decay, a phenomenon called Ostrogradsky instability, see Ref. [48]. However, it is possible to construct some healthy theories.

Probably the most famous example is $f(R)$ gravity, see Refs. [64, 65]. Here the Einstein-Hilbert action, which is linear in the Ricci scalar, is generalised to an arbitrary function of the Ricci scalar: $\mathcal{L} = \sqrt{-g} f(R)$. The resulting equations of motion are in general fourth order, but avoid Ostrogradsky instabilities because the theory is equivalent to a scalar-tensor theory with second order equations of motion. This can be seen by using a suitable conformal transformation of the metric ($\tilde{g}_{\mu\nu} = \frac{\mathrm{d}f}{\mathrm{d}R} g_{\mu\nu}$) and a field redefinition ($\phi \propto \ln \frac{\mathrm{d}f}{\mathrm{d}R}$), see e.g. Ref. [65]. Since the Horndeski-functions corresponding to $f(R)$ gravity automatically satisfy $G_{4,X} = 0 = G_5$, $f(R)$ gravity is not constrained by the neutron merger observations. Examples of well studied $f(R)$ models are the Hu-Sawicki, Ref. [66], and the Starobinsky model, Ref. [67], which evade solar-system constraints through the Chameleon screening mechanism which we discuss in Section 3.4.2.

By violating both the first and the second assumption in Lovelock's theorem, one can formulate beyond Horndeski and DHOST models. Beyond Horndeski models, Ref. [68], are scalar-tensor theories with third-order equations of motion

which generalise the Horndeski Lagrangians $\mathcal{L}_4$ and $\mathcal{L}_5$, see Eqs. (3.4) and (3.5). These theories are related to Horndeski by a disformal transformation ($\tilde{g}_{\mu\nu} = g_{\mu\nu} + \Gamma(\phi, X)\partial_\mu\phi\partial_\nu\phi$) if either $\mathcal{L}_4 = 0$ or $\mathcal{L}_5 = 0$. These models avoid Ostrogradsky instabilities due to the appearance of constraint equations which ensure that the propagating degrees of freedom obey second-order equations of motion, see Ref. [68].

Beyond Horndeski models can be generalised even further to DHOST theories, Ref. [69], which are the most general scalar-tensor theories with higher-order derivatives and with constraints reducing the number of degrees of freedom such that Ostrogradsky instabilities are avoided. DHOST theories are invariant under the most general disformal transformations ($\tilde{g}_{\mu\nu} = \Omega^2(\phi, X)g_{\mu\nu} + \Gamma(\phi, X)\partial_\mu\phi\partial_\nu\phi$).

The final class of modified gravity theories we consider are higher-dimensional models, which violate the third assumption of Lovelock's theorem.[3] From the perspective of string theory, the main contender for a unified theory of gravity and the other fundamental forces, these extensions of gravity are particularly well motivated since string theory requires the existence of 10 (or 11) dimensions. The problem with higher-dimensional theories of gravity is that the gravitational force would naively scale like $1/r^{D-2}$ in D-dimensional space time, which clearly contradicts our observations that the gravitational force seems to scale like $1/r^2$. Therefore, higher-dimensional gravity theories must be equipped with a mechanism to hide the extra dimensions.

There exist two fundamentally different approaches to hiding the extra dimensions. In Kaluza-Klein theory, Refs. [73, 74], the extra dimension is assumed to be small, which is achieved through compactification of the extra dimension. On scales larger than the compactification scale, which is usually assumed to be of order TeV^{-1} to avoid constraints from collider experiments, all laws of physics will appear 4-dimensional.

In the braneworld paradigm, Refs. [75, 76], on the other hand the extra dimensions, also dubbed 'bulk', can be large, but are only accessible to gravity, while the standard model particles are constrained to a thin 'brane', a $3+1$ dimensional hypersurface in the 'bulk'. Since the standard model particles only live on the brane, the constraints from collider experiments do not apply and the extra dimensions

[3] Other classes of modified gravity, which violate the fourth and fifth assumption of Lovelock's theorem, exist in terms of emergent gravity approaches and non-local gravity respectively, but are not relevant for this thesis. We therefore ignore them here for brevity. The interested reader is referred to Refs. [70–72].

may be larger. Braneworld models avoid the constraints on the $1/r^2$ force law of gravity in different ways. In the ADD model, Ref. [75], the extra dimensions are assumed to be of order $\sim 0.1\,\mathrm{mm}$. Extra dimensions of this size are consistent with the effective Planck mass measured in tests of gravity on scales larger than $\sim 0.1\,\mathrm{mm}$, while offering a solution to the hierarchy problem by reducing the fundamental Planck mass observable only on smaller scales. In the Randall-Sundrum model, Ref. [77], the extra dimension is non-compact and a warp factor ensures that gravity is localised close to the brane.

For late Universe cosmology the most relevant braneworld model is the DGP model, Ref. [78]. The DGP model will indirectly play an important role for this thesis since it reduces to the cubic Galileon model in the decoupling limit as demonstrated in Section 3.2. In DGP gravity the 5D Planck mass M_5 differs from the 4D Planck mass M_p. In this way the $1/r^2$ force law is recovered below a cross-over scale $r_c = M_p^2/2M_5^3$. DGP gravity admits two distinct branches, the normal branch and the self-accelerating branch. The latter can in principle explain the accelerated expansion of the Universe, however, it is plagued by instabilities, while the normal branch is healthy, see Ref. [79].

The action of DGP in its most basic form[4] is given by:

$$S_{\mathrm{DGP}} = M_5^3 \int_{\mathcal{M}} \mathrm{d}^5X\sqrt{-G}\mathcal{R}_5(G) + \frac{M_p^2}{2}\int_B \mathrm{d}^4x\sqrt{-g}R(g), \tag{3.6}$$

where the manifold $\mathcal{M}$ is the 5-dimensional bulk space with coordinates $X = (x^\mu, y)$ and metric G. $\mathcal{R}_5$ is the 5D Ricci scalar and M_5 is the 5D Planck mass, which could a priori take any value. The brane B is a 4D hypersurface located at $y = 0$ and with induced metric $g_{\mu\nu}(x) = G_{\mu\nu}(x, y = 0)$. If there is a hierarchy between the 5D and 4D Planck mass, the model will appear 5-dimensional on scales above the cross-over scale $r_c = M_p^2/2M_5^3$ and look like 4-dimensional gravity on scales below the cross-over scale.

This concludes our general overview of the most prominent modified gravity models. In the following sections we discuss scalar-tensor theories and their screening mechanisms in more detail since they are particularly relevant for this thesis.

[4]For simplicity we neglect external curvature and tension terms here.

3.2. The Cubic Galileon from DGP Gravity

The cubic Galileon model is especially important for this thesis since it is perhaps the simplest modified gravity model with Vainshtein screening, see Section 3.4.1, and will therefore be used as toy model in many places. Thus, it deserves a more detailed introduction.

The cubic Galileon was first obtained from DGP gravity, see Eq. (3.6), as the effective 4D theory in the decoupling limit, see Ref. [80]. We briefly sketch the calculation of the effective action here referring to the original paper for details.

We first consider a general braneworld field theory with the bulk action $S_{\mathcal{M}}[\Phi]$ and the brain action $S_{\partial\mathcal{M}}[\phi]$, where the bulk field Φ satisfies the boundary condition $\Phi|_{\partial\mathcal{M}} = \phi$. The partition function of this theory is given by the path integral ($\hbar = 1$):

$$Z = \int \mathcal{D}\Phi\mathcal{D}\phi \mathrm{e}^{\mathrm{i}(S_{\mathcal{M}}[\Phi]+S_{\partial\mathcal{M}}[\phi])}. \tag{3.7}$$

To obtain the effective action $\Gamma[\phi]$ on the brain we expand the bulk action around a solution $\bar{\Phi}$ of the bulk equation of motion with $\bar{\Phi} = \phi$ up to second order in the fluctuations $\Phi' = \Phi - \bar{\Phi}$ and integrate out Φ':

$$\mathrm{e}^{\mathrm{i}\Gamma[\phi]} \approx \mathrm{e}^{\mathrm{i}(S_{\mathcal{M}}[\bar{\Phi}]+S_{\partial\mathcal{M}[\phi]})} \int_{\Phi'|_{\partial\mathcal{M}}=0} \mathcal{D}\Phi' \exp\left(\frac{\mathrm{i}}{2}\int \Phi' \frac{\delta^2 S_{\mathcal{M}}}{\delta\Phi^2}(\Phi=\bar{\Phi})\Phi'\right). \tag{3.8}$$

For the case of DGP gravity, see Eq. (3.6), the bulk field is the 5D metric G_{MN} and we write it in terms of the flat Minkowski metric η_{MN}: $G_{MN} = \eta_{MN} + H_{MN}$. The boundary conditions require $H_{MN}(y = 0) = h_{MN}$. The resulting effective action is best written in terms of the fields π, N_μ and $h'_{\mu\nu}$, which are defined through:

$$-2\sqrt{-\partial^2}\pi = h_{yy}, \qquad N_\mu = G_{y\mu} - \partial_\mu\pi \qquad \text{and} \qquad h'_{\mu\nu} = h_{\mu\nu} + \frac{\pi}{r_c}\eta_{\mu\nu}. \tag{3.9}$$

The quadratic part of the effective action then becomes diagonal:

$$\Gamma_{\text{quadratic}} = \frac{M_p^2}{4}\int \mathrm{d}^4x \left[\frac{1}{2}h'^{\mu\nu}\Box h'_{\mu\nu} - \frac{1}{4}h'\Box h' - r_c^{-1}N^\mu\sqrt{\partial^2}N_\mu + \frac{3}{r_c^2}\pi\Box\pi\right]. \tag{3.10}$$

Of the higher-order terms in the effective action only the cubic term in π is relevant

in the limit $M_p, r_c, T_{\mu\nu} \to \infty$ and $M_p/M_5^2, T_{\mu\nu}/M_p = \text{const.}$:

$$\Gamma_{\text{interactions}} \approx -\frac{M_5^3}{2}\int \mathrm{d}^4x (\partial\pi)^2\Box\pi. \tag{3.11}$$

In this 'decoupling' limit the scalar field π decouples from the graviton $h'_{\mu\nu}$. In the presence of matter fields on the brain, the linearised brain action $S_{\partial\mathcal{M}}$ contains the interaction term $\frac{1}{2}\int \mathrm{d}^4x\, h_{\mu\nu}T^{\mu\nu}$. Since $h_{\mu\nu}$ is related to $h'_{\mu\nu}$ through Eq. (3.9), the scalar field couples to the trace of the energy-momentum tensor: $\frac{1}{2}\int \mathrm{d}^4x\, \frac{\pi}{r_c}T$. The field N_μ however does not couple to any other field and we can set it to 0.

The 4D effective DGP model in the decoupling limit is therefore a scalar-tensor theory. Its effective Lagrangian is given by $\mathcal{L} = \mathcal{L}_{\text{GR}} + \mathcal{L}_\pi$, where $\mathcal{L}_{\text{GR}}$ is the action of GR expanded to second order in $h_{\mu\nu}$ and $\mathcal{L}_\pi$ is the Lagrangian of the scalar field π coupled to the trace of the energy-momentum tensor:

$$\mathcal{L}_\pi = -\frac{3M_p^2}{4r_c^2}(\partial\pi)^2 - \frac{M_5^3}{2}(\partial\pi)^2\Box\pi + \frac{\pi}{2r_c}T. \tag{3.12}$$

Alternatively, one may rescale the scalar field π such that the standard kinetic term is canonically normalised:

$$\mathcal{L}_\pi = -\frac{1}{2}(\partial\pi)^2 - \frac{1}{2M^3}(\partial\pi)^2\Box\pi + \frac{\pi}{\sqrt{6}M_p}T, \tag{3.13}$$

with the mass scale $M \sim (M_p/r_c^2)^{1/3}$. Varying this Lagrangian with respect to π, we obtain the equation of motion:

$$\Box\pi + \frac{1}{M^3}\left((\Box\pi)^2 - (\partial_\mu\partial_\nu\pi)^2\right) = -\frac{T}{\sqrt{6}M_p} = \frac{\rho_m}{\sqrt{6}M_p}, \tag{3.14}$$

where we assumed that the energy momentum tensor is given by a pressure-less perfect fluid $T_{\mu\nu} = \rho_m u_\mu u_\nu$ with matter density ρ_m.

This equation of motion is remarkable in two aspects. First, it is only second order in the derivatives of π even though the Lagrangian already contains second derivatives. This marks this scalar-tensor theory as a Horndeski theory. Second, the equation of motion is invariant under the galilean transformation $\pi \to \pi + c + b_\mu x^\mu$. This scalar-tensor theory was thus dubbed Galileon in Ref. [51] in analogy to the non-relativistic galilean boost $\dot{x} \to \dot{x} + v$. Ref. [51] furthermore discovered that the model in Eq. (3.13) is only the cubic variant of a larger class of galilean

invariant theories with second-order equations of motion, which also contains the quartic and the quintic Galileon.

The covariant variant of the Galileon as formulated in Refs. [53, 54] breaks the invariance under the galilean transformation but maintains second-order equations of motion. It was later realised in Ref. [50] that the covariant Galileon models are a subclass of the Horndeski models as defined in Eq. (3.1). The traditional covariant Galileon model of Refs. [53, 54] is obtained by choosing the Horndeski functions G_3, G_4 and G_5 proportional to the standard kinetic term X. The action of the cubic Galileon with $G_3 = X/M^3$ and $K = X$ is equivalent to the effective DGP action in the decoupling limit, see Eq. (3.13), except for the coupling to matter. The coupling to matter can be added to the cubic Galileon through a conformal coupling, see Eq. (3.35).

3.3. Conformal Transformations and Fifth Forces

In Eq. (3.1) we introduced the Horndeski theory as the most general scalar-tensor theory with second-order equations of motion. In general the scalar field couples non-minimally to the gravitational field if either $G_4 \neq$ const. or $G_5 \neq 0$, thus modifying the gravitational field equations. This is the so-called Jordan-frame description of scalar-tensor theories, where the scalar field couples non-minimally to gravity, but the matter fields follow geodesics of the metric $g_{\mu\nu}$. In some cases, there also exists an Einstein-frame description of the same theory, where the non-minimal coupling terms disappear and the gravitational field equations are given by Einstein's equations, however the matter-fields couple to the metric through a function of the scalar field. In the Einstein-frame description matter moves on geodesics of a metric different from the one determined by Einstein's equations. In this way the emergence of a fifth force mediated by the scalar field becomes apparent.

For a very careful analysis on the criteria for the existence of an Einstein frame in Horndeski gravity we refer to Ref. [81]. For simplicity, we restrict ourselves here to the case where $G_5 = 0$ and $G_4 = G_4(\phi)$, i.e. the traditional scalar-tensor theories:

$$S = \int \mathrm{d}^4x \left[\sqrt{-g}\left(K(\phi, X) - G_3(\phi, X)\Box\phi + G_4(\phi)R\right) + \mathcal{L}_m\left[g_{\mu\nu}, \psi_m\right]\right] \qquad (3.15)$$

As we will demonstrate in the following, we can change to the Einstein frame with a conformal transformation:

$$g_{\mu\nu} \to \tilde{g}_{\mu\nu} = \Omega^2(\phi) g_{\mu\nu}. \tag{3.16}$$

The transformation behaviour of the Ricci-scalar, the d'Alembert operator, the metric determinant and the standard kinetic term X is given by:

$$\begin{aligned} R &= \Omega^2 \left(\tilde{R} + 6\tilde{\Box} \log\Omega - 6\tilde{g}^{\mu\nu}\partial_\mu \log\Omega \partial_\nu \log\Omega \right), && (3.17)\\ \Box A &= \Omega^2 \left(\tilde{\Box} A - 2\tilde{g}^{\mu\nu}\partial_\mu \log\Omega \partial_\nu A \right), && (3.18)\\ \sqrt{-g} &= \Omega^{-4}\sqrt{-\tilde{g}}, \qquad X = \Omega^2 \tilde{X}, && (3.19) \end{aligned}$$

where A is an arbitrary scalar field. These transformation rules together with the identity:

$$\int \mathrm{d}^4x \sqrt{-g} \frac{\Box A}{A^3} = 3 \int \mathrm{d}^4x \sqrt{-g} \frac{(\nabla A)^2}{A^4}, \tag{3.20}$$

which holds up to a negligible boundary term[5], enable us to write the action in Eq. (3.15) in terms of the new metric $\tilde{g}$:

$$S = \int \mathrm{d}^4x \left[\sqrt{-\tilde{g}} \left(\tilde{K}\left(\phi, \tilde{X}\right) - \tilde{G}_3\left(\phi, \tilde{X}\right) \tilde{\Box}\phi + \tilde{G}_4(\phi)\, \tilde{R} \right) + \mathcal{L}_m \left[\Omega^{-2}\tilde{g}_{\mu\nu}, \psi_m \right] \right]. \tag{3.21}$$

The transformation rules for the Horndeski functions are:

$$\begin{aligned} \tilde{K}\left(\phi, \tilde{X}\right) &= \Omega^{-4} K\left(\phi, \Omega^2\tilde{X}\right) - 4\frac{\Omega'}{\Omega^3} G_3\left(\phi, \Omega^2\tilde{X}\right)\tilde{X} - 12\frac{\Omega'^2}{\Omega^4} G_4(\phi)\tilde{X}\\ \tilde{G}_3\left(\phi, \tilde{X}\right) &= \Omega^{-2} G_3\left(\phi, \Omega^2\tilde{X}\right), \qquad \tilde{G}_4(\phi) = \Omega^{-2} G_4(\phi). \end{aligned} \tag{3.22}$$

Primes denote derivatives with respect to the scalar field ϕ.

From the transformation rules of the Horndeski functions we see that any non-minimal coupling in the form of $G_4(\phi)$ can always be removed by choosing the conformal factor $\Omega^2(\phi) = 2G_4(\phi)/M_p^2$. The action in the Einstein frame is then of the form:

$$S = \int \mathrm{d}^4x \left[\sqrt{-\tilde{g}} \left(\mathcal{L}_\phi + \frac{M_p^2}{2}\tilde{R} \right) + \mathcal{L}_m \left[\Omega^{-2}\tilde{g}_{\mu\nu}, \psi_m \right] \right], \tag{3.23}$$

[5] We assume that the derivatives of field A vanish at the boundary.

with the scalar-field Lagrangian $\mathcal{L}_\phi = \tilde{K} - \tilde{G}_3\Box\phi$. The Einstein equations now take their standard form with energy-momentum tensor:

$$\tilde{T}_{\mu\nu} = \tilde{T}^{\phi}_{\mu\nu} + \tilde{T}^{m}_{\mu\nu} = -\frac{2}{\sqrt{-\tilde{g}}}\frac{\delta\left(\sqrt{-\tilde{g}}\mathcal{L}_\phi\right)}{\delta\tilde{g}^{\mu\nu}} - \frac{2}{\sqrt{-\tilde{g}}}\frac{\delta\mathcal{L}_m}{\delta\tilde{g}^{\mu\nu}}. \tag{3.24}$$

In the Einstein frame the total energy-momentum tensor obeys a conservation equation $\nabla^\mu\tilde{T}_{\mu\nu} = 0$, however, the individual components $\tilde{T}^{\phi}_{\mu\nu}$ and $\tilde{T}^{m}_{\mu\nu}$ do not obey a conservation equation, since the matter fields couple to the Jordan-frame metric $g_{\mu\nu} = \Omega^{-2}\tilde{g}_{\mu\nu}$, which depends on ϕ. This is also called conformal coupling and leads to the emergence of a fifth force mediated by the scalar field as we demonstrate in the following.

Non-relativistic test objects moving on geodesics of the Jordan-frame metric experience the acceleration:

$$\frac{\mathrm{d}x^i}{\mathrm{d}t^2} \approx -\Gamma^i_{00} = -\tilde{\Gamma}^i_{00} + \tilde{g}_{00}\frac{\mathrm{d}\log\Omega}{\mathrm{d}\phi}\partial^i\phi, \tag{3.25}$$

where the Christoffel symbols Γ^i_{00} and $\tilde{\Gamma}^i_{00}$ are computed from the Jordan-frame and Einstein-frame metrics respectively. Since the equations of motion for the Einstein-frame metric are the standard Einstein equations, the metric in the stationary weak-field limit is given by $\tilde{g}_{00} \approx -1 - 2\Phi_N$, with the Newtonian potential Φ_N. Therefore, the acceleration of a non-relativistic test particle becomes:

$$\frac{\mathrm{d}x^i}{\mathrm{d}t^2} \approx -\partial^i\Phi_N + \frac{\mathrm{d}\log\Omega}{\mathrm{d}\phi}\partial^i\phi. \tag{3.26}$$

We see that the test particle experiences a fifth force mediated by the scalar field ϕ in addition to the Newtonian gravitational force.

We now take a look at the equation of motion for the scalar field in the Einstein frame. Variation of the action in Eq. (3.23) with respect to the scalar field results in the equation of motion:

$$\begin{aligned}\frac{\delta\mathcal{L}_\phi}{\delta\phi} &= \frac{-1}{\sqrt{-\tilde{g}}}\frac{\delta\mathcal{L}_m\left[\Omega^{-2}\tilde{g}_{\mu\nu},\psi_m\right]}{\delta\phi} = 2\frac{\mathrm{d}\log\Omega}{\Omega^2\mathrm{d}\phi}\frac{\tilde{g}_{\mu\nu}}{\sqrt{-\tilde{g}}}\frac{\delta\mathcal{L}_m\left[g_{\mu\nu},\psi_m\right]}{\delta g_{\mu\nu}} \\ &= \frac{\mathrm{d}\log\Omega}{\mathrm{d}\phi}\tilde{T}^m.\end{aligned} \tag{3.27}$$

The scalar field thus couples to the trace of the Einstein-frame energy-momentum

tensor of the matter fields, which in the pressure-less, perfect-fluid case is given by the Einstein-frame matter density $-\tilde{\rho}_m$.

Comparison of Eq. (3.27) with the equation of motion for the field π in the decoupling limit of DGP, see Eq. (3.14), demonstrates that we have reproduced the same coupling between the scalar field and matter if we choose the conformal factor to be

$$\Omega = \exp\left(-\phi/\sqrt{6}M_p\right). \tag{3.28}$$

The acceleration of a test particle due to the fifth force, see Eq. (3.26), is then proportional to $\propto \partial^i\phi/M_p$.

For the rest of this thesis we will skip the tilde on Einstein-frame quantities for brevity. We will always work in the Einstein frame unless otherwise stated.

3.4. Screening of Fifth Forces

If our goal is the construction of a cosmologically relevant scalar-tensor theory, we would expect the strength of the fifth force to be similar to that of gravity. Furthermore, the fifth force has to be a long-range force with a mass $m \lesssim H_0$ to be of cosmological interest. However, long-range fifth forces with couplings as strong as gravity are excluded by tests of gravity in the Solar System and laboratory experiments, see e.g. Refs. [6, 7]. For the scalar-tensor theory to be viable, it therefore must be highly non-linear such that the strength or the range of the force is strongly suppressed on small scales, but is still cosmologically relevant. Such non-linear theories are said to have a 'screening mechanism'.

Various categorisations of the known screening mechanisms have been proposed in the literature. Here we define two different classes of screening mechanisms, the 'Vainshtein-type' and the 'Chameleon-type' mechanisms. We define Vainshtein-type screening mechanisms as models with non-linear kinetic terms in the equation of motion. On scales where the non-linear terms dominate over the linear term, the $1/r^2$-force law is modified and the fifth force is suppressed compared to gravity. This class includes the traditional Vainshtein screening, Refs. [82, 83], as well as kinetic screening, Ref. [84], and DBIonic screening, Ref. [85].

On the other side are Chameleon-type screening mechanisms which have a standard kinetic term, but have a non-linear effective potential which depends on the local matter density. In these models the scalar field value minimising the effec-

tive potential depends on the local matter distribution. Quantities like the mass or the coupling strength of the scalar field are thus environmentally dependent. The classic Chameleon mechanism, Ref. [86], and the Symmetron mechanism, Ref. [87], fall into this class of screening mechanisms.

We will discuss both classes in more detail in the following two sections. For a more detailed review of screening mechanisms we refer to Ref. [88].

3.4.1. The Vainshtein screening mechanism

For simplicity, we consider a scalar-tensor theory with the shift-symmetry $\phi \to \phi + c$. In this case, the equation of motion for the scalar-field may always be written in the form:

$$\nabla_\mu J^\mu = \frac{\xi}{M_p}\rho_m. \tag{3.29}$$

We have assumed here that the conformal factor is given by $\Omega = \exp\left(-\xi\phi/M_p\right)$ with ξ being an order one parameter. The current J^μ can be split into the linear part $\partial^\mu\phi$ which stems from the standard kinetic term in the Lagrangian, $X \in \mathcal{L}_\phi$, and a non-linear current $J^\mu_{\rm nl}$:

$$J^\mu = \partial^\mu\phi + J^\mu_{\rm nl}\left(\nabla\phi, \nabla^2\phi\right). \tag{3.30}$$

The non-linear current has to be a function of the first and second derivatives of the scalar field to obey the shift-symmetry. The dependence on second derivatives is only possible, if the resulting third order terms in $\nabla_\mu J^\mu_{\rm nl}$ cancel out as is the case for any Horndeski scalar-tensor theory.

Around a static, compact and spherically symmetric mass M_0, the equation of motion, Eq. (3.29), can be integrated over a sphere S_r of radius r using Gauss' law:

$$\frac{\xi}{M_p}M_0 = \int_{S_r} \mathrm{d}\vec{S}_r \cdot \vec{J} = 4\pi r^2 J^r = 4\pi r^2\left(\partial_r\phi + J^r_{\rm nl}\right), \tag{3.31}$$

where J^r is the radial component of the spatial 3-vector current $\vec{J}$. We have assumed that the curvature is low around mass M_0, such that all covariant derivatives ∇ can be written as partial derivatives ∂. From Eq. (3.31) we can read off the radial dependence of the fifth force in the two relevant regimes. In the regime where the non-linear terms are negligible, we recover the $1/r^2$-force law of gravity, i.e. there is no active screening of the fifth force.

The situation is different in the regime where the non-linearities dominate. To further simplify the analysis here, we assume that the non-linear current is polynomial[6] in the derivatives of ϕ:

$$J^r_{\rm nl} \propto (\partial_r\phi)^n \left(\partial_r^2\phi\right)^m \propto r^{-(n+2m)}\phi^{n+m}, \tag{3.32}$$

where m and n are natural numbers with $m+n \geq 2$. This results in a force law:

$$\partial_r\phi \propto r^{\frac{m-2}{n+m}}, \tag{3.33}$$

where the exponent $\frac{m-2}{n+m} \geq -1$. The ratio of the fifth force with respect to the gravitational force scales as:

$$\frac{\partial_r\phi}{\partial_r\Phi_N} \propto r^{\frac{m-2}{n+m}+2} = r^\alpha, \tag{3.34}$$

where $\alpha \geq 1$. This demonstrates that the fifth force is strongly suppressed compared to gravity for small r.

We conclude that Vainshtein screening is effective below a scale r_V, called Vainshtein radius, which marks the scale where $J^r_{\rm nl} \sim \partial_r\phi$.

As an example we consider the cubic Galileon model conformally coupled to matter, which will be of great importance for this thesis:

$$S = \int \mathrm{d}^4x\sqrt{-g}\left[M_p^2\frac{R}{2} - \frac{1}{2}(\partial\phi)^2 - \frac{1}{2M^3}\Box\phi\,(\partial\phi)^2\right] + S_M\left[\mathrm{e}^{2\xi\phi/M_p}g_{\mu\nu}, \psi_m\right]. \tag{3.35}$$

The resulting equation of motion:

$$\Box\phi + \frac{1}{M^3}\left((\Box\phi)^2 - R_{\mu\nu}\nabla^\mu\phi\nabla^\nu\phi - (\nabla_\mu\nabla_\nu\phi)(\nabla^\mu\nabla^\nu\phi)\right) = \frac{\xi}{M_p}\rho_m, \tag{3.36}$$

is completely analogous to the decoupling limit of DGP, see Eq. (3.14), if we choose $\xi = 1/\sqrt{6}$ and consider low curvatures.

The appearance of the Ricci-tensor $R_{\mu\nu}$ can easily be understood. Variation of the action in Eq. (3.35) with respect to the scalar field gives the third-order terms $\nabla_\mu\phi\nabla_\nu\nabla^\nu\nabla^\mu\phi$ and $-\nabla_\mu\phi\nabla^\mu\nabla_\nu\nabla^\nu\phi$. These third-order terms can be eliminated by commuting the covariant derivatives, however, in this way we pick up a Ricci

[6]This is not possible in the case of DBIonic screening. See Ref. [85] for details.

tensor. This mixing of second derivatives of the metric and the scalar field is also called kinetic braiding, see Ref. [89]. A consequence is that even in the absence of a conformal coupling, the Galileon field still couples to matter indirectly due to its coupling to the metric.

In the static, low-curvature case, the equation of motion, Eq. (3.36), has the form of Eq. (3.29) with the non-linear current:

$$J^i_{\rm nl} = \frac{1}{M^3}\left(\Delta\phi\partial^i\phi - \left(\partial^i\partial^j\phi\right)\partial_j\phi\right). \tag{3.37}$$

The cubic Galileon is thus of type $m = 1$, $n = 1$, see Eq. (3.32), and the force-law should be of the form $\partial_r\phi \propto 1/\sqrt{r}$ inside the Vainshtein radius. Indeed the exact solution around a spherical mass M_0 is given by:

$$\partial_r\phi = \frac{M^3}{4}r\left(1 - \sqrt{1 + \frac{r_V^3}{r^3}}\right). \tag{3.38}$$

The Vainshtein radius is defined through:[7]

$$r_V^3 := \frac{2\xi M_0}{\pi M_p M^3}. \tag{3.39}$$

Examining the solution in Eq. (3.38), we find as expected $\partial_r\phi \propto 1/r^2$ at scales larger than the Vainshtein radius, $r \gg r_V$, and on small scales compared to the Vainshtein radius, $r \ll r_V$, we obtain $\partial_r\phi \propto 1/\sqrt{r}$. Thus, the strength of the fifth force compared to gravity is constant in space outside the Vainshtein radius but decays as $(r/r_V)^{3/2}$ towards smaller radii.

3.4.2. Chameleon-type screening mechanisms

We now discuss the Chameleon and Symmetron screening mechanisms. For this purpose we consider a scalar-tensor theory of the form:

$$S = \int \mathrm{d}^4x\sqrt{-g}\left(M_p^2\frac{R}{2} - \frac{1}{2}(\partial\phi)^2 - V(\phi)\right) + S_m\left[\Omega^{-2}(\phi)g_{\mu\nu}, \psi_m\right], \tag{3.40}$$

[7] In the case of an evolving background, kinetic braiding adds an extra contribution to the effective coupling and modifies the Vainshtein radius as demonstrated in Eq. (A.31) in Appendix A.2.

where the potential $V(\phi)$ is arbitrary for now. The equation of motion is of the form, see Eq. (3.27):

$$\Box\phi = \frac{\mathrm{d}V}{\mathrm{d}\phi} - \frac{\mathrm{d}\log\Omega}{\mathrm{d}\phi}\rho_m =: \frac{\mathrm{d}V^{\mathrm{eff}}}{\mathrm{d}\phi}. \tag{3.41}$$

We have assumed here that the trace of the energy-momentum tensor is given by $-\rho_m$. The effective potential has the form:

$$V^{\mathrm{eff}}(\phi, \rho_m) = V(\phi) - \log\Omega\,\rho_m, \tag{3.42}$$

and thus depends on the local matter distribution. If the field is varying only slowly over time and space, such that the kinetic term in the equation of motion may be ignored, the field will lie at the minimum of the effective potential which is environmentally dependent $\bar{\phi} = \phi(\rho_m)$.

In the case of the Chameleon field, the potential $V(\phi)$ is typically assumed to decrease monotonically with ϕ. A prominent example is the Ratra-Peebles potential $V \propto \phi^{-n}$ with $n > 0$.[8] The minimum of the effective potential then scales as $\bar{\phi} \propto \rho_m^{1/(n+1)}$ if we choose the conformal factor to be an exponential function of ϕ:

$$\Omega(\phi) = \exp\left(-\xi\frac{\phi}{M_p}\right). \tag{3.43}$$

As a consequence, the effective mass $m^2(\rho) \coloneqq V^{\mathrm{eff}}_{,\phi\phi}(\bar{\phi}, \rho_m)$ of fluctuations around the minimum $\bar{\phi}$ is environmentally dependent and scales as $m^2 \propto \rho_m^{(n+2)/(n+1)}$. The mass thus increases in regions of high densities, which decreases the range of the fifth force.

For the Symmetron one typically assumes a $\mathbb{Z}_2$-symmetric potential of the form:

$$V(\phi) = -\frac{\mu^2}{2}\phi^2 + \frac{\lambda}{4}\phi^4, \tag{3.44}$$

together with the quadratic conformal factor:

$$\Omega(\phi) = \exp\left(-\xi^2\frac{\phi^2}{M_p^2}\right). \tag{3.45}$$

A non-zero matter density modifies the quadratic term in the potential $-\mu \to$

[8] Negative n have also been discussed in the literature, see e.g. Ref. [90]. For the sake of simplicity, we only consider positive n in this Chapter.

$\xi\rho_m/M_p - \mu$. The $\mathbb{Z}_2$ is restored with $\bar{\phi} = 0$ if the density term dominates over μ, but is spontaneously broken in regions of low density. Due to the quadratic nature of the conformal factor, the coupling of the fifth force to matter is proportional to the scalar field value $\bar{\phi}$ and thus vanishes in regions of high density.

We will now demonstrate how Chameleon-type screening behaves around compact objects by considering a static, spherically symmetric matter source M with radius R and constant density ρ_M, which is embedded in a homogeneous background density ρ_{bg}. We assume that the mass M is large or dense enough that the field inside the object is given by the minimum of the effective potential $\phi_M = \phi(\rho_M)$, except for a thin shell at the boundary. We will specify later what 'large enough' means. Far away from the mass, the field becomes $\phi_{bg} = \phi(\rho_{bg})$. In the close vicinity of the object, the field is given by a solution which matches these two boundary conditions:

$$\phi(r > R) = \phi_{bg} - \frac{R}{r}\left(\phi_{bg} - \phi_M\right) \mathrm{e}^{-m(\rho_{bg})(r-R)}. \tag{3.46}$$

We have assumed here that the effective potential outside the object is well approximated by a quadratic with mass $m^2(\rho_{bg}) = V^{\mathrm{eff}}_{,\phi\phi}(\rho_{bg})$. For both the Chameleon and Symmetron model the minimum of the effective potential decreases with increasing density. Thus, it is safe to assume $\phi_{bg} \gg \phi_M$, if the object has a significantly higher density than the background. We may therefore write:

$$\phi(r > R) = \phi_{bg} - \lambda \frac{\xi M}{4\pi M_p r} \mathrm{e}^{-m(\rho_{bg})(r-R)}, \tag{3.47}$$

where the screening or thin-shell factor λ is defined as:

$$\lambda = \frac{3M_p(\phi_{bg} - \phi_M)}{\xi\rho_M R^2} = \frac{\phi_{bg} - \phi_M}{2\xi M_p \Phi_N(R)} \approx \frac{\phi_{bg}}{2\xi M_p \Phi_N(R)}. \tag{3.48}$$

We used that the gravitational potential at the surface of the object is given by $\Phi_N = M/8\pi M_p^2 R$.

The meaning of the screening factor λ becomes clear when comparing the gradient of the scalar field with the gradient of the gravitational potential: $\partial_r\phi/\partial_r\phi_N \propto \lambda\xi M_p$, if $r \ll m(\rho_{bg})$. A small screening factor $\lambda \ll 1$ typically indicates that the fifth force is screened compared to the gravitational force. To be more precise, the exact magnitude of the fifth force on a test particle is given by $\partial^i\phi \, \mathrm{d}\log\Omega/\mathrm{d}\phi$, see

Eq. (3.26). In the case of an exponential conformal factor like for the Chameleon, see Eq. (3.43), the fifth force is directly proportional to the gradient of the scalar field and a small λ guarantees a small fifth force if $\xi \sim 1$. However, for the Symmetron the fifth force is proportional to $\phi\partial^i\phi$, i.e. the magnitude of the fifth force relative to gravity around the central object is approximately $\phi_{bg}\lambda/M_p$. The magnitude of the fifth force thus depends more subtly on both λ and the background field ϕ_{bg}/M_p.

The screening due to a small screening factor λ has a nice interpretation in terms of the thin-shell effect. Since the mass of the Chameleon is large inside of the object, the range of the fifth force is small ($\sim m^{-1}(\rho_M)$) and only the outermost shell of the object can source a fifth force of longer range ($m^{-1}(\rho_{bg})$). Similarly for the Symmetron, the inner part of the object, where the $\mathbb{Z}_2$-symmetry is restored, has a vanishing coupling to matter and thus does not contribute to the fifth force of the object.

In Ref. [91] a much more careful derivation of the thin-shell solution in Eq. (3.47) is presented in the context of Chameleon gravity. Ref. [91] shows that $\lambda \ll 1$ also guarantees consistency with our assumption that the object is 'large enough' for the field inside the object to be given by the minimum of the effective potential.

4. The Shape Dependence of Vainsthein Screening in the Matter Bispectrum

As stated in the introduction, see Chapter 1, it is our desire to find observable features of screening mechanisms. One such feature is the shape dependence of Vainshtein screening, i.e. the observation that the effectiveness of Vainshtein screening around matter sources depends on the shape of the sources, see Ref. [92]. We demonstrate in this chapter that this shape dependence affects the matter bispectrum in a very intuitive way and with a unique time dependence which could be used to minimize degeneracies with other cosmological parameters. We use a conformally coupled cubic Galileon as toy model and perform a second-order perturbative analysis to derive analytic, integral expressions for the bispectrum. The latest version of the `hi_class`-code is used to demonstrate the time dependence of the effect. We leave a careful data comparison for future analyses and concentrate on the phenomenology in this work.

This work was published in Ref. [3] together with my coauthors Clare Burrage and Daniela Saadeh, who gave excellent advice throughout this work and helped me with some of the numerical aspects of the `hi_class` code. Ref. [3] is replicated here with only minor changes, which establish the connections to the introductory chapters 2 and 3 in this thesis.

4.1. Motivation

In Section 3.4.1 we have introduced Vainshtein screening as one of the main contenders for a screening mechanism which suppresses fifth forces in regions of high second-order derivatives of the scalar field. Remarkably, it was realized in Refs. [92, 93] that the effectiveness of Vainshtein screening is strongly dependent

on the shape of the source mass. The screening is most effective around spherical sources, less effective around cylindrical bodies and non-existent in systems with planar symmetry.

The discovery of this shape-dependence motivated us to look for this effect in the cosmic web, where lots of different shapes are present, from clusters to filaments and walls.[1] The dynamics of the cosmic web are investigated here using cosmological perturbation theory. Since Vainshtein screening is intrinsically non-linear, we have to go to at least second order in perturbation theory to observe any shape-dependent effects: we will therefore use the matter bispectrum as our observable. The matter bispectrum is especially suitable to test for shape dependence as it is sensitive to three wavenumbers, which form a closed triangle upon imposing background homogeneity. Different triangle shapes correspond to different shapes in real space, which have differing screening properties[2].

The simplest model exhibiting Vainshtein screening is the cubic Galileon, see Sections 3.2 and 3.4.1. It was shown in Ref. [98] that the cubic Galileon without coupling to matter is ruled out as the only energy component driving the late-time accelerated expansion of the Universe, as it predicts a negative integrated Sachs-Wolfe effect in conflict with current obervations. Similarly, a cubic Galileon which couples to matter conformally, is constrained by solar-system bounds on the variation of Newton's constant, see Refs. [5, 99] and Chapter 5. Therefore, we include a cosmological constant in our model and keep the Galileon energy density as a subdominant energy component throughout the entire evolution of the Universe. A cosmological model with such a sub-dominant cubic Galileon component was also considered in Ref. [100], where it was shown that independent initial perturbations in the Galileon field can break the usual correlation between density and velocity power spectra and lead to a form of stochastic bias.

The matter bispectrum was first studied for cubic Galileon models in Ref. [101] and, subsequently, generalised to Horndeski theories [102–105]. These analyses did not include an explicit conformal coupling to matter, only an indirect coupling due kinetic braiding, see the discussion after Eq. (3.36). Our analysis includes an explicit conformal coupling of the Galileon field to matter, which generally results in a stronger fifth force and stronger effects from screening. Furthermore, we

[1] The morphology dependence of Vainshtein screening in the cosmic web was previously explored with simulations in Ref. [94]. For further numerical studies of Vainshtein screening see also Refs. [95, 96].

[2] See Ref. [97] for a very insightful interpretation of the different shapes of the bispectrum.

demonstrate for the first time how the shape-dependence of Vainshtein screening affects the bispectrum.

4.2. The Shape-Dependence of Isolated Objects

In this section we review the effect of shape-dependent Vainshtein screening. As a simple proxy for an extension of general relativity with Vainshtein screening we consider a cubic Galileon model with a conformal coupling to the matter fields similar to the one introduced in Eq. (3.35). In addition to the model in Eq. (3.35) we include a cosmological constant Λ since the cubic Galileon cannot be the sole source of the late-time accelerated expansion of the Universe as mentioned in the previous section. The model we consider has the form:

$$S = \int \mathrm{d}^4x \left[M_p^2 \sqrt{-g} \left(\frac{R}{2} - \Lambda + \mathcal{L}_\phi \right) + \mathcal{L}_m \left[(1+\phi)\, g_{\mu\nu}, \psi_m \right] \right], \tag{4.1}$$

with the Lagrangian for the Galileon field being:

$$\mathcal{L}_\phi = -\frac{C_2}{2}(\nabla\phi)^2 - \frac{C_3}{2}(\Box\phi)(\nabla\phi)^2. \tag{4.2}$$

This model differs from the cubic Galileon defined in Eq. (3.35) in two ways. First, we approximated the exponential conformal factor of Eq. (3.35) linearly[3]. This is a very good approximation as long as the dimensionless field ϕ is small compared to 1, which it always will be since we are not interested in a self-accelerating Galileon model, i.e. an explanation of the late-time accelerated expansion of the Universe through a time-varying conformal factor.

The second difference between our cubic Galileon model here and Eq. (3.35) is the normalisation of the scalar field. We have rescaled the scalar field such that it is dimensionless ($2\xi\phi/M_p \to \phi$). As a consequence, the kinetic term is not canonically normalised. Due to this rescaling our expressions are very closely related to the calculations in Ref. [101], the first paper studying the bispectrum in the (non-conformally coupled) cubic Galileon model. We were thus able to use some of their expressions for the extremely involved calculation of the second-order

[3]This linear approximation of the conformal factor is in principle not necessary as all consecutive expressions in this Chapter would be similarly simple if we kept the full exponential dependence. However, we chose to work with the linear approximation in Ref. [3] and for consistency with our publication, we choose to do the same here.

cosmological perturbations[4]. The parameters C_2 and C_3 of our model here, Eq. (4.1), are related to the parameters ξ and M of the model in Eq. (3.35) by:

$$C_2 = \frac{1}{4\xi^2}, \qquad C_3 = \frac{M_p}{6M^3\xi^3}. \tag{4.3}$$

The parameter C_2 is thus dimensionless and C_3 has inverse mass dimension 2.

Since we will use the `hi_class` code for numerical analyses later on, we will use the `hi_class` normalization for densities in this Chapter, such that the Friedmann equation takes the form $H^2 = \sum_i \rho_i$ (the same normalization will be used for pressures). For the energy-momentum tensor of the matter fields we make the standard cosmological assumption that matter is non-relativistic and can thus be treated as a pressureless, perfect fluid with velocity field u_μ. With the `hi_class` normalization of densities the energy-momentum tensor takes on the form $T^m_{\mu\nu} = 3M_p^2\rho_m u_\mu u_\nu$.

Variation of the action Eq. (4.1) with respect to the Galileon field gives the field equation (see also Eq. (3.36)):

$$C_2\Box\phi + C_3\left((\Box\phi)^2 - R_{\mu\nu}\nabla^\mu\phi\nabla^\nu\phi - (\nabla_\mu\nabla_\nu\phi)\,(\nabla^\mu\nabla^\nu\phi)\right) = \frac{3\rho_m}{2(1+\phi)}. \tag{4.4}$$

Variation of the action with respect to the metric leads to the Einstein equations:

$$G_{\mu\nu} = M_p^{-2}\left(T^m_{\mu\nu} + T^\phi_{\mu\nu}\right) - \Lambda g_{\mu\nu}, \tag{4.5}$$

with the energy-momentum tensor of the Galileon field being:

$$\begin{aligned}\frac{T^\phi_{\mu\nu}}{M_p^2} &= C_2(\partial_\mu\phi)(\partial_\nu\phi) - \frac{C_2}{2}g_{\mu\nu}(\nabla\phi)^2 \\ &\quad + C_3\left((\partial_\mu\phi)(\partial_\nu\phi)\Box\phi - \nabla_{\{\mu}\phi\nabla_{\nu\}\alpha}\phi\nabla^\alpha\phi + g_{\mu\nu}\nabla^\alpha\phi\nabla_{\alpha\beta}\phi\nabla^\beta\phi\right).\end{aligned} \tag{4.6}$$

Furthermore, the Bianchi identities give rise to the conservation equations:

$$\nabla^\mu\left(T^m_{\mu\nu} + T^\phi_{\mu\nu}\right) = 0. \tag{4.7}$$

In order to demonstrate the shape dependence of the Vainshtein screening mech-

[4]To be precise, there still remains a small difference in signs and normalisations between our expressions and the calculations in Ref. [101]. Expressions in Ref. [101] can be used in our analysis when replacing $C_2 \to -C_2$ and $C_3/M^3 \to -C_3$

anism we examine Eq. (4.4) in the static and curvature free case and assume that $\phi \ll 1$:

$$C_2\Delta\phi + C_3\left((\Delta\phi)^2 - (\partial_i\partial_j\phi)(\partial^i\partial^j\phi)\right) = \frac{3\rho_m}{2}, \tag{4.8}$$

where Δ is the static spatial Laplacian. This equation can be solved for various different shapes of the source ρ_m, see Ref. [92]:

- **Planar Symmetry:** For simplicity, we assume here that the source has the constant density ρ_0 if $|z| \leq z_0$ and zero otherwise. Any other configuration with planar symmetry qualitatively has the same result. We consider the fifth force outside of the source and its relative strength with respect to the gravitational force $\vec{F}_G$:

$$\partial_z\phi = \frac{3\rho_0 z_0}{2C_2}, \qquad \Rightarrow \qquad \frac{|\vec{F}_5|}{|\vec{F}_G|} = \frac{M_p^2}{2C_2}. \tag{4.9}$$

  For any configuration with planar symmetry the non-linear (C_3) term in Eq. (4.8) vanishes completely, there is no screening and the relative strength of the fifth force with respect to the gravitational force is constant in space.

- **Cylindrical Symmetry:** We assume the source to have constant density ρ_0 inside the radius r_0 (radius being defined as $r^2 = x^2 + y^2$ here) and the density is zero otherwise:

$$\partial_r\phi = \frac{C_2 r}{2C_3}\left(\sqrt{1 + \frac{r_V^2}{r^2}} - 1\right) \qquad \text{with} \qquad r_V \coloneqq \sqrt{\frac{3r_0^2\rho_0 C_3}{C_2^2}}. \tag{4.10}$$

  r_V is called the Vainshtein radius and determines the scale below which the non-linear terms become important. Within the Vainshtein radius ($r_0 < r \ll r_V$):

$$\frac{|\vec{F}_5|}{|\vec{F}_G|} = \frac{M_p^2}{C_2}\frac{r}{r_V}. \tag{4.11}$$

  We see that the fifth force becomes weaker than the graviational force inside the Vainshtein radius and is thus screened.

- **Spherical Symmetry:** The source is defined in the same way as for the cylindrical case except now radii are defined by $r^2 = x^2+y^2+z^2$. Equivalently

to Eq. (3.38), we obtain:

$$\partial_r \phi = \frac{C_2 r}{4C_3}\left(\sqrt{1+\frac{r_V^3}{r^3}}-1\right) \qquad \text{with} \qquad r_V := \left(\frac{4r_0^3\rho_0 C_3}{C_2^2}\right)^{1/3}. \tag{4.12}$$

The relative strength of the fifth force inside the Vainshtein radius is now given by:

$$\frac{|\vec{F}_5|}{|\vec{F}_G|} = \frac{M_p^2}{C_2}\frac{r^{3/2}}{r_V^{3/2}}. \tag{4.13}$$

We observe that the fifth force is screened more effectively inside the Vainshtein radius than for the cylindrical case.

To summarize, the more evenly the Galileon field depends on the three directions of space, the larger is the non-linear term in Eq. (4.8) and the more effective is Vainshtein screening. All of the above mentioned source symmetries appear on cosmological scales as walls, filaments and halos. Therefore, we will search for this shape-dependent effect in the distribution of cosmic structure.

More specifically, the shape-dependent term in Eq. (4.8) is non-linear, so that its effects can only manifest at second or higher order in cosmological perturbation theory. We will therefore study the matter bispectrum, which is sensitive to both non-linearitLi:2013nuaies and shapes, due to its dependence on three wavevectors forming a closed triangle. Based on our observations of the shape dependence in real space, we expect the non-linearities to be largest for the equilateral configuration, which corresponds to the highest degree of symmetry, and to vanish for the flattened configuration, where all three sides of the triangle are parallel thus containing only one-dimensional information in Fourier space.

4.3. Cosmological Perturbation Theory in the Einstein Frame

In order to compute the bispectrum for our Galileon model, we have to perform a perturbative analysis up to second order in the matter density contrast. For this we start by analysing the background evolution and then proceed with a first and second order calculation. A similar analysis without an explicit coupling to matter was performed in Ref. [101]. For the rest of this Chapter we will set $M_p = 1$.

4.3.1. Background evolution

At the background level, the metric is given by the FLRW-metric, see Eq. (2.9), and the Einstein equations become the Friedmann equations, Eqs. (2.11) and (2.12):

$$\frac{\mathcal{H}^2}{a^2} = \rho_m + \rho_\phi + \frac{\Lambda_c}{3}, \tag{4.14}$$

$$\frac{1}{a^2}\left(\mathcal{H}^2 + 2\mathcal{H}'\right) = -p_\phi + \frac{\Lambda_c}{3}, \tag{4.15}$$

where the background Galileon density and pressure are defined by:

$$\rho_\phi = \frac{C_2}{6a^2}\phi'^2 - \frac{C_3}{a^4}\mathcal{H}\phi'^3, \tag{4.16}$$

$$p_\phi = \frac{C_2}{6a^2}\phi'^2 + \frac{C_3}{3a^4}\phi'^2\left(\phi'' - \mathcal{H}\phi'\right). \tag{4.17}$$

The background Galileon equation of motion takes on the form:

$$-\frac{C_2}{a^2}\left(\phi'' + 2\mathcal{H}\phi'\right) + \frac{3C_3}{a^4}\phi'\left(2\mathcal{H}\phi'' + \mathcal{H}'\phi'\right) = \frac{3\rho_m}{2(1+\phi)}. \tag{4.18}$$

Finally, the 0-component of the conservation equations becomes:

$$-\rho_m' - 3\mathcal{H}\rho_m + \frac{\rho_m\phi'}{2(1+\phi)} = 0. \tag{4.19}$$

4.3.2. Cosmological Vainshtein screening

Before we solve the Galileon field equation, Eq. (4.18), numerically with `hi_class`, we can obtain useful analytical understanding by applying the simplifying assumption $\phi \ll 1$ which is typically true if the Galileon density, Eq. (4.16), is subdominant on the background. This assumption enables us to approximate the continuity equation, Eq. (4.19), by $\rho_m' = -3\mathcal{H}\rho_m$ if we additionally assume $\phi' \sim \mathcal{H}\phi$. Both assumptions have been checked numerically for all the models we study in Section 4.4. Under these assumptions the continuity equation has the solution $\rho_m = \rho_{m,0}a^{-3}$. It is now straightforward to solve the Galileon equation of motion if $C_3 > 0$:

$$\phi_{1/2}' = \frac{C_2 a^2}{6C_3\mathcal{H}}\left(1 \pm \sqrt{1+\lambda_V(a)}\right), \quad \text{with} \quad \lambda_V(a) \coloneqq 18H\rho_m t\frac{C_3}{C_2^2}, \tag{4.20}$$

where t is the physical time. Variants of this solution, which assumed C_2 to be negligibly small, have already been derived in Refs. [100, 106]. By solving the equation of motion numerically using `hi_class` we found for all models studied in Section 4.4 that only the negative branch of the solution is stable on a cosmological background. This is analogous to the two branches of the DGP model, of which only the normal branch is stable, see Ref. [79].

The solution in Eq. (4.20) is called the cosmological Vainshtein solution, because it exhibits a time-like Vainshtein screening effect. The function λ_V measures the magnitude of the non-linear terms in the equation of motion against the linear terms and is the time-like equivalent of $(r_V/r)^3$ in the spatial solution around a spherical source, see Eq. (4.12). We will show in the next Section that the linearised fifth force will be screened at early times where $\lambda_V \gg 1$ compared to a situation where $\lambda_V \ll 1$.

4.3.3. Linear Perturbation Theory

We now look at scalar linear perturbations in the cosmic fluid. Similar to our approach to structure formation in general relativity, see Section 2.3, we choose Newtonian gauge:

$$\mathrm{d}s^2 = a^2 \left[-(1+2\Psi)\mathrm{d}\tau^2 + (1-2\Phi)\delta_{ij}\mathrm{d}x^i\mathrm{d}x^j\right]. \tag{4.21}$$

In addition to the perturbative quantities (δ, v, v^0, Φ and Ψ) in the general relativistic case, see Eq. (2.20), we now have to consider the perturbed Galileon field, which we write as $\phi + \delta\phi$, where ϕ is the background field and $\delta\phi = \phi^{(1)} + \phi^{(2)}/2 + \ldots$ is the perturbative variable in terms of the first and second-order perturbations. The Galileon, Einstein and Conservation equations, Eqs. (4.4), (4.5) and (4.7), expanded at linear order are listed in Appendix A.1.1. Analogous to our calculation in Section 2.3 we combine these equations using the quasi-static approximation, which is valid on subhorizon modes ($\mathcal{H}^2 \ll k^2$)[5]. We arrive at a second-order differential equation for the density contrast (compare to Eq. (2.27)

[5]The validity of the quasi-static approximation has been demonstrated for theories with Vainshtein screening in Ref. [107]

for the general relativistic analogue):

$$\delta^{(1)\prime\prime} + \left(\mathcal{H} + \frac{\phi'}{2(1+\phi)}\right)\delta^{(1)\prime} = \alpha_\delta(\tau)\delta^{(1)}, \tag{4.22}$$

where

$$\alpha_\delta \;\coloneqq\; \frac{3a^2\bar{\rho}}{2}\left[1 + \frac{\alpha_\phi^2}{2A(\tau)}\right], \quad \alpha_\phi \coloneqq \frac{1}{1+\phi} + \frac{C_3\phi'^2}{a^2}, \tag{4.23}$$

$$A(\tau) \;\coloneqq\; C_2 - \frac{2C_3}{a^2}(\phi'' + \mathcal{H}\phi') - \frac{C_3^2\phi'^4}{2a^4}. \tag{4.24}$$

In the square brackets, the gravitational force of strength one ($M_p^{-2} = 1$) is accompanied by a fifth force of strength $\alpha_\phi^2/(2A)$. The first term in α_ϕ reflects the conformal coupling between matter and the Galileon field, and the second term is a consequence of kinetic braiding, i.e. the indirect coupling of the scalar field to matter through the metric.

Inserting the cosmological Vainshtein solution of Eq. (4.20) into the expression for $A(\tau)$ enables us to observe the cosmological screening of the linearised fifth force. Assuming matter domination for simplicity (radiation domination just gives different numerical factors), $A(\tau) \approx C_2(1 + \lambda_V(a)/3) \approx C_2$ if $\lambda_V(a) \ll 1$, and $A \approx C_2(1 + 2\sqrt{\lambda_V}/3) \approx 2C_2\sqrt{\lambda_V}/3$ if $\lambda_V \gg 1$. Similarly, we obtain $\alpha_\phi \sim 1$, and thus, the strength of the fifth force relative to gravity is given by A^{-1}. We conclude that for $\lambda_V \ll 1$ the fifth force is unscreened with strength $\sim C_2^{-1}$ relative to the gravitational force and for $\lambda_V \gg 1$ the fifth force is suppressed with relative strength $(C_2\sqrt{\lambda_V})^{-1}$.

4.3.4. Breakdown of Perturbation Theory

In general relativity, cosmological perturbation theory is restricted to scales that obey $\delta \ll 1$, see also the discussion around Eq. (2.42). Below the non-linearity scale, the hierarchy between background, linear and non-linear terms in the Continuity and Euler equations breaks down. Similarly, for the background Galileon equation of motion, Eq. (4.18), we had to assume $|\Box\delta\phi(\tau,\vec{x})| \ll |\Box\phi(\tau)|$, i.e. we neglected second derivatives of the Galileon field perturbation $\delta\phi$ compared to second derivatives of the background field ϕ. This means that there is a second non-linearity scale in our system, the scale where $|\Box\delta\phi(\tau,\vec{x})| \sim |\Box\phi(\tau)|$. Our perturbative analysis breaks down on smaller scales.

The same assumption had to be made when we derived the linearised Galileon equation of motion, Eq. (A.5). We assumed that terms non-linear in $\delta\phi$, like $C_3(\Box\delta\phi)^2$, are small compared to the term $(C_2 + C_3\Box\phi)\Box\delta\phi$, which is linear in $\delta\phi$.[6] This makes the connection between this new non-linearity scale and the Vainshtein radius clear as both indicate the scale at which the non-linearities of the spatially dependent Galileon field become relevant in the equation of motion.

If this new non-linearity scale is larger than the standard non-linearity scale defined by $\delta \sim 1$, our analysis is even more restricted than a conventional perturbative analysis without the Galileon field. Therefore, it is important to check how the assumption

$$\left|\frac{\Box\delta\phi(\tau,\vec{x})}{\Box\phi(\tau)}\right| \ll 1 \tag{4.25}$$

compares to the assumption $\delta \ll 1$.

The Galileon field perturbation $\delta\phi$ on the left-hand side of Eq. (4.25) is in principle given by the full series $\delta\phi = \sum_{n=1}^{\infty}\phi^{(n)}/n!$ making the expression a non-perturbative statement about the perturbativity of the system. However, this makes it unfeasible to check the condition in practice. We therefore assume in the following that the order of magnitude of the non-linearity scale can be estimated if we simplify $\delta\phi \approx \phi^{(1)}$. This simplification is true on all scales up to the non-linearity scale, so the estimate for the non-linearity scale obtained in this way should be of the correct order of magnitude. Furthermore, we assume that the quasi-static approximation is valid, i.e. we can neglect the time derivatives in $\Box\delta\phi$ compared to the spatial derivatives. This assumption is valid as long as the non-linearity scale is a sub-horizon scale.

With these assumptions the ratio on the left-hand side of Eq. (4.25) is given by:

$$\frac{\Delta\phi^{(1)}}{(\phi'' + 2\mathcal{H}\phi')} = \frac{3\bar{\rho}\alpha_\phi a^2}{2A(\tau)(\phi'' + 2\mathcal{H}\phi')}\delta^{(1)}. \tag{4.26}$$

We used in the first step that, on a linear level, the Einstein and Galileon field equations, Eqs. (A.3) and (A.5), can be combined to:

$$\Delta\phi^{(1)} = \frac{3\bar{\rho}\alpha_\phi}{2A(\tau)}\delta^{(1)}. \tag{4.27}$$

[6] For simplicity, we ignore C_2 compared to $C_3\Box\phi$ in the following. This is consistent with our goal to study meaningful cubic galileon models, i.e. models where the galileon term dominates over the standard kinetic term.

We define the quantity:

$$\lambda(\tau) := \left| \frac{2A(\tau)(\phi'' + 2\mathcal{H}\phi')}{3\bar{\rho}\alpha_\phi a^2} \right|. \tag{4.28}$$

As long as $\lambda \gtrsim 1$ the assumption in Eq. (4.25) is fulfilled automatically if $\delta \ll 1$. Thus, the new non-linearity scale leads to no additional restrictions of the perturbative analysis beyond the requirement $\delta \ll 1$.

We will check the condition $\lambda \gtrsim 1$ for every model we study in Section 4.4 and plot the quantity λ as a function of time in Figure 4.2. In a simplified, analytically tractable setting, where we assume matter domination together with $C_2 = 0$, we find $\lambda \equiv 2$, i.e. the two non-linearity scales are of the same order of magnitude. What appears to be a coincidence at first sight is actually a consequence of the particular Galileon model we chose. The conformal coupling of the Galileon field with matter causes the background equation of motion to require $C_3(\Box\phi)^2 \sim \bar{\rho}$ and the linear equation to enforce $C_3\Box\phi\Box\delta\phi \sim \bar{\rho}\delta$. Combining these two scaling relations, results in $\left|\frac{\Box\delta\phi(\tau,\vec{x})}{\Box\phi(\tau)}\right| \sim \delta$. Since it is not trivial that the two non-linearity scales will be equivalent for any Vainshtein screening model, we propose that the condition in Eq. (4.25) should be checked for any perturbative study of Vainshtein screening.

4.3.5. Second-Order Perturbation Theory

In order to compute the matter bispectrum we have to proceed to second order in perturbation theory as prescribed in Section 2.3. This enables us to capture the onset of non-linear dynamics and the Vainshtein screening mechanism. Computing the Galileon, Einstein and Conservation equations, Eqs. (4.4), (4.5), (4.7), at second order and combining them appropriately, results in the inhomogeneous equation:

$$\delta^{(2)\prime\prime} + \left(\mathcal{H} + \frac{\phi'}{2(1+\phi)}\right)\delta^{(2)\prime} = \alpha_\delta(\tau)\delta^{(2)} + S^{(\delta)}, \tag{4.29}$$

where the inhomogeneity $S^{(\delta)}$ captures the non-linear physics. Compared to the non-linearities in pure GR, see Eq. (2.34), $S^{(\delta)}$ now includes additional terms from the Galileon field. In A.1.2 we state the source function $S^{(\delta)}$ in terms of the source functions $S^{(1)}$, $S^{(4)}$, $S^{(5)}$, $S^{(6)}$ and $S^{(7)}$ which were defined in the Appendix of

Ref. [101] and are sufficiently long that we don't reproduce them here. However, we would like to point out the appearance of one crucial term, which was also found in Ref. [102]:

$$S^{(\delta)} \supset -\frac{C_3\alpha_\phi}{a^2A(\tau)}\left[\left(\Delta\phi^{(1)}\right)^2 - \left(\partial_i\partial_j\phi^{(1)}\right)\left(\partial^i\partial^j\phi^{(1)}\right)\right]. \tag{4.30}$$

This term has the same structure as the non-linear part of Eq. (4.8) and thus encodes the shape dependence of the Vainshtein screening mechanism.

The kernel $\mathcal{K}$ of the inhomogeneity $S^{(\delta)}$ as defined in Eq. (2.34) is now given by:

$$\begin{aligned}\mathcal{K}(a,\vec{k}_1,\vec{k}_2) &= 2\left(\mathcal{H}^2f^2(\tau)+\alpha_\delta(\tau)\right)\alpha(\vec{k}_1,\vec{k}_2) + 2\beta(\vec{k}_1,\vec{k}_2)\mathcal{H}^2f^2(\tau) \\ &\quad -\frac{9C_3\bar{\rho}^2a^2\alpha_\phi^3}{4A^3(\tau)}\gamma(\vec{k}_1,\vec{k}_2)\end{aligned} \tag{4.31}$$

Compared to the pure GR kernel in Eq. (2.35), we introduced an extra form factor

$$\gamma(\vec{k}_1,\vec{k}_2) \coloneqq 1 - \frac{(\vec{k}_1\cdot\vec{k}_2)^2}{k_1^2k_2^2}. \tag{4.32}$$

The additional form factor γ originates directly as a Fourier transform of the non-linear term in Eq. (4.30) and reflects very intuitively the shape dependence of Vainshtein screening. If the modes $\vec{k}_1$ and $\vec{k}_2$ are parallel, the term vanishes and no screening can occur. $\vec{k}_1$ and $\vec{k}_2$ being parallel means that we only capture one-dimensional information which is equivalent to a situation in real space with planar symmetry where, similarly no screening occurs, compare with Eq. (4.9). The appearance of γ in Horndeski theories was already noted in Refs. [102, 105] and earlier for DGP gravity in Ref. [108], but without making the connection to the shape dependence of Vainshtein screening.

In order to solve the inhomogeneous differential equation for $\delta^{(2)}$, Eq. (4.29), we make the same ansatz for $\delta^{(2)}$ as in the pure GR case, see Eq. (2.36):

$$\delta^{(2)}(\tau,\vec{k}) = \int \mathrm{d}^3k_1\mathrm{d}^3k_2\,\delta(\vec{k}-\vec{k}_1-\vec{k}_2)\,F_2(\tau,\vec{k}_1,\vec{k}_2)\,\delta^{(1)}(\tau,\vec{k}_1)\,\delta^{(1)}(\tau,\vec{k}_2). \tag{4.33}$$

We adopt the technique used in Ref. [101] to solve Eq. (4.29) with Green's method:

$$F_2(\tau,\vec{k}_1,\vec{k}_2) = \int_{\tau_i}^{\tau}\mathrm{d}\tilde{\tau}\,G(\tau,\tilde{\tau})\,\mathcal{K}(\tilde{\tau},\vec{k}_1,\vec{k}_2)\frac{D_+^2(\tilde{\tau})}{D_+^2(\tau)}. \tag{4.34}$$

The Green's function G is defined by:

$$G(\tau, \tilde{\tau}) \coloneqq \frac{D_1(\tau)D_2(\tilde{\tau}) - D_2(\tau)D_1(\tilde{\tau})}{W(\tilde{\tau})}\Theta(\tau - \tilde{\tau}), \tag{4.35}$$

with the Wronskian W:

$$W(\tau) \coloneqq D_1'(\tau)D_2(\tau) - D_2'(\tau)D_1(\tau). \tag{4.36}$$

The functions D_1 and D_2 are two independent solutions of the linear growth equation, Eq. (4.22). In our numerical analysis in Section 4.4.2 we will associate D_1 and D_2 with the growing and decaying modes D_+ and D_-.

Using the kernel in Eq. (4.31), F_2 can be cast into the form:

$$F_2(\tau, \vec{k}_1, \vec{k}_2) = \mathcal{A}_{GR}(\tau)\alpha(\vec{k}_1, \vec{k}_2) + \mathcal{B}_{GR}(\tau)\,\beta(\vec{k}_1, \vec{k}_2) + \mathcal{B}_{\phi}(\tau)\,\gamma(\vec{k}_1, \vec{k}_2). \tag{4.37}$$

The time dependent functions $\mathcal{A}_{GR}$, $\mathcal{B}_{GR}$ and $\mathcal{B}_{\phi}$ are defined in Appendix A.1.1. While the functions $\mathcal{A}_{GR}$ and $\mathcal{B}_{GR}$ always appear in general relativity, $\mathcal{B}_{\phi}$ is a purely Galileon contribution describing the shape-dependent non-linearities in the Galileon equation of motion. We demonstrate in Appendix A.1.3 that there is a relation between $\mathcal{A}_{GR}$ and $\mathcal{B}_{GR}$:[7]

$$\mathcal{A}_{GR}(\tau) = 2 - \mathcal{B}_{GR}(\tau). \tag{4.38}$$

Defining μ as the cosine of the angle between $\vec{k}_1$ and $\vec{k}_2$, we thus conclude:

$$F_2(\tau, \vec{k}_1, \vec{k}_2) = 2 + \frac{\mu}{k_1 k_2}\left(k_1^2 + k_2^2\right) - \mathcal{B}(\tau)\left(1 - \mu^2\right), \tag{4.39}$$

where

$$\mathcal{B}(\tau) \coloneqq \mathcal{B}_{GR}(\tau) - \mathcal{B}_{\phi}(\tau). \tag{4.40}$$

We observe that the contribution from GR described by $\mathcal{B}_{GR}$ has the same shape-dependence as the Vainshtein screening contribution, $\mathcal{B}_{\phi}$, since both multiply $(1 - \mu^2)$ in Eq. (4.39). The origin of this shape-dependence in GR may be traced back to the kernel of the displacement field in second-order Lagrangian perturbation theory, which is proportional to $(1 - \mu^2)$, see Ref. [109].[8]

[7] We thank Emilio Bellini for pointing out this relation to us.

[8] Since first-order Lagrangian perturbation theory is exact in one dimension, second-order per-

The bispectrum and the reduced bispectrum may now be computed by means of Eqs. (2.46) and (2.47) respectively. The form factor F_2 appears in three copies in the bispectrum: $F_2(\vec{k}_1, \vec{k}_2)$, $F_2(\vec{k}_1, \vec{k}_3)$ and $F_2(\vec{k}_2, \vec{k}_3)$. The contribution from Vainshtein screening to the form factor F_2, i.e. the term $\mathcal{B}_\phi(\tau)(1-\mu^2)$, vanishes for parallel wavevectors ($\mu = 1$). Thus, in the case of the flattened limit, where all the three wavevectors are approximately parallel, the contribution from Vainshtein screening to the bispectrum vanishes completely. In this case, the real-space, plane-wave density perturbations associated with these three wavevectors will only depend on one direction of space which is equivalent to the planar symmetry discussed in Section 4.2, where no Vainshtein screening occurred. The vanishing of the contributions from Vainshtein screening to the bispectrum thus coincides with our expectations.

The signal imprinted by Vainshtein screening on the bispectrum vanishes where the fifth force is unscreened and is maximum where the screening is also largest. This is because stronger screening requires larger non-linearities, which are detected by the bispectrum. A situation of no screening corresponds to no additional non-linearities.

It is possible to compute the function $\mathcal{B}_\phi$ analytically in a simplified setting. For this purpose we assume matter domination together with $C_2 = 0$ for the rest of this section. During matter domination, $D_+ \propto a$ and $D_- \propto a^{-3/2}$ with $a = \rho_{m,0}\tau^2/4$, so the Green's function takes on the form:

$$G(\tau, \tilde{\tau}) = \frac{1}{5}\left(\frac{\tau^2}{\tilde{\tau}} - \frac{\tilde{\tau}^4}{\tau^3}\right). \tag{4.41}$$

The negative (stable) branch of the solution to the Galileon field equation, Eq. (4.20), becomes (assuming the initial conditions $\phi = \phi' = 0$ at $\tau = 0$):

$$\phi' = -\sqrt{\frac{\rho_{m,0}t}{2C_3\mathcal{H}}} = -\frac{a}{\sqrt{3C_3}} \quad \Rightarrow \quad \phi = \frac{2\phi'}{3\mathcal{H}} \quad \text{and} \quad \phi'' = \mathcal{H}\phi'. \tag{4.42}$$

This enables us to compute:

$$\alpha_\phi = \frac{4}{3}, \qquad A(\tau) = -\frac{8}{9\phi} - \frac{1}{18} \approx -\frac{8}{9\phi}, \tag{4.43}$$

turbations only exist for higher-dimensional systems. This is equivalent to the Vainshtein case where non-linearities require systems of dimension two or higher.

where we assumed $\phi \ll 1$. Using Eq. (4.16) we find $\rho_\phi/\rho_m = -\phi/2$ and we conclude:

$$-\frac{9C_3\bar{\rho}^2a^2\alpha_\phi^3}{4A^3(\tau)} = \frac{9}{8}\mathcal{H}^2\phi = -\frac{9}{4}\mathcal{H}^2\frac{\rho_\phi}{\rho_m}. \tag{4.44}$$

Finally, we can integrate for $\mathcal{B}_\phi$:

$$\mathcal{B}_\phi = -\int_{\tau_i}^{\tau} \mathrm{d}\tilde{\tau}\, G(\tau,\tilde{\tau})\frac{9C_3\bar{\rho}^2a^2\alpha_\phi^3}{4A^3(\tau)}\frac{D_+^2(\tilde{\tau})}{D_+^2(\tau)} = -\frac{9}{50}\frac{\rho_\phi}{\rho_m}. \tag{4.45}$$

The fraction ρ_ϕ/ρ_m is small due to the assumption of matter domination. During matter domination, $\mathcal{B}_{GR}$ has the standard value of 4/7, see e.g. Ref. [110], and will thus be significantly larger than $\mathcal{B}_\phi$. In the presence of the Galileon field $\mathcal{B}_{GR}$ receives small corrections relative to its GR value 4/7 due to the impact of the Galileon field on the background evolution. These corrections are difficult to compute analytically but will be studied numerically in Section 4.4.3 and turn out to be small compared to $\mathcal{B}_\phi$, see Figure 4.6.

Summarising, we saw that the contribution $\mathcal{B}_\phi$ to the bispectrum from Vainshtein screening is degenerate with the GR term $\mathcal{B}_{GR}$, see Eq. (4.40). However, in contrast to the GR term, which is constant during matter domination, it evolves in time $\propto \frac{\rho_\phi}{\rho_m}$, which might help break the degeneracy.

4.4. Numerical analysis with `hi_class`

In order to back up our analytic approximation in Eq. (4.45), and to generalise it beyond matter domination, we will evaluate the functions $\mathcal{B}_{GR}$ and $\mathcal{B}_\phi$ with `hi_class`[9], a Boltzmann solver for Horndeski-type models based on CLASS, see Refs. [111–113]. While previous public versions of `hi_class`, see Ref. [112], required one to parameterise the time evolution of the Horndeski α functions[10] in order to fully evolve the system, the latest version of the code, see Ref. [113], is able to integrate the full equation of motion of any Horndeski theory, including the Galileon.

Since `hi_class` works in the Jordan frame, we have to transform our Einstein-frame action, Eq. (4.1), into the Jordan frame. As declared at the end of Section

[9] www.hiclass-code.net

[10] The α functions are a set of four functions $\alpha_M(a)$, $\alpha_K(a)$, $\alpha_B(a)$ and $\alpha_T(a)$, which fully describe the evolution of linear perturbations in any Horndeski theory, see Ref. [114].

3.3 we have dropped the tildes on Einstein-frame quantities so far, however, we will briefly reinstate them here for clarity. We apply the conformal transformation

$$\tilde{g}_{\mu\nu} \to g_{\mu\nu} = \Omega^{-2}\tilde{g}_{\mu\nu}, \quad \text{where} \quad \Omega^{-2} \coloneqq 1 + \phi. \tag{4.46}$$

This transformation brings our model into the Jordan frame and allows it to be formulated in terms of the Jordan-frame Horndeski functions $G_i(\phi, X)$ as defined in Eq. (3.1). The form of the Horndeski functions for our model is shown in Appendix A.1.1.

When working with both the Jordan and Einstein frame, one has to make sure to correctly connect between physical quantities in both frames. More specifically, we have to consider the density contrast in Einstein ($\tilde{\delta}$) and Jordan (δ) frame which are related by:

$$\delta^{(1)} = \tilde{\delta}^{(1)} - 2\frac{\phi^{(1)}}{1+\phi}. \tag{4.47}$$

Using Eq. (4.27), we can show that:

$$\delta^{(1)} - \tilde{\delta}^{(1)} = -2\frac{\phi^{(1)}}{1+\phi} \sim \frac{\mathcal{H}^2}{k^2}\tilde{\delta}^{(1)}. \tag{4.48}$$

Therefore, on subhorizon scales the density contrast becomes approximately the same in both frames, see also Refs. [115, 116]. As we are only interested in the subhorizon scales where non-linear dynamics become important, the density contrast is effectively invariant under the conformal transformation and so is the matter bispectrum.

Other quantities like the conformal Hubble function $\mathcal{H}$, the matter density ρ_m, the scale factor a, have to be transformed carefully under the conformal transformation. A summary of these transformations is given in Appendix A.1.1.

4.4.1. Background evolution

We now analyse the background evolution of the Universe in our Galileon model numerically using `hi_class`.

There is a subtlety with regards to the Galileon density ρ_ϕ when working in the Jordan frame, because the structure of the Friedmann equation (4.14) changes

significantly. In the Jordan frame we have:

$$\frac{1}{a^2(1+\phi)}\left(\mathcal{H}^2 - \frac{\mathcal{H}\phi'}{1+\phi} + \frac{\phi'^2}{4(1+\phi)^2}\right) = \frac{1}{1+\phi}\frac{C_2\phi'^2}{6a^2} + \frac{C_3\phi'^3}{a^4}\left(\mathcal{H} - \frac{\phi'}{2(1+\phi)}\right) + \rho_m + \frac{\Lambda}{3(1+\phi)^2}. \quad (4.49)$$

This equation can be cast into the traditional form of a Friedmann equation, which is assumed by `hi_class`, by defining an effective Galileon energy density:

$$\frac{\mathcal{H}^2}{a^2} = \rho_m + \rho_{\phi,\text{eff}} + \frac{\Lambda}{3}, \quad (4.50)$$

where

$$\rho_{\phi,\text{eff}} \coloneqq \frac{1}{1+\phi}\frac{C_2\phi'^2}{6a^2} + \frac{C_3\phi'^3}{a^4}\left(\mathcal{H} - \frac{\phi'}{2(1+\phi)}\right) + \frac{1}{a^2(1+\phi)}\left(\mathcal{H}^2\phi + \frac{\mathcal{H}\phi'}{1+\phi} - \frac{\phi'^2}{4(1+\phi)^2} - \Lambda\frac{2\phi+\phi^2}{3(1+\phi)}\right). \quad (4.51)$$

This effective Galileon density measures all deviations from a ΛCDM cosmology at the background level. Similarly, an effective Galileon pressure $p_{\phi,\text{eff}}$ can be defined.

The `hi_class` code checks for instabilities of the background by calculating the sign of the kinetic term and the sound speed of the scalar field. For all our models it turns out that stability is guaranteed if the Galileon field is negative, i.e. the negative branch of the two solutions in Eq. (4.20) is chosen. As a consequence, $\rho_{\phi,\text{eff}}$ turns out to be negative as well. However, this is not indicating that the model is pathological since the physical Galileon density, i.e. Eq. (4.16), or in terms of Jordan-frame quantities, the first line of Eq. (4.51), will always be positive.

In this analysis we will restrict ourselves to models, where $\Omega_{\phi,\text{eff}} \coloneqq \rho_{\phi,\text{eff}}/\rho_{\text{crit}}$ is small and the background evolution is at least roughly inside of current observational limits. Since the main goal of this analysis is to get a qualitative understanding of the shape-dependence effect, we postpone a thorough data analysis to future works.

We construct our background models with `hi_class` in the following way: Our Galileon model has two free parameters, C_2 and C_3. Since we are mostly interested in the effect of shape dependence which is proportional to C_3, we consider C_2 to be either zero or subdominant on the background level. Thus, the value of $\Omega_{\phi,\text{eff},0}$

Model name	$\Omega_{\phi,\mathrm{eff},0}$	C_3 [Mpc^2]	C_2
Gal 1	-0.01	4.276×10^9	0
Gal 2	-0.02	1.063×10^9	0
Gal 3	-0.03	4.699×10^8	0
Gal 4	-0.01	6.127×10^9	-5.925
Gal 5	-0.01	1.918×10^9	5.925
ΛCDM	0	0	0

Table 4.1.: Definition of the Galileon models we use. The value of C_3 is obtained by means of a shooting algorithm in order to match the required $\Omega_{\phi,\mathrm{eff},0}$. The models Gal 1-3 test the effects of $\Omega_{\phi,\mathrm{eff},0}$, and Gal 4 and Gal 5 enable us to study the influences of C_2 while keeping $\Omega_{\phi,\mathrm{eff},0}$ constant.

depends mostly on C_3. When we give `hi_class` a target value for $\Omega_{\phi,\mathrm{eff},0}$ as input, the code performs a shooting algorithm that fits the value of C_3 corresponding to the given $\Omega_{\phi,\mathrm{eff},0}$. The parameter of Ω_Λ will always be used to fulfil the closure condition $1 = \sum_i \Omega_{i,0}$. This also ensures that the sum of the energy densities driving the late time acceleration of the Universe $\Omega_{DE} \coloneqq \Omega_\Lambda + \Omega_{\phi,\mathrm{eff}}$ will be identical to Ω_Λ in a purely ΛCDM model.

The Galileon models that we use throughout this work, labelled Gal 1-5, are defined in Table 4.1. The models Gal 1-3 enable us to study the effects of increasing $\Omega_{\phi,\mathrm{eff},0}$, whereas the models Gal 4 and Gal 5 test the influences of the parameter C_2 while keeping $\Omega_{\phi,\mathrm{eff},0}$ constant. We compare these models to ΛCDM, which corresponds to vanishing $\Omega_{\phi,\mathrm{eff},0}$ achieved by the limit $C_2 \to 0$, $C_3 \to \infty$. Although `hi_class` checks the stability of the considered models on the cosmological background, it is not guaranteed that these models will be stable on any background. However, for the sake of studying phenomenological aspects of Vainshtein screening, only stability on a cosmological background is paramount.

In order to check how much the inclusion of the Galileon field affects the background evolution, we consider an effective equation of state parameter w_{eff} defined as:

$$w_{\mathrm{eff}} \coloneqq \frac{p_\Lambda + p_{\phi,\mathrm{eff}}}{\rho_\Lambda + \rho_{\phi,\mathrm{eff}}}, \tag{4.52}$$

i.e. the equation of state parameter of all the energy components driving the late time acceleration of the Universe. The deviations of this quantity from -1 are

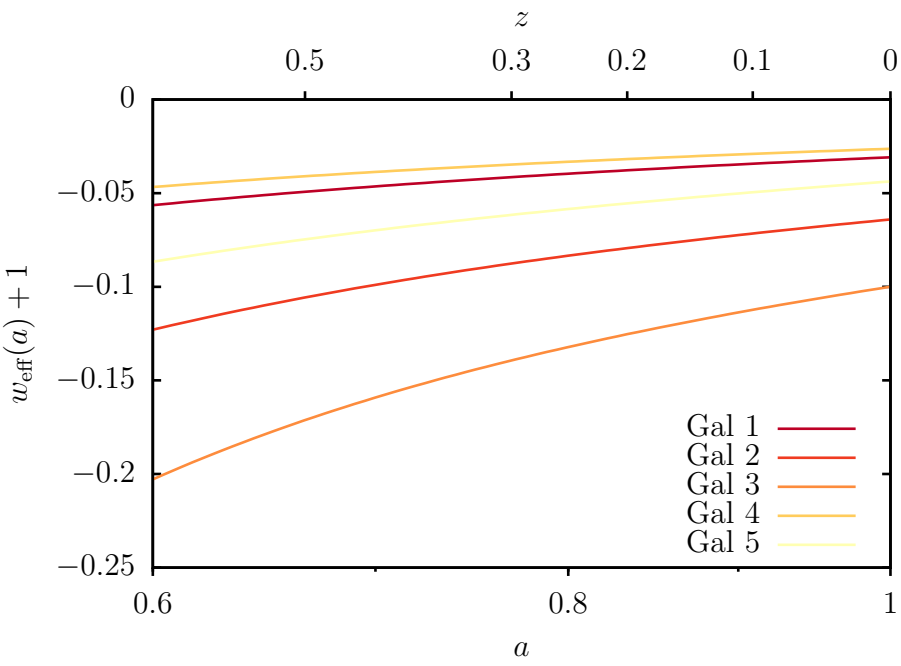

Figure 4.1.: Deviations from -1 of the effective equation of state parameter $w_{\rm eff}$ of the energy components driving the late-time acceleration of the Universe as a function of scale factor and redshift for the models Gal 1-5 defined in Table 4.1. The dark energy density becomes dominant over the matter density at $z \approx 0.33$.

plotted in Figure 4.1. The value of $w_{\rm eff}$ is always smaller than -1 but tends towards -1 at late times. Deviations from -1 become large at early times, but dark energy only becomes dominant over the matter density at $z \approx 0.33$ for all considered models. As already mentioned in Chapter 2.5, current bounds on the equation of state parameter of dark energy from the DES [41] indicate the values $w_p = -1.01^{+0.04}_{-0.04}$ and $w_a = -0.28^{+0.37}_{-0.48}$ for a parametrisation $w = w_p + w_a\,(a_p - a)$ with the pivot redshift $z_p = 1/a_p - 1 = 0.2$.

Before we compute the first and second order perturbations, we have to check the condition in Eq. (4.25) for perturbativity of the Galileon equation of motion as outlined in Section 4.3.4. For this we plot the quantity λ defined by Eq. (4.28) as a function of time in Figure 4.2. We find that the condition $\lambda \gtrsim 1$ is satisfied for all the considered models and for the entire evolution of the Universe, confirming the validity of our perturbative analysis. Figure 4.2 confirms our analytic prediction that $\lambda = 2$ during matter domination. However, we also observe that λ decreases

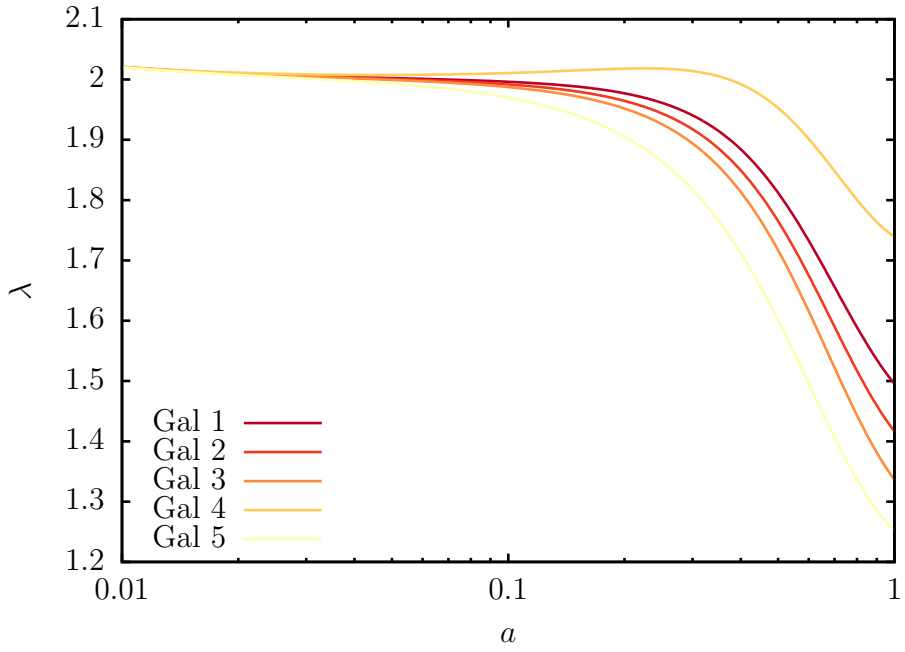

Figure 4.2.: The quantity λ defined in Eq. (4.28) describing the relative size of the non-linearity scales of standard perturbation theory with respect to the cubic Galileon is plotted for the models Gal 1-5 defined in Table 4.1. If this quantity is larger than 1, perturbativity of the cubic Galileon is assured as long as the standard condtion $\delta^{(1)} \ll 1$ is fulfilled. Although this is fulfilled for all the models studied in this work, it is not a trivial test and should be done for all future perturbative analyses of theories with Vainshtein screening.

over time in the late Universe, suggesting that perturbativity of the Galileon equation might be more restricted for a de-Sitter Universe. In particular, the value of C_2 appears to have significant impact on the late behaviour of λ. This indicates that the validity of perturbation theory in Vainshtein screened theories is not trivial and we would like to emphasise the importance of testing the validity of perturbation theory for any theory with Vainshtein screening.

4.4.2. Linear growth

In this section we compute the linear growth rate numerically. In order to obtain the Green's function in Eq. (4.35), we need two independent solutions of the linear growth equation, Eq. (4.22) – let them be D_1 and D_2. To obtain them numerically,

we solve Eq. (4.22) for two different initial conditions. To establish an approximate connection between the solution D_1 and the growing mode and solution D_2 and the decaying mode, respectively, we set the initial conditions to be the solutions of the Meszaros equation, see Ref. [117, 118], valid during radiation and matter domination:

$$\begin{aligned} D_1(a_i) &= 2 + 3y_i \\ D_2(a_i) &= (4 + 6y_i) \coth^{-1}\left(\sqrt{1+y_i}\right) - 6\sqrt{1+y_i}, \end{aligned} \tag{4.53}$$

where $y \coloneqq a/a_{eq}$ is the scale factor relative to the scale factor at radiation-matter equality a_{eq}. The thereby obtained solutions $D_1(a)$ and $D_2(a)$ are afterwards normalized such that $D_1(a = 1) = 1$.

As an example we show the results of the integration for the model Gal 1 in Figure 4.3. Since we ignore the presence of a cosmological constant and the Galileon field when setting the initial conditions in the early Universe, D_2 deviates slightly from the true decaying mode at late times. This small deviation is not a concern for the purposes of this work as all we need is the growing mode and another independent solution.

In order to quantify the linear growth in our models we consider the growth rate f. In Figure 4.4 we present deviations of f from the ΛCDM result $f_{\Lambda\mathrm{CDM}}$. We see that deviations do not exceed 5 % and that the growth rate is enhanced due to the presence of a fifth force. This is roughly within current observational bounds, which indicate order 10 % relative uncertainties for $f\sigma_8$ assuming a ΛCDM cosmology, where σ_8 is the amplitude of the power spectrum. See Ref. [119] for a compendium on past constraints on $f\sigma_8$ and Refs. [120–125] for some recent developments.

4.4.3. The matter bispectrum

We can now integrate the functions $\mathcal{B}_{GR}$ and $\mathcal{B}_\phi$ in Eq. (A.7) and Eq. (A.8), where we recall (compare Eqs. (4.39) and (4.40)) that $\mathcal{B}_\phi$ and $\mathcal{B}_{GR}$ describe the contributions to the bispectrum proportional to $(1-\mu^2)$ originating from the shape dependence of Vainshtein screening, $\mathcal{B}_\phi$, and from the non-linearities coming from the continuity and Euler equations, which are also present for a ΛCDM cosmology with standard GR, i.e. $\mathcal{B}_{GR}$.

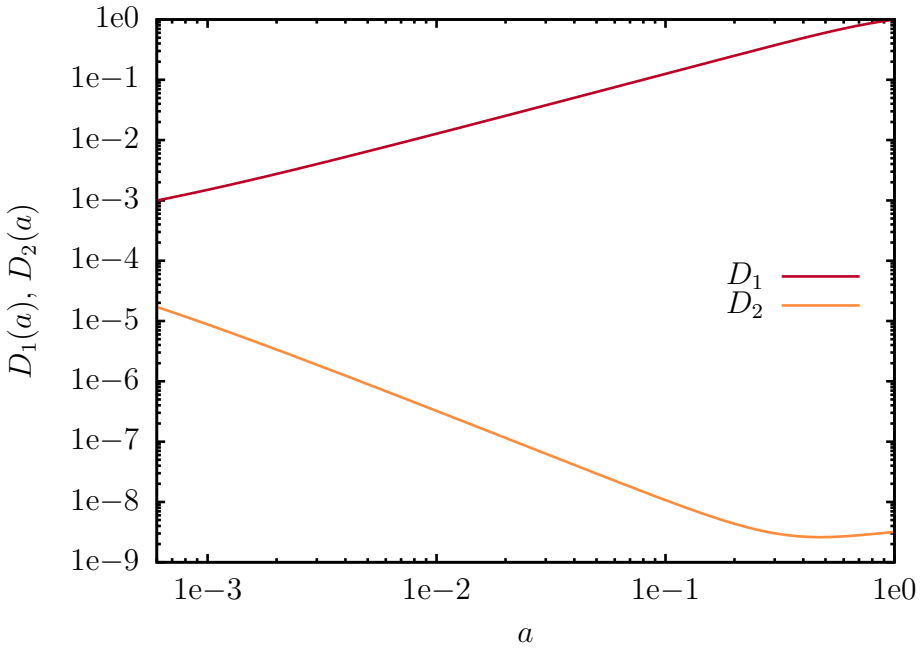

Figure 4.3.: The two independent solutions D_1 and D_2 for the model Gal 1 as a function of the scale factor. The solution D_1 is equivalent to the growing mode and the solution D_2 can roughly be associated with the decaying mode. The solutions are normalised such that $D_1(a = 1) = 1$.

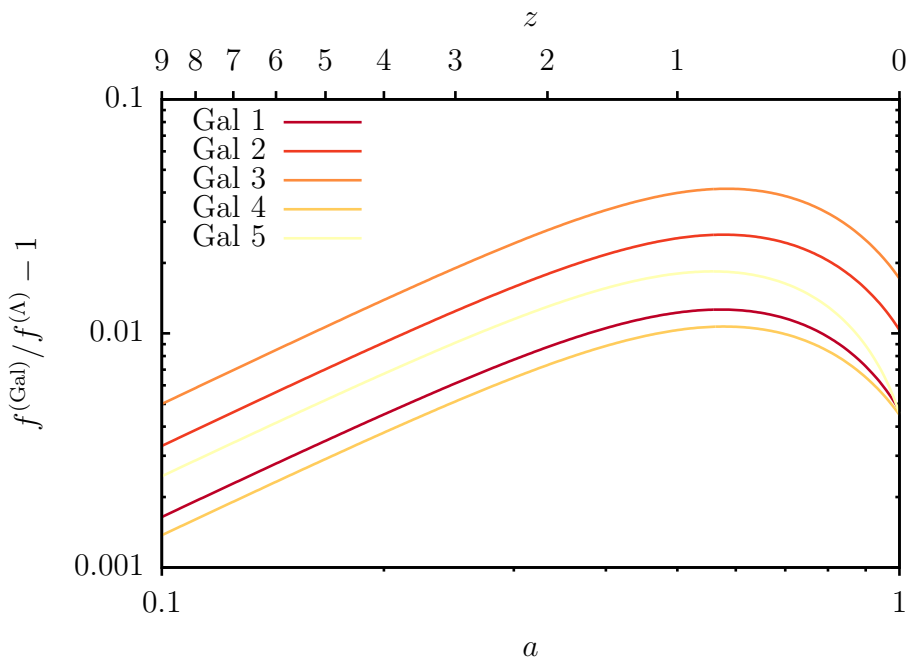

Figure 4.4.: The deviations of the linear growth rate f from the ΛCDM growth rate for the models Gal 1-5 defined in Table 4.1 as a function of scale factor and redshift.

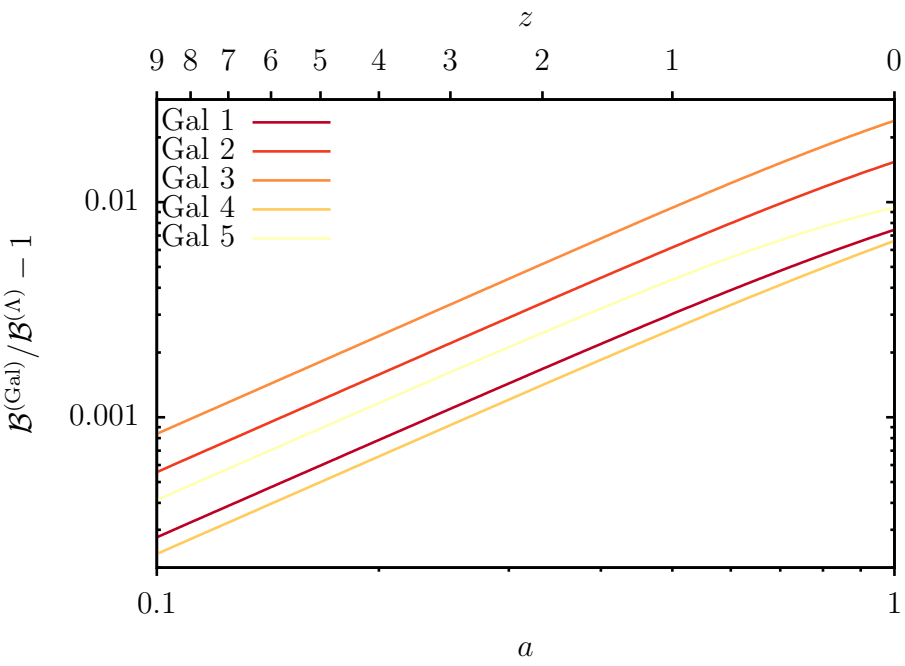

Figure 4.5.: The relative difference between $\mathcal{B} = \mathcal{B}_{GR} - \mathcal{B}_{\phi}$ for the Galileon models Gal 1-5 defined in Table 4.1 and the ΛCDM model. The function $\mathcal{B}_{\phi}$ describes the effect of the shape-dependence on the form factor F_2, the function $\mathcal{B}_{GR}$ is a standard GR contribution to F_2 which is degenerate with $\mathcal{B}_{\phi}$, see Eq. (4.39). The slope of $a^{3/2}$ of $\mathcal{B}_{\phi}$ during matter domination is a distinctive prediction of our model.

In Figure 4.5, we show the relative difference between $\mathcal{B} = \mathcal{B}_{GR} - \mathcal{B}_{\phi}$ as computed for the five Galileon models and as obtained for ΛCDM. The relative difference scales as $\Omega_{\phi} \propto a^{3/2}$ during matter domination, in agreement with our analytical result derived in Eq. (4.45). The slope remains approximately the same at late times, but it appears to be mildly sensitive to the value of C_2. In fact, we can see that the Galileon model Gal 5, characterised by $C_2 > 0$, displays a shallower slope at $z < 1$ compared to the other models.

In general, deviations in the bispectrum from ΛCDM are larger for models which also display significant modifications in the background evolution and linear growth rate. For example, we observe the largest deviations in the bispectrum for the model Gal 3, where they are of order $2 - 3\%$ at redshift $z = 0$. However, the Gal 3 model also modifies the background evolution and the linear growth the most compared to ΛCDM, as comparison with the Figures 4.1 and 4.4 demonstrates.

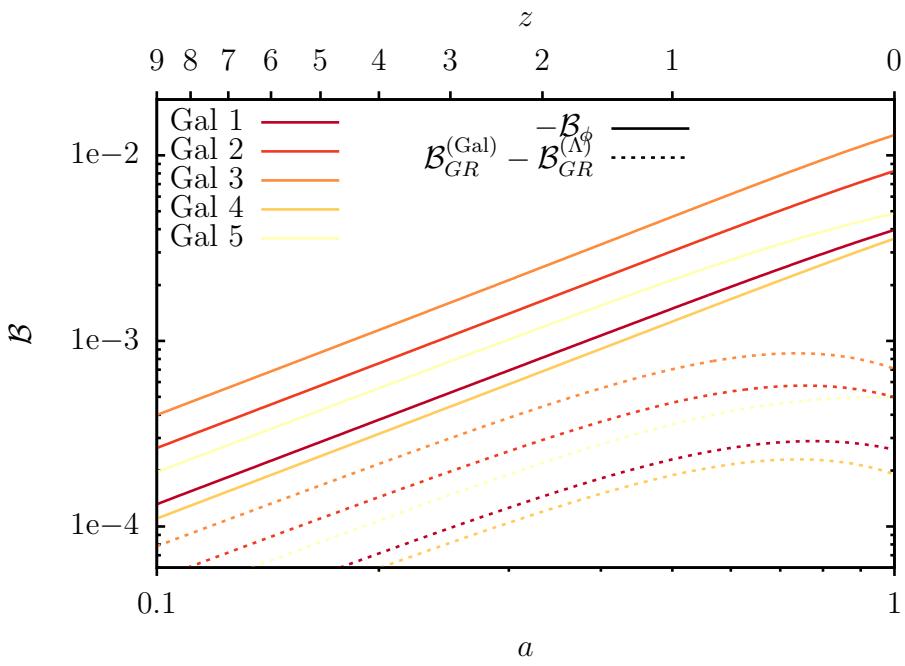

Figure 4.6.: Comparison of $\mathcal{B}_\phi$ (solid lines) and $\mathcal{B}_{GR}^{(\mathrm{Gal})} - \mathcal{B}_{GR}^{(\Lambda)}$ (dashed lines), for the Galileon models Gal 1-5 defined in Table 4.1. While $\mathcal{B}_\phi$ represents the effect of the shape-dependence on the bispectrum, $\mathcal{B}_{GR}^{(\mathrm{Gal})} - \mathcal{B}_{GR}^{(\Lambda)}$ measures the modification of the bispectrum due to the altered evolution of the linear perturbations. $\mathcal{B}_{GR}^{(\mathrm{Gal})}$ and $\mathcal{B}_{GR}^{(\Lambda)}$ describe a GR contribution evaluated on a Galileon or a ΛCDM background respectively.

The deviations with respect to ΛCDM of the term $\mathcal{B}$ in the Galileon models have two different origins. First, the term $\mathcal{B}_\phi$ describing the shape-dependence of Vainshtein screening is altogether absent in ΛCDM, and second, the term $\mathcal{B}_{GR}$ depends on the evolution of linear perturbations, see Eq. (A.7), which are also modified for the Galileons, see Figure 4.4.

To determine which of these two contributions is dominant, we compare in Figure 4.6 the shape-dependence part $\mathcal{B}_\phi$ with the expression $\mathcal{B}_{GR}^{(\mathrm{Gal})} - \mathcal{B}_{GR}^{(\Lambda)}$, i.e. the difference between the term $\mathcal{B}_{GR}$ evaluated on a Galileon and on a standard ΛCDM background. It becomes apparent that the shape-dependence is by far the dominant effect modifying the bispectrum compared to ΛCDM.

Finally, we consider the reduced bispectrum as defined in Eq. (2.47). As mentioned in Section 2.4 the reduced bispectrum has the advantage of being mostly independent of scale and linear growth. In Figure 4.7, we show the relative dif-

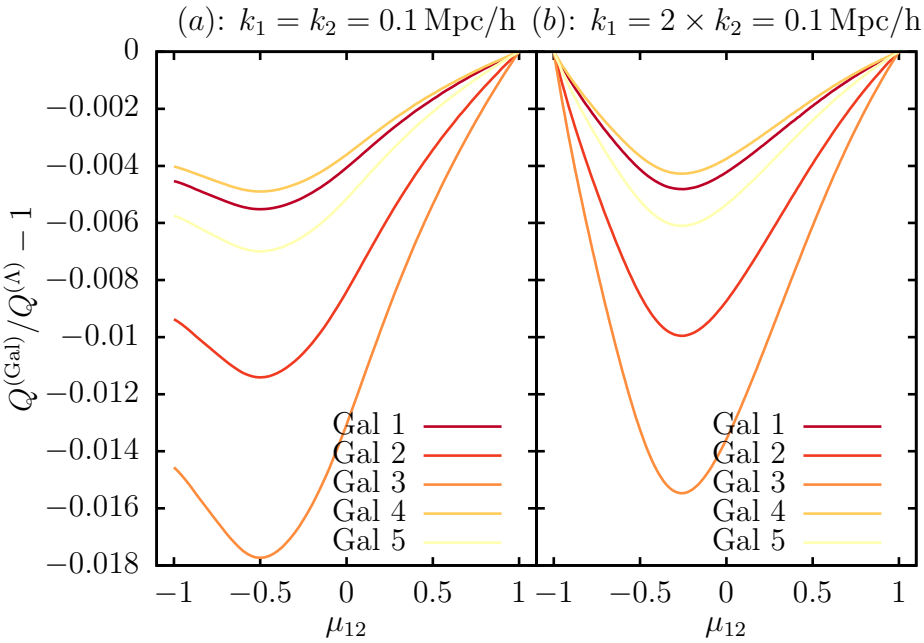

Figure 4.7.: The relative difference of the reduced bispectrum for the Galileon models Gal 1-5 defined in Table 4.1 with respect to the ΛCDM result at $z = 0$ is plotted against μ_{12} – the cosine of the angle between $\vec{k}_1$ and $\vec{k}_2$. In plot (a) the wavenumbers k_1 and k_2 are equal and in plot (b) we have $k_1 = 2 \times k_2$; in both cases $k_1 = 0.1\,\mathrm{Mpc/h}$.

ference between the reduced bispectrum for the Galileon models and ΛCDM. The triangle $\vec{k}_1 + \vec{k}_2 + \vec{k}_3 = 0$ is parametrized by μ_{12}, the cosine of the angle between $\vec{k}_1$ and $\vec{k}_2$, and the absolute values of $\vec{k}_1$ and $\vec{k}_2$. In both plots in Figure 4.7 we keep k_1 and k_2 constant while varying μ_{12}; in the left panel (a), we set $k_1 = k_2$, whereas in the right panel (b), we use $k_1 = 2 \times k_2$.

In panel (a), deviations from ΛCDM vanish for $\mu_{12} = 1$. This corresponds to the flattened limit of the triangle with $k_3 = 2 \times k_1$. This is in agreement with our expectations that planar symmetry, the real-space equivalent of the flattened limit, will result in no Vainshtein screening, see Section 4.3.5. The deviations from ΛCDM are maximal for $\mu_{12} = -0.5$, which corresponds to an equilateral triangle, i.e. the most symmetric configuration. The signal is only slightly smaller in the squeezed limit $\mu_{12} = -1$.

In plot (b), where $k_1 = 2 \times k_2$, the configurations $\mu_{12} = -1$ and $\mu_{12} = 1$ both correspond to the flattened limit and the signal vanishes. The signal is maximal

for $\mu = -0.25$ which corresponds to $k_3 = k_1$, i.e. an isosceles triangle, which, for $k_1 = 2 \times k_2$ is the most symmetric configuration possible. In Refs. [102, 103] a qualitatively similar behaviour of the reduced bispectrum in general Horndeski theories was observed, but without making the connection to the shape dependence of Vainshtein screening.

Summarizing, the shape dependence of Vainshtein screening as seen by the bispectrum is perfectly analogous to the shape dependence in real space outlined in Section 4.2: in real space, the non-linearities responsible for Vainshtein screening are larger the more evenly the field depends on all three directions of space; in the bispectrum, the non-linearities are largest for the most symmetric triangle configurations.

4.5. Conclusion

In this Chapter, we investigated the effects of the shape dependence of Vainshtein screening on the cosmic matter bispectrum. The dependence of Vainshtein screening on the shape of the source mass was first found in Ref. [92], which showed that more symmetric sources lead to a more effective suppression of the fifth force. If Vainshtein screening is present in nature, we can then expect that it will leave an imprint on cosmic structures, given that the cosmic web is characterised by many differently shaped objects like walls, filaments and clusters.

The simplest modified gravity model displaying the Vainshtein screening mechanism is the cubic Galileon, which we used as a proxy to test the effects of the shape-dependence on the matter bispectrum.[11] Unlike previous work on the bispectrum in Galileon theories, we assumed the Galileon field to be conformally coupled to matter, so as to make the fifth force mediated by the Galileon field explicit. We also restricted ourselves to models where the Galileon energy density is subdominant throughout the entire evolution of the Universe, to reflect constraints ruling out the Galileon as the single component driving the accelerated expansion of the Universe.

Previous analyses like Refs. [101–103] seemed to indicate that there was no

[11] It is reasonable to expect that more complicated models with Vainshtein screening behave qualitatively similarly. For example, a quartic galileon theory contains a cubic term in the equations of motion of the form $(\Box\phi)^3 - 3\Box\phi(\nabla_\mu\nabla_\nu\phi)(\nabla^\mu\nabla^\nu\phi)$. At second order in perturbation theory this term becomes $3\Box\bar{\phi}\left((\Box\phi^{(1)})^2 - (\nabla_\mu\nabla_\nu\phi^{(1)})(\nabla^\mu\nabla^\nu\phi^{(1)})\right)$, i.e. equivalent to the shape-dependent term in the cubic galileon, see Eq. (4.30).

qualitatively new information in the bispectrum that was not already present in the power spectrum, which is also easier to measure. However, in this work we have shown that a unique signature emerges in the bispectrum, imprinted by the shape dependence of Vainshtein screening, that would not be observable in the power spectrum alone. We performed an analytic, perturbative analysis of our coupled Galileon model in the Einstein frame, checking explicitly that the emergence of a new non-linearity scale associated to the Vainshtein radius does not lead to a breakdown of perturbation theory.

The non-linearities of Vainshtein screening leave an imprint on the form factor $F_2(\vec{k}_i, \vec{k}_j)$ of the reduced bispectrum, adding a time-dependent term $\mathcal{B}_\phi(\tau)(1-\mu^2)$ which depends on the cosine μ of the angle between the two wavevectors $\vec{k}_i, \vec{k}_j$. This μ dependence reflects the real-space shape dependence found in Ref. [92]: in fact, we observe that the non-linearities are largest for the most symmetric configuration of the bispectrum triangle – i.e. the equilateral one – whereas they vanish for the flattened limit, which corresponds to a planar symmetry in real space.

A simplified, analytic computation of $\mathcal{B}_\phi$ assuming matter domination revealed that $\mathcal{B}_\phi$ scales with the Galileon density, which was confirmed by a numerical analysis using the `hi_class` code. The effect of the shape dependence on the matter bispectrum is found to be at percent level today for Galileon models where the Galileon energy density $\Omega_{\phi,\mathrm{eff},0}$ is at percent level as well.

Critically, the shape dependence of Vainshtein screening displays a distinctive time dependence $\propto a^{3/2}$, see Figure 4.5, which is dominant over the corrections to the bispectrum originating from modifications of the linear growth, see Figure 4.6. This signature is an observational effect of Vainshtein screened modified gravity theories independent from modifications of the background evolution or the linear growth factor. Since it might be difficult to differentiate between different models of modified gravity from observations of the background evolution and the linear growth alone, the bispectrum may be used to break possible degeneracies between theories of modified gravity.

It is important to remark that it is very difficult to measure individual triangle configurations of the bispectrum with current and future galaxy surveys. The observability strongly depends on the binning of the triangle configurations. While past constraints from the SDSS, see Ref. [126], show measurements of individual triangles with order 10 % error bars (five times larger than the largest signal in

Figure 4.7), forecasts for the upcoming Euclid mission in Ref. [127] conclude that individual triangles have a signal-to-noise too low for detections of the bispectrum indicating the usage of much narrower bins. Estimating the detectability of the Vainshtein screening signal in the bispectrum with future surveys thus requires a careful forecast dedicated to this specific signal, which goes beyond the purpose of this work.

5. Constraining Scalar-Tensor Theories with Local Measurements of the Time Variation of G

It has been argued in the past by different authors, see Refs. [99, 128–131], that some screened fifth force models are subject to constraints on the time evolution of the gravitational constant from lunar laser ranging experiments even though the fifth force is effectively screened on solar-system scales. The arguments presented in these references usually apply only to a subclass of screening models. In this chapter we use a unified framework, which incorporates all known screening mechanisms in the context of scalar field theory, to determine the conditions for which the constraints from lunar laser ranging on the time evolution of the *local* gravitational constant can be extrapolated to impose constraints on the time evolution of the *cosmological* gravitational constant. This results in strong late Universe constraints on the running of the cosmological Planck mass described by the Horndeski function $|\alpha_M| \lesssim 0.002$. We find that our assumptions are valid for most Vainshtein and kinetic screening models, where the internal structure of test objects is irrelevant due to an approximate shift-symmetry $\phi \to \phi + c$ on small scales, but are violated by some Chameleon and Symmetron screening models, where the macroscopic equivalence principle is broken.

This work was published in Ref. [5] together with my coauthor Clare Burrage who helped making this analysis as thorough as possible through excellent advice. Ref. [5] is reproduced here with only minor changes.

5.1. Fifth Forces and the Gravitational Constant

In Chapter 3 we have introduced fifth forces mediated by a conformally coupled scalar field as a popular modification of general relativity, see Eq. (3.23). In these models matter particles move on geodesics of the Jordan-frame metric, and thus, a non-relativistic test mass will, in addition to the gravitational acceleration, experience an acceleration due to the gradient of the conformal factor, see Eq. (3.26):

$$\vec{a}_5 = \vec{\nabla} \log \Omega \coloneqq -\frac{1}{2}\vec{\nabla} \log A. \tag{5.1}$$

In Ref. [5], we defined the Jordan-frame metric through $g_{\mu\nu} = \Omega(\phi)\tilde{g}_{\mu\nu}$. However, to not cause confusion with the rest of this thesis, where we defined the Jordan-frame metric as $g_{\mu\nu} = \Omega^{-2}\tilde{g}_{\mu\nu}$, see Eq. (3.16), we introduce $A(\phi) = \Omega^{-2}(\phi)$ here.

In a theory with a conformal coupling, the observed, Jordan-frame gravitational constant[1] will be modified by the conformal factor $A(\phi)$:

$$G(\phi) = A(\phi)G_N. \tag{5.2}$$

This can be read off the transformation law for the Horndeski function G_4 in Eq. (3.22) using that in the Einstein frame $G_4 = M_p^2/2 = 1/(16\pi G_N)$. This gives rise to a variation of the observed gravitational constant in time on both cosmological and solar-system scales if the field evolves in time on those scales.

If the gravitational constant varies on scales where cosmological perturbation theory remains linear, this variation is characterised by the Horndeski parameter[2]:

$$\alpha_M \coloneqq -H^{-1}\dot{G}/G\ . \tag{5.3}$$

On cosmological scales, a time varying gravitational constant can provide an explanation for the late-time accelerated expansion of the Universe alternative to the cosmological constant or the quintessence scenario, and is called self-acceleration,[3]

[1] We call the Jordan-frame gravitational constant the 'observed' one, since this is the gravitational constant matter fields experience.

[2] The four Horndeski α-functions (α_M, α_B, α_K and α_T) were introduced in Ref. [114] as independent functions describing the linear growth of structure in any Horndeski theory without redundancy.

[3] In the literature, the term 'self-acceleration' is sometimes used more generally for modified gravity solutions to the accelerated expansion of the Universe without the use of a negative pressure component. In this work we only refer to non-minimally coupled theories with acceleration in the Jordan frame but not the Einstein frame.

see e.g. Ref. [51]. Here the expansion of the Universe is accelerated only in the (observed) Jordan frame, but not in the Einstein frame. This solution is characterised by the Horndeski parameter α_M being of order 1. Recently, self-acceleration for Horndeski scalar-tensor theories has come under heavy pressure from a combination of cosmological data including CMB, BAO and ISW data, see Ref. [98], the multi-messenger observation of a neutron star merger, see Refs. [55–58], and theoretical constraints from gravitational wave instabilities, see Refs. [132, 133]. For the most recent constraints combining these evidences see Ref. [133], which essentially rules out $\alpha_M = \mathcal{O}(1)$. Predating this, Ref. [128] argues that self-acceleration in Chameleon and Symmetron models is ruled out as soon as we require that the fifth force is smaller than the gravitational force everywhere.

Within the Solar System the ϕ dependence of the gravitational constant in Eq. (5.2) is subject to constraints on the time evolution of the gravitational constant, in particular from lunar laser ranging, see Ref. [134]:

$$\left|\frac{\dot{A}}{A}\right| = \left|\frac{\dot{G}}{G}\right| \lesssim 0.002 H_0. \tag{5.4}$$

This constraint on the time evolution of the conformal factor A is a priori only valid on solar-system scales. The goal of this Chapter is to show under which circumstances these constraints from solar-system scales can be used to constrain the cosmological evolution of the gravitational constant, i.e. α_M, in the late Universe. Models only varying the gravitational constant in the early Universe, see e.g. Ref. [135] for a review and Refs. [136, 137] for recent developments, are not affected by our constraints. Constraints on the variation of the gravitational constant in the early Universe come from analyses of the Big Bang Nucleosynthesis and the CMB, see Refs. [138, 139] respectively.

The central idea of this Chapter, which is described in detail in Section 5.2.2, is very similar to the approach used in Ref. [128]. If we assume that the acceleration of test particles due to the fifth force, Eq. (5.1), is small everywhere compared to the acceleration due to the gravitational force $-\nabla\Phi_N$, where Φ_N is the gravitational potential, we can integrate both quantities from far outside the Milky Way to inside the Solar System. This leads to the statement that the local, solar-system value and the cosmological value of the conformal factor, A_l and A_0 respectively, can only deviate by a term proportional to the local value of the gravitational

potential, which is of order 10^{-6} in the Solar System:

$$|A_l - A_0| \lesssim 10^{-6} A_0. \tag{5.5}$$

Therefore, the constraints from lunar laser ranging in Eq. (5.4) on A_l also apply to the cosmological solution A_0 and thus to α_M. While it was already shown in Refs. [99, 129–131] that theories invariant under the shift symmetry $\phi \to \phi + c$ are subject to the constraints from lunar laser ranging, our result serves as a confirmation of their results with an independent approach and applies to a wider range of fifth force models including some Chameleon and Symmetron models.

Our analysis depends on a number of assumptions, which we detail in Section 5.2.1 and whose validity will depend on the specific fifth force model under consideration. While we find that our assumptions are valid for most theories which obey the shift symmetry $\phi \to \phi + c$ (this includes the most common Vainshtein-type screening models, see Section 3.4.1), they are not exclusively valid for shift-symmetric theories. We carefully examine under which conditions non shift-symmetric theories like the Chameleon and Symmetron models could potentially escape our constraints due to a violation of the macroscopic equivalence principle, see Section 5.3.2. With regard to the Chameleon and the Symmetron, our conclusions are thus more conservative than the claim in Ref. [128], which rules out self-acceleration entirely for these models.

5.2. From the Solar System to Cosmological Scales

In this section we will prove, with minimal assumptions, that the deviation of the local conformal factor A_l from the cosmological average A_0 must be small. Therefore, constraints on the time evolution of the Planck mass from local, solar-system observations also constrain the cosmological evolution of the Planck mass for fifth force models respecting those assumptions. While our formal proof in Section 5.2.2 will be completely model independent, it relies on a number of assumptions, which are summarized in Section 5.2.1 and whose validity has to be checked for any fifth force model individually.

5.2.1. Model-dependent assumptions

So far, observations from cosmological to local, solar-system scales have not detected a fifth force with high significance, which makes it very unlikely that a fifth force, which is significantly stronger than gravity could be observed on any of these scales. The situation might be different on laboratory scales where strong fifth forces could still exist in Chameleon or Symmetron scenarios, see Ref. [91], although even here experimental constraints are strong, see Ref. [90]. However, these scales are not relevant for the purposes of this work. We therefore arrive at our first assumption:

$$\textbf{Weak fifth force assumption:} \qquad \left|\vec{F}_5\right| < \beta \left|\vec{F}_N\right|, \tag{5.6}$$

which is assumed to be valid from cosmological ($\sim H_0^{-1}$) to solar-system scales ($\sim 1\,\mathrm{AU} \approx 5 \times 10^{-6}\,\mathrm{pc}$). We define $\vec{F}_N$ as the Newtonian gravitational force and β is a constant roughly of order 1. We will actually see later (in the discussion around Eq. (5.21)) that β could be as large as 10 for our purposes.

Next, we assume that the weak fifth force assumption can be directly translated into a constraint on the acceleration of test particles:

$$\textbf{Equivalence principle assumption:} \qquad \frac{1}{2}\left|\nabla \log A\right| < \beta \left|\nabla \Phi_N\right|. \tag{5.7}$$

This step will in general not be valid for fifth force models which break the macroscopic equivalence principle. We will discuss this in great detail in Section 5.3. The validity of this assumption is therefore model dependent.

Furthermore, we assume that the fifth force and the gravitational force are parallel throughout the space time region we consider. This is motivated by the fact that both the fifth force and the weak-field gravitational force are sourced by matter in a similar way, compare Eqs. (2.24) and (3.27), and that scalar mediated fifth forces are attractive[4], see Ref. [142]. We can therefore write:

$$\textbf{Parallelism assumption:} \qquad \frac{1}{2}\nabla \log A = \beta(\vec{x}) \nabla \Phi_N, \tag{5.8}$$

[4]Unless the equation of state parameter of the scalar field is phantom, see Ref. [140], in which case the theory is unstable. Another possible exception is described in Ref. [141].

where we have promoted the constant β to a function of space-time which fulfils:

$$0 < \beta(\vec{x}) \leq \beta_{\max} \lesssim 10, \quad \forall \vec{x}. \tag{5.9}$$

Finally, we assume that the time today, t_0, is not a special point in the evolution of the Universe. This is an important assumption because the fifth force on solar-system scales can not be tested over cosmological time scales. More formally, we assume that Eq. (5.8) is valid for an extended period of time Δt on cosmological scales (we will specify this more explicitly around Eq. (5.21)):

$$\textbf{Naturalness assumption:} \quad \frac{1}{2}\nabla \log A = \beta(\vec{x})\nabla\Phi_N \quad \text{for} \quad t \in [t_0 - \Delta t : t_0]). \tag{5.10}$$

Not only would it be unnatural for the strength of the fifth force to be suppressed only during a short (with respect to cosmological time scales) time interval around t_0, but we are also not aware of a realistic cosmological model predicting this.

We will make two additional very technical assumptions in the following, see Eqs. (5.13) and (5.14) and the discussions before these equations. These assumptions are however independent of the fifth force model, and therefore, are not mentioned here.

5.2.2. Model-independent proof

We split the conformal factor $A(\vec{x}, t)$ into its spatially averaged value $A_0(t)$ plus an inhomogeneous part $\alpha(\vec{x}, t)$:

$$A = A_0(t) + \alpha(\vec{x}, t), \qquad \text{with} \quad \langle \alpha(\vec{x}, t) \rangle = 0, \tag{5.11}$$

where $\langle \dots \rangle$ represents a spatial average. The function $A_0(t)$ represents the cosmological background solution, and α describes inhomogeneities sourced by the highly non-linear density distribution in the late Universe.

We first show that on solar-system scales α has to be small compared to A_0, meaning that the local conformal factor has to be very close to the cosmological conformal factor. For this we integrate the final assumption, Eq. (5.10), along a path γ from a point $\vec{x}_2$ far outside an overdensity, such as the Milky Way, to a

point $\vec{x}_1$ inside, e.g. deep inside the Solar System:

$$\frac{1}{2}\log\frac{A(\vec{x}_1)}{A(\vec{x}_2)} = \int_\gamma \beta(\vec{x})\nabla\Phi_N \cdot \mathrm{d}\vec{x}. \tag{5.12}$$

The integral on the right-hand side must be independent of the path γ between the points $\vec{x}_2$ and $\vec{x}_1$ since $\nabla \log A = 2\beta(\vec{x})\nabla\Phi_N$ is a conservative vector field. We now make the technical assumption that we can choose a path γ where Φ_N is decreasing from $\vec{x}_2$ to $\vec{x}_1$. This assumption will certainly hold for an isolated overdensity whose density increases monotonically towards the center of the object (such monotonically increasing density profiles are expected for any self-gravitating object). Since $\beta(\vec{x}) > 0$, the integral in Eq. (5.12) has to be smaller than 0 and we can estimate:

$$0 > \int_\gamma \beta(\vec{x})\nabla\Phi_N \cdot \mathrm{d}\vec{x} \geq \beta_{\max}\int_\gamma \nabla\Phi_N \cdot \mathrm{d}\vec{x} = \beta_{\max}\left(\Phi_N(\vec{x}_1) - \Phi_N(\vec{x}_2)\right). \tag{5.13}$$

This statement can be made far more precise and constraining for a specific fifth force model, where $\beta(\vec{x}) \ll \beta_{\max}$ in screened regions. We demonstrate this for a simple cubic Galileon model in Appendix A.2. Therefore, we believe that Eq. (5.13) should be considered a very conservative estimate.

We now choose the point $\vec{x}_2$ such that $A(\vec{x}_2) = A_0$ (so far we only assumed that $\vec{x}_2$ lies far outside the overdensity). Furthermore, we make the assumption[5] that $|\Phi_N(\vec{x}_2)| \ll |\Phi_N(\vec{x}_1)|$. Typical values for the gravitational potential inside of the Milky Way or the Solar System are of order $0 > \Phi_N(\vec{x}_1) \gtrsim -10^{-6}$. We therefore arrive at:

$$0 > \frac{1}{2}\log\frac{A(\vec{x}_1)}{A(\vec{x}_2)} = \frac{1}{2}\log\left(1 + \frac{\alpha(\vec{x}_1)}{A_0}\right) \gtrsim -10^{-6}\beta_{\max}. \tag{5.14}$$

Since the absolute value of the right-hand side is small compared to 1, we can Taylor expand the logarithm on the left side and multiply by $2A_0$:

$$0 > \alpha_l \gtrsim -2 \times 10^{-6}\beta_{\max}A_0, \tag{5.15}$$

where $\alpha_l \coloneqq \alpha(\vec{x}_1)$ is a typical, local (solar-system scale) value of α. This proves that, even using the most conservative estimate in Eq. (5.13), $|\alpha|$ on solar-system scales has to be small compared to A_0.

[5] This is the second and final technical assumption that we hinted at in Section 5.2.1.

For a Chameleon-type screening mechanism, the statement in Eq. (5.15) is phrased more intuitively in terms of only the cosmological conformal factor A_0. For Chameleon-type screening the scalar field is very small in the solar system due to the high density, see Section 3.4.2. The local conformal factor will thus be very close to one, $A(\vec{x}_1) \approx 1$, and is independent of the cosmological value A_0 which depends on the background density. The result in Eq. (5.15) that the difference between the local and cosmological conformal factors has to be small, should therefore be phrased as a constraint on A_0 instead of α_l. Using $\alpha_l \approx 1 - A_0$ we obtain from Eq. (5.15):

$$1 < A_0 \lesssim 1 + 2 \times 10^{-6} \beta_{\max} A_0, \tag{5.16}$$

i.e. A_0 has to be very close to 1.

We are now in a position to examine the consequences of the lunar laser ranging constraints in Eq. (5.4) on the evolution of the cosmological conformal factor A_0 for any screened fifth force obeying the assumptions in Section 5.2.1. The constraints on the local gravitational constant demand:

$$0.002 H_0 \gtrsim \left| \frac{\dot{A}(\vec{x}_1)}{A(\vec{x}_1)} \right| = \left| \frac{\dot{A}_0 + \dot{\alpha}_l}{A_0 + \alpha_l} \right| \approx \left| \frac{\dot{A}_0 + \dot{\alpha}_l}{A_0} \right|. \tag{5.17}$$

In the last step we have assumed $\alpha_l \ll A_0$ in accordance with Eq. (5.15). The constraints in Eq. (5.17) are technically only valid over the time period during which lunar laser ranging tests were performed, i.e. over a few decades. However, in accordance with our naturalness assumption (see Eq. (5.10)), we assume that the constraints are valid for an extended cosmological time period Δt.

There are now two possibilities for the two terms $\dot{A}_0/A_0$ and $\dot{\alpha}_l/A_0$ on the right-hand side of Eq. (5.17):

- Both terms are individually smaller than the left-hand side of Eq. (5.17). In this case we conclude that the cosmological evolution of the gravitational constant, typically characterised by the Horndeski parameter α_M, is constrained in the same way as the evolution of the local gravitational constant:

$$|\alpha_M| \coloneqq H^{-1} \left| \frac{\dot{A}_0}{A_0} \right| \lesssim 0.002. \tag{5.18}$$

- The two terms on the right-hand side of Eq. (5.17) cancel each other, i.e. $\dot{\alpha}_l \approx -\dot{A}_0$. This will always be the case for Chameleon-type screening where $\alpha_l \approx 1 - A_0$. In this case the constraints from lunar laser ranging do not apply directly, however, equivalent constraints may be derived in the following way. By assumption the cancellation $\dot{\alpha}_l \approx -\dot{A}_0$ has to be valid for an extended period of time Δt. Assuming that $\dot{A}_0$ can be treated as approximately constant over a time interval $\delta t \leq \Delta t$, we can integrate $\dot{\alpha}_l$:

$$\alpha_l(t_0) - \alpha_l(t_0 - \delta t) = \int_{t_0-\delta t}^{t_0} \dot{\alpha}_l(t)\mathrm{d}t \approx -\int_{t_0-\delta t}^{t_0} \dot{A}_0(t_0)\mathrm{d}t \approx -\dot{A}_0(t_0)\delta t. \quad (5.19)$$

  Since $\delta t < \Delta t$, both terms on the left-hand side have to fulfil Eq. (5.15) and we obtain:

$$\frac{\left|\dot{A}_0(t_0)\right|}{A_0} \lesssim 2 \times 10^{-6} \frac{\beta_{\max}}{\delta t}. \quad (5.20)$$

  We can assume here that the approximation $\dot{A}_0 \approx$ const used in Eq. (5.19) is valid for at least a cosmologically short time interval δt of order $0.01 H_0^{-1}$. Otherwise, the strong change in the evolution of A_0 in the recent history of the Universe would make this small period of time a special point in the evolution of the Universe, which violates our Naturalness assumption. Therefore, the constraint

$$|\alpha_M| \lesssim 0.002 \quad (5.21)$$

  still holds as long as $\beta_{\max} \lesssim 10$. In other words the time interval Δt, during which the fifth force is assumed to be weak in our naturalness assumption, see Eq. (5.10), has to fulfil $\Delta t > \delta t = 0.001 H_0^{-1} \beta_{\max}$ for our constraints on α_M to be valid.

We conclude that according to our assumptions, the evolution of the cosmological gravitational constant is strongly constrained:

$$|\alpha_M| \lesssim 0.002. \quad (5.22)$$

This is the central result of this Chapter. This bound on α_M is a significant improvement over previous bounds, see Ref. [133], and is independent of parametrisations of α_M, but relies on the assumptions summarised in Section 5.2.1.

5.3. Discussion of the central assumptions

Although our proof in Section 5.2.2 is independent of the underlying fifth force model, the assumptions summarized in Section 5.2.1 are model dependent statements. Therefore, it is possible to evade the constraints from lunar laser ranging if the fifth force model violates one or more of these assumptions. In this section we will discuss these assumptions in light of the most common screening models, which we categorised in Section 3.4 as Vainshtein- and Chameleon-type screening mechanisms.

5.3.1. Weak fifth force assumption

The weak fifth force assumption in Eq. (5.6) states that the fifth force between two objects, whose sizes range from solar-system to cosmological scales, can not be significantly larger than the gravitational force between the two objects. We saw in our discussion around Eq. (5.20) that 'significantly larger' means more than an order of magnitude larger than the gravitational force. The goal of this section is to summarise some of the observational bounds on the strength of a fifth force.

On solar-system scales a strong fifth force is decisively ruled out by precision measurements of general relativity in the Solar System, see Ref. [6]. On galactic scales some evidence has been found in the past for a very weak screened fifth force, see Ref. [143], but was ruled out again by a subsequent analysis with more stringent data cuts, see Ref. [144]. Even if a weak force of this form exists, it still satisfies our assumption that a fifth force, if it exists, can't be substantially stronger than gravity. In general, it is difficult to make definite statements about the presence of a fifth force on galactic scales because of degeneracies with uncertainties in our knowledge of the physics of galaxy formation. However, it seems unlikely that a fifth force that is an order of magnitude stronger than the gravitational force would have evaded detection.

For a fifth force model which screens effectively on small scales, such as within the Solar System, the strongest constraints on the strength of a fifth force come from observations of the largest scales in the universe, where the growth of structure can be treated linearly. On these scales screening is generally less effective than on smaller scales due to the low densities of the density perturbations on these scales. Therefore, we expect the effects of the fifth force to be strongest there. A strong fifth force would significantly modify the linear growth of struc-

ture $D_+(a)$, which in GR is described by Eq. (2.28), but in the presence of a fifth force has the form:

$$D''_+ + \mathcal{H}D'_+ = \frac{3}{2}\mathcal{H}^2\Omega_m(a)\,(1+\beta(a))\,D_+, \tag{5.23}$$

where $\beta(a)$ is the relative strength of the fifth force with respect to the gravitational force on linear scales as a function of the scale factor a. The function $\beta(a)$ is strongly constrained by observations of redshift-space distortions. The study in Ref. [41] using data from the DES 1-year results constrains $\beta(a)$ (called $\mu(a)$ in Ref. [41]) and, making use of the parametrisation $\mu(a) = \mu_0\Omega_\Lambda(a)/\Omega_{\Lambda,0}$, concludes: $\mu_0 = -0.11^{+0.42}_{-0.46}$. Similarly, Ref. [145] constrains $G_M \coloneqq 1+\beta(a)$ by binning it into two redshift intervals and obtains $G_M(z<0.5) = 1.26 \pm 0.32$ and $G_M(z>0.5) = 0.986 \pm 0.022$. This clearly rules out fifth forces with strength relative to gravity of order $\beta \sim 10$.

It is important to make one caveat when using redshift-space distortion data in order to constrain modified theories of gravity. Several steps in the analysis of redshift-space distortion data assume a certain cosmology, typically ΛCDM. The effects of this assumption have been estimated in Refs. [146, 147] and were shown to be important for future galaxy surveys, but are negligible for the precision of current data. Therefore, this should not affect the validity of the weak fifth force assumption.

Finally, we note that it is very unlikely that a theory of modified gravity could have a fifth force which is stronger than gravity on linear scales without significantly changing the expansion history of the Universe, which is well constrained. This makes a violation of the weak fifth force assumption even more unlikely.

5.3.2. Equivalence principle assumption

The Equivalence principle assumption of Eq. (5.7) is the assumption which is the most likely to be violated by theories of screened fifth forces. Eq. (5.7) assumes that small fifth forces imply small gradients of the conformal factor, a result which would follow immediately from the weak fifth force assumption, Eq. (5.6), if a macroscopic equivalence principle holds for all the astrophysical and cosmological objects used as tracers in tests of gravity. This is true for some, but not all, fifth force models as was shown in Ref. [148]. We will review the results of Ref. [148] here and discuss their implications for the validity of our constraints in Eq. (5.22)

for different fifth force models depending on their screening models.

The fifth force on an extended, non-relativistic test object B due to another object A can be computed through:

$$F_5^i = -\int_S T_\phi^{ji} n_j \mathrm{d}S, \tag{5.24}$$

where S is a surface enclosing object B, n is the unit vector normal to S and T_ϕ is the energy-momentum tensor of the scalar field. We will assume spherical symmetry for the test object B in the following.

In simple scenarios we can solve the surface integral in Eq. (5.24) analytically. Let us assume that the total gradient of the scalar field on the surface S is well approximated by adding the gradients of the fields ϕ_A and ϕ_B linearly, where ϕ_A and ϕ_B are the field profiles we would compute around objects A and B if they were isolated. Furthermore, we assume that the field profile ϕ_B is well described by a $1/r$ power law and that the gradient of ϕ_A is constant over the surface S. With these assumptions the gradient of the total scalar field on the surface S is given by:

$$\partial_i \phi = \partial_i \phi_A + \partial_i \phi_B = \partial_i \phi_A + \frac{Q_B}{4\pi} \frac{x_i}{r^3}, \tag{5.25}$$

where Q_B is the scalar charge of object B. Finally, we assume that the energy-momentum tensor of the scalar field is given by:

$$T_\phi^{ij} = \partial^i \phi \partial^j \phi - \frac{1}{2} \delta^{ij} \partial_k \phi \partial^k \phi, \tag{5.26}$$

where we have neglected time derivatives of the scalar field compared to spatial derivatives, which is reasonable for non-relativistic objects. Under these assumptions we find the simple result:

$$F_5^i = -Q_B \partial^i \phi_A. \tag{5.27}$$

We will use this result in the following two subsections in order to discuss the equivalence principle assumption in the context of Vainshtein- and Chameleon-type screening mechanisms.

Equivalence principle assumption – Vainshtein

The first type of screening mechanisms we would like to discuss in this context are Vainshtein-type screening mechanisms, see Section 3.4.1. Summarising our findings in Section 3.4.1, these screening mechanisms weaken the fifth force in regions of high derivatives of the scalar field; second derivatives in case of Vainshtein screening and first derivatives for kinetic screening. Around compact matter sources, there will typically be a non-linearity radius r_V (also Vainshtein radius), within which the fifth force is screened and outside which the fifth force behaves just like non-relativistic gravity.

Typically, Vainshtein screened fifth force models are invariant under the shift symmetry $\phi \to \phi + c$. Around an isolated mass M_B the equation of motion, Eq. (3.29), may be integrated using Gauss' law, see Eq. (3.31). For the far field ($r \gg r_V$) we obtain:

$$\partial_r \phi_B(r \gg r_V) = \frac{\xi M_B}{4\pi M_p r^2} = \frac{Q_B}{4\pi} \frac{1}{r^2}, \tag{5.28}$$

where we defined the scalar charge $Q_B = \xi M_B / M_p$. It is important to note that this solution is not only valid for spherically symmetric masses, but also applies to arbitrary complicated matter configurations in the far-field limit, where multipoles may be ignored.

We are now interested in the fifth force acting on object B due to another object A assuming that the distance between the two objects is much larger than the Vainshtein radii of the two objects. In this case we may choose the surface S for the integration in Eq. (5.24) to lie outside the Vainshtein radius of object B, where the fifth force behaves like gravity. Thus, the result in Eq. (5.27) applies in this simplified, unscreened scenario.

A different scenario where Eq. (5.27) applies is the following. We may choose ϕ_A as the field of the linearly evolving large scale density fluctuations. In this regime, the fifth force is unscreened and behaves like gravity since the terms non-linear in the second derivatives may be ignored[6]. We now take the object B to be a tracer galaxy probing the field ϕ_A, e.g. through redshift-space distortions. If the wavelength of ϕ_A is much longer than the Vainshtein radius of the tracer galaxy, we may treat $\partial\phi_A$ as constant over a surface S lying outside the Vainshtein radius

[6]This is guaranteed if the scale of the density fluctuations is above the non-linearity scale of the Galileon field, see the discussion in Chapter 4.3.4.

of the tracer galaxy, where $\phi_B \sim 1/r$, and thus Eq. (5.27) applies.[7]

In the cases where Eq. (5.27) applies, the magnitude of the fifth force acting on object B relative to the gravitational force on B can be expressed through the gradient of the conformal factor $A(\phi_A)$ at the position of object B:

$$\frac{\left|\vec{F}_5\right|}{\left|\vec{F}_N\right|} = \frac{\left|-Q_B\vec{\nabla}\phi_A\right|}{\left|-M_B\vec{\nabla}\Phi_{N,A}\right|} = \frac{1}{M_p}\frac{\left|\xi\vec{\nabla}\phi_A\right|}{\left|\vec{\nabla}\Phi_{N,A}\right|} = \frac{\left|\vec{\nabla}\log A^{1/2}(\phi_A)\right|}{\left|\vec{\nabla}\Phi_{N,A}\right|}, \tag{5.29}$$

where $\Phi_{N,A}$ is the gravitational potential of object A at the position of object B. We conclude that the equivalence principle assumption, Eq. (5.7), directly follows from the weak fifth force assumption, Eq. (5.6), in the unscreened regime.

But what happens in the screened regime, where the Vainshtein radii of the two objects are relevant? It was demonstrated in Ref. [149] (see also Chapter 6) that in the screened regime the self-field of the test-object interacts non-linearly with the tested field ϕ_A. In this way the equivalence principle is broken. However, for the purposes of this study this breaking of the equivalence principle is irrelevant. Due to the nature of Vainshtein-type screening, the ratio $\nabla\log A^{1/2}/\nabla\Phi_N$ is largest in the unscreened regime and decreases quickly for scales below the Vainshtein radius, see Eq. (3.34). Therefore, if we constrain the ratio $\nabla\log A^{1/2}/\nabla\phi_N$ through observations of the largest structures in the Universe, which are typically unscreened, we have constrained the ratio $\nabla\log A^{1/2}/\nabla\Phi_N$ everywhere. We have seen in Section 5.3.1 that the fifth force from the largest structures is well constrained by observations of redshift-space distortions. The assumption in Eq. (5.7), which we naively dubbed 'equivalence principle assumption', thus holds on all scales regardless of equivalence principle violations on small scales, as long as the equivalence principle holds on the largest scales.

For completeness we mention the only possible way for Vainshtein-type screening models to violate the equivalence principle assumption in the form of Eq. (5.7). It might in principle be possible to construct Vainshtein-screened fifth force models, where the Vainshtein radius of any tracer galaxy, which is used in galaxy surveys to map the fifth force on cosmological scales, is of the same scale as the largest structures in the Universe. In this case, the equivalence principle would be broken

[7] The statement that $\partial\phi_A = \text{const.}$ over the surface S only makes sense since ϕ_A was assumed to be an unscreened, linear field with small enough second derivatives. In this way the second derivatives of ϕ_A may be neglected compared to the derivatives of ϕ_B outside the Vainshtein radius of B.

even on the largest cosmological scales and Eq. (5.29) would not be valid anywhere. However, if the Vainshtein radius of single galaxies was as large as the largest structures in the Universe, the fifth force would be screened everywhere in the Universe and it seems unlikely that such a model would be cosmologically or otherwise relevant. We are not aware of a study which analyses such highly non-linear theories. Thus, we draw the conservative conclusion that these theories, if they turn out to be consistent, might potentially escape our constraints.

Equivalence principle assumption – Chameleon

We now turn our attention to Chameleon-type screening mechanisms as defined in Section 3.4.2. For Chameleon-type screening mechanisms the minimum of the effective potential depends on the local matter density, see Eq. (3.42). In case of the classic Chameleon, the effective mass is therefore large in high-density regions, thus reducing the range of the fifth force. For the Symmetron mechanism, the coupling vanishes in regions of high densities due to the restoration of the $\mathbb{Z}_2$ symmetry which is spontaneously broken in regions of low densities. The consequence for both the classic Chameleon and the Symmetron is a thin-shell effect, i.e. only a thin shell at the boundary of any object with high density contributes to the fifth force. This thin-shell effect changes the discussion of the equivalence principle assumption significantly compared to the Vainshtein screening case, where the density of an object was found to be irrelevant in the far-field limit.

We recall that the thin-shell solution for the field profile around a spherical object B of constant density and radius R_B is given by Eq. (3.47):

$$\phi_B(r > R_B) = \phi_{bg} - \lambda_B \frac{\xi M_B}{4\pi M_p} \frac{\mathrm{e}^{-m(\rho_{bg})(r-R_B)}}{r}, \tag{5.30}$$

where the screening factor λ_B is:

$$\lambda_B \approx \frac{\phi_{bg}}{2\xi M_p \Phi_N(R_B)}. \tag{5.31}$$

As discussed in Section 3.4.2 the object B is said to be screened if $\lambda_B \ll 1$. A small screening factor means that the scalar charge $Q_B = \xi \lambda_B M_B/M_p$ is proportional to only a fraction of the entire mass of object B.

We can now compute the fifth force acting on object B due to another object A

by means of Eq. (5.24) by choosing the surface S just outside the object B such that the exponential decay in the solution (5.30) can be neglected:

$$F_5^i = -\lambda_B M_B \frac{\xi}{M_p} \partial^i \phi_A. \tag{5.32}$$

The strength of the fifth force relative to the gravitational force acting on object B is thus given by:

$$\frac{\left|\vec{F}_5\right|}{\left|\vec{F}_N\right|} = \lambda_B \frac{\xi}{M_p} \frac{\left|\vec{\nabla}\phi_A\right|}{\left|\vec{\nabla}\Phi_{N,A}\right|}, \tag{5.33}$$

where ϕ_A and $\Phi_{N,A}$ are taken at the position of object B. Analogous to the Vainshtein case, see Eq. (5.29), we can express the right-hand side of Eq. (5.33) in terms of the derivative of the conformal factor A. For the chameleon ($\log A^{1/2} = \xi\phi/M_p$) we have:

$$\frac{\left|\vec{F}_5\right|}{\left|\vec{F}_N\right|} = \lambda_B \frac{\left|\vec{\nabla}\log A^{1/2}(\phi_A)\right|}{\left|\vec{\nabla}\Phi_{N,A}\right|}, \tag{5.34}$$

and for the Symmetron ($\log A^{1/2} = \xi^2\phi^2/2M_p^2$):

$$\frac{\left|\vec{F}_5\right|}{\left|\vec{F}_N\right|} = \lambda_B \frac{M_p}{\xi\phi_A} \frac{\left|\vec{\nabla}\log A^{1/2}(\phi_A)\right|}{\left|\vec{\nabla}\Phi_{N,A}\right|}. \tag{5.35}$$

In contrast to the Vainshtein case a small fifth force, i.e. a small left-hand side in Eqs. (5.34) and (5.35), does not necessarily mean that the gradient of the conformal factor has to be small. For the Chameleon it depends on the properties of the test object B whether the gradient of the conformal factor is constrained by observations of small fifth forces. If the test object is screened, $\lambda_B \ll 1$, the conformal factor is less constrained than if the test object is unscreened, $\lambda_B = 1$. For the Symmetron it additionally depends on the field ϕ_A at the position of the test object.

Therefore, the equivalence principle assumption, Eq. (5.7), can be violated by Chameleon-type screening if all relevant astrophysical and cosmological test objects are screened. In this case the constraint on α_M in Eq. (5.22) could be violated by Chameleon-type screening models. This can be shown by integrating Eq. (5.33) in the same way we have integrated the equivalence principle assumption in Sec-

tion 5.2.2: We define $\beta(\vec{x}) \coloneqq \left|\vec{F}_5\right| / \left|\vec{F}_N\right|$, multiply by $\left|\vec{\nabla}\Phi_{N,A}\right|$ and integrate from a point far outside of object A, where ϕ_A is equal to the cosmological solution ϕ_{bg}, to a point inside object A, where ϕ_A is given by the local value of the scalar field ϕ_l. Estimating the integral in the same way as in Section 5.2.2 through the maximum value $\beta_{\max}$ of $\beta(\vec{x})$, gives the following constraint on the difference between the cosmological and the local field:

$$0 > \lambda_B \frac{\xi}{M_p} (\phi_l - \phi_{bg}) \gtrsim \beta_{\max} \Phi_{N,l} \sim -10^{-6} \beta_{\max}, \tag{5.36}$$

where we introduced the local gravitational potential $\Phi_{N,l}$. For simplicity of the calculation we have assumed that the screening factor λ_B is the same for all tracer objects which are used to test the fifth force on all relevant scales from far outside to inside object A.[8] If we could treat all tracer objects as unscreened, i.e. $\lambda_B = 1$, Eq. (5.36) becomes equivalent to Eq. (5.14) in the sense that the value of the local conformal factor would again be constrained to be very close to the cosmological value for both the Chameleon ($\log A^{1/2} = \xi\phi/M_p$) and the Symmetron ($(\log A^{1/2})^{1/2} = \xi\phi/\sqrt{2}M_p$). In this case our constraints on α_M in Eq. (5.22) still hold. However, if the tracer objects are screened, i.e. $\lambda_B \ll 1$, the local and cosmological field values could potentially deviate enough to allow for a self-accelerating solution of the cosmological field characterised by $\alpha_M \sim 1$.

It has been pointed out in the literature, see e.g. Ref. [88], that $\lambda_B \ll 1$ is only possible for an extended period of time if the field excursion of the cosmological background field $\Delta\phi_{bg}$ is small because λ_B is proportional to ϕ_{bg}, see Eq. (5.31). This argument would suggest that $\alpha_M \sim \xi\Delta\phi_{bg}/M_p \sim 1$ is still ruled out even if the theory avoids the equivalence principle assumption. However, if $\xi^2 \gg \Phi_N^{-1}(R_B)$, λ_B could remain small even if the field excursion is large, see Eq. (5.31). Therefore, α_M is unconstrained for models with large couplings $\xi^2 \gg 10^6$ since all tracers can be consistently screened for an extended period of time thereby violating our equivalence principle assumption.

In the related study Ref. [128], which establishes a no-go theorem for self-acceleration from Chameleon and Symmetron fields, the violation of the macroscopic equivalence principle was ignored with the argument that a huge backreaction effect on the expansion history is expected if all tracers were screened. While

[8] This is a significant simplification and is not true in general, but it serves here to demonstrate the central idea.

we agree that the background evolution should be reconsidered in this case, we are not aware of an argument showing that this reconsidered background evolution can not have $|\alpha_M| \sim 1$. Even if all cosmological tracers are screened, very low density regions in the Universe, which are unobserved and thus can not be used as tracers, could still be unscreened and have a substantial impact on the background evolution. Therefore, we would like to draw a more conservative conclusion by stating that a large coupling ξ could potentially invalidate our constraint in Eq. (5.22). Hopefully, a future analysis of this backreaction effect will shine some light on this issue.

5.3.3. Parallelism assumption

The assumption that the fifth force is parallel to the gravitational force, Eq. (5.8), is a technical assumption enabling us to make the simple estimate in Eq. (5.13). Small violations of this assumption are not problematic as long as the estimate of Eq. (5.13) still holds.

Since both the fifth force and the gravitational force are sourced by matter, they will always be parallel around spherically symmetric matter sources. The same is going to be true far away from a matter source, where the monopole of the matter distribution dominates. However, close to irregular matter distributions the two forces are only guaranteed to be parallel if they obey the same force law, i.e. the Poisson equation[9] $\Delta\phi \propto \rho$.

For the Vainshtein-type screening mechanisms the Poisson equation will be approximately valid outside the Vainshtein radius, where the force is unscreened, and for Chameleon type screening the Poisson equation is a good approximate description of the field profile close to the matter source, where the Yukawa damping can be neglected. Violations of the parallelism assumption, coming from deviations of the equation of motion from the Poisson equation, occur only in regions where the gradient of the scalar field is suppressed compared to the gradient of the gravitational potential. Thus, the effect of these violations of the parallelism assumption should be irrelevant for the estimate in Eq. (5.13). For Vainshtein screening we show this explicitly in Appendix A.2, where Eq. (A.44) is the analogue of the estimate in Eq. (5.13) and depends only on the fields outside the Vainshtein radius,

[9] We are assuming non-relativistic matter sources here because all objects of interest for our purposes, i.e. the Solar System, the Milky Way and other sub-horizon structures, are non-relativistic.

i.e. where the scalar field and the gravitational field both obey a Poisson equation.

5.4. Conclusion

In this Chapter, we have considered a general fifth force model, where a scalar field couples conformally to matter, and demonstrated that the constraints from lunar laser ranging on the time evolution of the local gravitational constant strongly constrain the evolution of the cosmological gravitational constant, i.e. α_M, under a specific set of assumptions. We have assumed that 1. the fifth force is weak compared to the gravitational force on any scale from cosmological to solar-system scales, see Eq. (5.6), that 2. a macroscopic equivalence principle holds for the objects used as tracers in tests of gravity on those scales, see Eq. (5.7), that 3. the fifth force and the gravitational force are mostly parallel, see Eq. (5.8), and that 4. all of those assumptions hold for an extended period of time on cosmological scales, see Eq. (5.10).

Furthermore, we made two model independent, technical assumptions in Section 5.2.2. If $\vec{x}_1$ is a point inside an overdensity like the Solar System and $\vec{x}_2$ is a point far outside the overdensity such that the conformal factor $A(\vec{x}_2)$ is given by the cosmological average A_0, we assumed that there exists a path γ from $\vec{x}_1$ to $\vec{x}_2$ where the gravitational potential is monotonically increasing, and we assumed that $|\phi_N(\vec{x}_2)| \ll |\phi_N(\vec{x}_1)|$.

Under all of these assumptions we showed that the conformal factor in the Solar System has to be relatively close to the cosmological average, see Eq. (5.15). Due to the strong constraints on the time evolution of the gravitational constant in the Solar System, the running of the Planck mass on cosmological scales in the late Universe is therefore heavily constrained: $|\alpha_M| \lesssim 0.002$. This is a significant improvement over previous constraints on α_M in the literature, see Ref. [133], and furthermore has the advantage of being independent of a parametrisation of α_M. Using this bound on the evolution of the cosmological gravitational constant should lead to significant improvements of constraints on cosmological models as is shown in, for example, Ref. [150].

The validity of our assumptions should be considered for every fifth force model individually. For models of current interest, the most likely assumption to be invalid is the equivalence principle assumption. For shift-symmetric theories like Vainshtein and kinetic screening models, we argued that the macroscopic equiv-

alence principle is valid on large cosmological scales, where the fifth force is unscreened, independent of the internal structure of the tracer galaxies, which are used to map out the fifth force on these scales. On smaller scales, the equivalence principle is broken, however, due to the nature of Vainshtein screening, the spatial variations of the conformal factor have to be strongly suppressed compared to the variations of the gravitational field on these scales. Thus, the assumption in Eq. (5.7) holds on any scales if it holds in the unscreened regime. For theories which predict the Vainshtein radius of tracer galaxies to be of the order of the largest structures in the universe, the macroscopic equivalence principle would break down and our constraints might not be valid. However, it remains to be seen if such a theory, which is non-linear everywhere, can be consistent with cosmological data. We therefore conclude that most Vainshtein and kinetic screening models should be subject to our constraints on α_M. This validates the conclusions reached in Ref. [99] with an independent approach and extends upon them since our analysis is also valid for some Chameleon-type screening mechanisms.

Chameleon and Symmetron mechanisms can violate the macroscopic equivalence principle and therefore can, in some regions of their parameter space, evade our constraints if the squared coupling scale ξ^2 is large compared to the inverse gravitational potential on the surface of any tracer object. It remains an open question whether there might be a large backreaction effect for theories which violate the macroscopic equivalence principle as is suggested in Ref. [128].

We note that the gravitational constant determining the propagation of gravitational waves can in principle differ from the gravitational constant describing the strength of the gravitational force between massive objects, see Ref. [151] where it is argued that this could lead to a novel way of probing the fifth force. The difference between these two couplings was calculated explicitly for the chameleon in Ref. [152]. The analysis in Ref. [152] assumes that the local and cosmological conformal factors are close to each other, which we confirmed here for the case of large couplings ξ.

We close by remarking that modifications of gravity without a conformal coupling, for example theories with kinetic braiding like in Ref. [89], where the gravitational force is modified through a mixing of the kinetic terms of the metric and the scalar field, are not affected by our constraints. This is also part of the reason why the constraints on α_M derived here do not make our analysis in Chapter 4 irrelevant. Although all Galileon models (Gal 1-5) violate the constraints on α_M due

to the conformal coupling we assumed[10], the core message of the Chapter remains untouched if we simply remove the conformal coupling such that the Galileon field interacts with matter only through kinetic braiding. The shape-dependence of Vainshtein screening will affect the shape of the bispectrum qualitatively in the same way for a Galileon model without conformal coupling.

[10]The values of α_M at redshift $z = 0$ for the 5 models are: Gal 1: 2.72×10^{-2}, Gal 2: 5.69×10^{-2}, Gal 3: 8.95×10^{-2}, Gal 4: 2.62×10^{-2}, Gal 5: 3.18×10^{-2}.

6. The Galileon Two-Body System

Due to the non-linearities in the Galileon equation of motion, it is generally very difficult to find analytical solutions for non-trivial matter sources. Here, we present a calculation of the Galileon field in a hierarchical two-body system, where one mass is significantly larger than the other mass. We find an analytic solution in the proximity of the smaller mass. Remarkably, there exists a regime where the field profile around the smaller mass has elliptical symmetry rather than spherical symmetry. A consequence is that the fifth force will not be parallel to the gravitational force in this regime, which might help break degeneracies with the gravitational force when searching for fifth forces. While the effects of this ellipticity are bound to be small in the Solar System due to very effective screening, the ellipticity might play a role on intergalactic scales, where the magnitude of the fifth force could be of order 4 % of the gravitational force.

The work in this chapter has not been published yet since numerical simulations are necessary to compute a more realistic estimate of the observable consequences of the elliptic field profile on intergalactic scales. We only present very rough order of magnitude estimates for the fifth force here.

6.1. Non-Linearities in the Cubic Galileon

We consider a cubic Galileon model, which couples to matter conformally, see Eq. (3.35). Here, we are mostly interested in studying the non-linear behaviour of the cubic Galileon for non-relativistic matter sources. This means that time-derivatives can be neglected compared to spatial derivatives and the field equation has the form:

$$\Delta\phi + \frac{1}{M^3}\left((\Delta\phi)^2 - (\partial_i\partial_j\phi)\left(\partial^i\partial^j\phi\right)\right) = \frac{\xi}{M_p}\rho. \tag{6.1}$$

It has been shown in the past that the non-linear term in the equation of motion can lead to some unique phenomenology. It was demonstrated in Ref. [149] that

these non-linearities lead to equivalence principle violations in a two body system if the two bodies A and B lie inside of each others Vainshtein radii. This is due to the fact that the individual fields of the two bodies when isolated, ϕ_A and ϕ_B, are not a viable solution to the equation of motion when added $\phi \neq \phi_A + \phi_B$. In other words, the gradient of ϕ_A, which leads to a fifth force acting on object B, is affected by the self-field of object B. Ref. [149] showed that the fifth force acting on object B sourced by object A is reduced by this self-shielding effect.

Some aspects of the two-body system in Galileon gravity have recently been studied both analytically and numerically. The authors of Ref. [153] and Ref. [154] use an effective one-body approach to compute the potential energy stored in a two-body system and the energy dissipated through radiation respectively. The Galileon field profile of the Sun-Earth system has been studied numerically using the finite-difference method in Ref. [155].

Despite those efforts to study the two-body system in Galileon gravity, the Galileon field profile around the Earth has not been analysed analytically yet. This motivated us to investigate the Galileon field profile in the two-body system more closely which lead to the discovery of a fascinating new phenomenon: an induced ellipticity of the field around the smaller mass. This ellipticity makes the fifth force acting on a (third) test particle orbiting the smaller mass dependent on the angular position in the orbit. This effect could in principle be searched for in the Solar System, where the earth takes on the role of the smaller mass and the sun is the larger mass. On intergalactic scales one might identify the larger mass with a large galaxy cluster and the smaller mass with a galaxy outside the cluster.

6.2. The Two-Body Galileon Equation of Motion

We consider two compact, spherical objects, A and B, with masses M_A and M_B. The distance vector between the centres of the two objects shall define the z axis of our coordinate system with the smaller mass M_B sitting at the origin and the larger mass M_A at $z = z_0$, see also Figure 6.1. Due to the axial symmetry of the system, we write the equation of motion, Eq. (6.1), in cylindrical coordinates ($r^2 \coloneqq x^2 + y^2$):

$$\partial_r^2\phi + \frac{1}{r}\partial_r\phi + \partial_z^2\phi + \frac{2}{M^3}\left(\partial_r^2\phi\partial_z^2\phi - \left(\partial_r\partial_z\phi\right)^2 + \frac{1}{r}\partial_r\phi\left(\partial_r^2\phi + \partial_z^2\phi\right)\right) = \frac{\xi}{M_p}\rho. \quad (6.2)$$

We now decompose the field ϕ as:

$$\phi = \phi_A + \varphi. \tag{6.3}$$

The field ϕ_A is defined as the field of the mass M_A if it were isolated.[1] The gradient of ϕ_A outside the mass M_A is a well known result, see Eq. (3.38), if expressed through the radius $R^2 \coloneqq r^2 + (z - z_0)^2$:

$$\partial_R \phi_A(R) = -\frac{M^3}{4} R \left(1 - \sqrt{1 + \frac{r_{V,A}^3}{R^3}} \right), \tag{6.4}$$

with the Vainshtein radius of mass A defined as:

$$r_{V,A}^3 \coloneqq \frac{2\xi M_A}{\pi M_p M^3}. \tag{6.5}$$

The derivatives of ϕ_A with respect to r and z are given by:

$$\begin{aligned}
\partial_r \phi_A = \tfrac{r}{R} \partial_R \phi_A, \quad \partial_r^2 \phi_A &= \frac{r^2}{R^2} \left(\partial_R^2 \phi_A - \frac{\partial_R \phi_A}{R} \right) + \frac{\partial_R \phi_A}{R}, \\
\partial_z \phi_A = \tfrac{z - z_0}{R} \partial_R \phi_A, \quad \partial_z^2 \phi_A &= \frac{(z - z_0)^2}{R^2} \left(\partial_R^2 \phi_A - \frac{\partial_R \phi_A}{R} \right) + \frac{\partial_R \phi_A}{R}, \\
\partial_r \partial_z \phi_A &= \frac{r(z - z_0)}{R^2} \left(\partial_R^2 \phi_A - \frac{\partial_R \phi_A}{R} \right).
\end{aligned} \tag{6.6}$$

We now substitute the decomposition $\phi = \phi_A + \varphi$ into the equation of motion, Eq. (6.2), and obtain:

$$\begin{aligned}
&\Delta\varphi + \frac{1}{M^3} \left((\Delta\varphi)^2 - (\partial_i \partial_j \varphi) \left(\partial^i \partial^j \varphi \right) \right) - \frac{\xi}{M_p} \rho_B \\
&\quad = -\frac{2}{M^3} \left(\partial_r^2 \varphi \partial_z^2 \phi_A + \partial_r^2 \phi_A \partial_z^2 \varphi - 2 \partial_r \partial_z \varphi \partial_r \partial_z \phi_A + \frac{\partial_r \phi_A}{r} \left(\partial_r^2 \varphi + \partial_z^2 \varphi \right) \right. \\
&\qquad \left. + \frac{\partial_r \varphi}{r} \left(\partial_r^2 \phi_A + \partial_z^2 \phi_A \right) \right) \qquad (6.7) \\
&\quad = -\frac{2}{M^3} \left(\partial_R^2 \phi_A - \frac{\partial_R \phi_A}{R} \right) \left(\frac{(z - z_0)^2}{R^2} \partial_r^2 \varphi + \frac{r^2}{R^2} \partial_z^2 \varphi - 2 \frac{r(z - z_0)}{R^2} \partial_r \partial_z \varphi + \frac{\partial_r \varphi}{r} \right) \\
&\qquad - \frac{4}{M^3} \frac{\partial_R \phi_A}{R} \Delta\varphi. \qquad (6.8)
\end{aligned}$$

[1] A similar field decomposition is also used in Ref. [153] to compute the energy dissipated in radiation in a two-body system.

$$= \frac{3}{4}\frac{r_{V,A}^3}{R^3}\left(1+\frac{r_{V,A}^3}{R^3}\right)^{-1/2}\left(\frac{(z-z_0)^2}{R^2}\partial_r^2\varphi + \frac{r^2}{R^2}\partial_z^2\varphi - 2\frac{r(z-z_0)}{R^2}\partial_r\partial_z\varphi + \frac{\partial_r\varphi}{r}\right) + \left(1-\sqrt{1+\frac{r_{V,A}^3}{R^3}}\right)\Delta\varphi. \tag{6.9}$$

We have used that the field ϕ_A satisfies:

$$\Delta\phi_A + \frac{1}{M^3}\left((\Delta\phi_A)^2 - (\partial_i\partial_j\phi_A)\left(\partial^i\partial^j\phi_A\right)\right) = \frac{\xi}{M_p}\rho_A. \tag{6.10}$$

We can simplify the equation of motion, Eq. (6.9), further by subtracting the expression $\Delta\varphi\left(1-\sqrt{1+r_{V,A}^3/R^3}\right)$:

$$\begin{aligned}&\sqrt{1+\tfrac{r_{V,A}^3}{R^3}}\Delta\varphi + \tfrac{1}{M^3}\left((\Delta\varphi)^2 - (\partial_i\partial_j\varphi)\left(\partial^i\partial^j\varphi\right)\right) - \tfrac{\xi}{M_p}\rho_B \\ &= \tfrac{3}{4}\tfrac{r_{V,A}^3}{R^3}\left(1+\tfrac{r_{V,A}^3}{R^3}\right)^{-1/2}\left(\tfrac{(z-z_0)^2}{R^2}\partial_r^2\varphi + \tfrac{r^2}{R^2}\partial_z^2\varphi - 2\tfrac{r(z-z_0)}{R^2}\partial_r\partial_z\varphi + \tfrac{\partial_r\varphi}{r}\right).\end{aligned} \tag{6.11}$$

Since the premise of this study is to examine the field profile of two masses in the deeply non-linear regime, i.e. the regime where the small mass B lies deep within the Vainshtein radius of mass A, we assume $R \ll r_{V,A}$:

$$\begin{aligned}&\sqrt{\frac{r_{V,A}^3}{R^3}}\Delta\varphi + \frac{1}{M^3}\left((\Delta\varphi)^2 - (\partial_i\partial_j\varphi)\left(\partial^i\partial^j\varphi\right)\right) - \frac{\xi}{M_p}\rho_B \\ &\qquad = \frac{3}{4}\sqrt{\frac{r_{V,A}^3}{R^3}}\left(\frac{(z-z_0)^2}{R^2}\partial_r^2\varphi + \frac{r^2}{R^2}\partial_z^2\varphi - 2\frac{r(z-z_0)}{R^2}\partial_r\partial_z\varphi + \frac{\partial_r\varphi}{r}\right).\end{aligned} \tag{6.12}$$

6.3. The Galileon Field around the small mass

In the following, we are only interested in the field profile close to the small mass B. Therefore, we can assume $z_0 \gg |z|, r$ and arrive at the final equation of motion:

$$\sqrt{\frac{r_{V,A}^3}{z_0^3}}\left(\partial_z^2\varphi + \frac{1}{4}\left(\partial_r^2\varphi + \frac{\partial_r\varphi}{r}\right)\right) + \frac{1}{M^3}\left((\Delta\varphi)^2 - (\partial_i\partial_j\varphi)\left(\partial^i\partial^j\varphi\right)\right) = \frac{\xi}{M_p}\rho_B. \tag{6.13}$$

Similar to the isolated mass case, where the terms quadratic in $\partial^2\varphi$ are dominant inside the Vainshtein radius $r_{V,B}$ and subdominant outside, there exist two regimes here, see Figure 6.1. First, the regime inside the 'modified Vainshtein

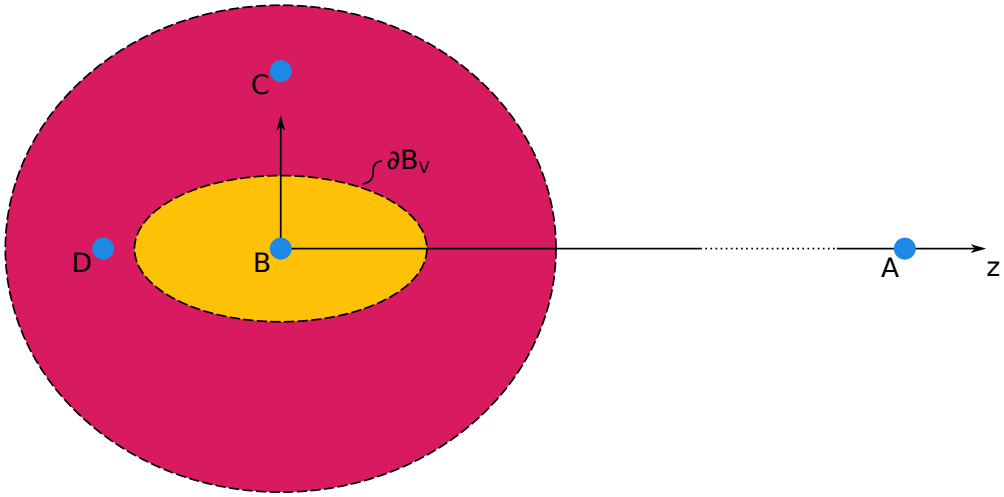

Figure 6.1.: Schematic picture of the relevant regimes for the Galileon field around the smaller object B in a two-body system. The roughly ellipsoidal Vainshtein boundary ∂B_V denotes the transition between the orange regime where the quadratic terms in φ dominate in Eq. (6.14) and the red regime, where the linear terms dominate and the field becomes ellipsoidal. Outside of the red regime, the assumption $z_0 \gg |z|, r$ is violated and numerical calculations are necessary. The points C and D denote the position of two test objects, which are subject to the elliptic fifth force.

boundary' ∂B_V, which is indirectly defined through the relation[2] $|\partial^2\varphi(\partial B_V)| \sim M^3\sqrt{r_{V,A}^3/z_0^3} \sim \partial_z^2\phi_A$. This regime is the equivalent to the regime inside the Vainshtein radius $r_{V,B}$ for the isolated mass since the equation of motion has exactly the same form:

$$\frac{1}{M^3}\left((\Delta\varphi)^2 - (\partial_i\partial_j\varphi)\left(\partial^i\partial^j\varphi\right)\right) = \frac{\xi}{M_p}\rho_B. \tag{6.14}$$

Here, we are much more interested in the solution to the equation of motion outside the Vainshtein boundary ∂B_V. We write the equation of motion, Eq. (6.13), as:

$$\vec{\nabla}\cdot\vec{J} = \sqrt{\frac{z_0^3}{r_{V,A}^3}}\frac{\xi}{M_p}\rho_B, \tag{6.15}$$

where the Galileon current $\vec{J}$ is defined as:

$$\vec{J} \coloneqq \begin{pmatrix} 1/4\partial_x\varphi \\ 1/4\partial_y\varphi \\ \partial_z\varphi \end{pmatrix} + \frac{1}{M^3}\sqrt{\frac{z_0^3}{r_{V,A}^3}}\left(\Delta\varphi\vec{\nabla}\varphi - \left(\vec{\nabla}\partial_i\varphi\right)\partial_i\varphi\right). \tag{6.16}$$

We integrate Eq. (6.15) over a volume V containing all of mass B and use Gauss' theorem:

$$\int_E \vec{J}\cdot\mathrm{d}\vec{E} = \sqrt{\frac{z_0^3}{r_{V,A}^3}}\frac{\xi}{M_p}M_B, \tag{6.17}$$

where $E = \partial V$. Outside the Vainshtein boundary we can neglect the non-linear terms in Eq. (6.16). Defining $\sigma^2 \coloneqq 4(x^2+y^2)+z^2$ the Galileon current becomes:

$$\vec{J} \approx \begin{pmatrix} 1/4\partial_x\varphi \\ 1/4\partial_y\varphi \\ \partial_z\varphi \end{pmatrix} = \frac{\partial_\sigma\varphi}{\sigma}\begin{pmatrix} x \\ y \\ z \end{pmatrix}, \tag{6.18}$$

We now choose the boundary E of our integral in Eq. (6.17) to be an ellipsoid defined as a surface of constant σ. Introducing ellipsoidal coordinates:

$$\vec{x} = \sigma\begin{pmatrix} 1/2\sin\theta\cos\phi \\ 1/2\sin\theta\sin\phi \\ \cos\theta \end{pmatrix}, \tag{6.19}$$

[2]This relation doesn't necessarily define a radius since the spherical symmetry is broken. Therefore the terminology Vainshtein 'boundary' was introduced.

the infinitesimal area vector $\mathrm{d}\vec{E}$ is given by:

$$\mathrm{d}\vec{E} = \frac{\partial\vec{x}}{\partial\theta} \times \frac{\partial\vec{x}}{\partial\phi}\mathrm{d}\theta\mathrm{d}\phi = \frac{\sigma^2}{4}\sin\theta \begin{pmatrix} 2\sin\theta\cos\phi \\ 2\sin\theta\sin\phi \\ \cos\theta \end{pmatrix} \mathrm{d}\theta\mathrm{d}\phi. \tag{6.20}$$

We thus obtain the direct product of the current $\vec{J}$ and the infinitesimal area vector $\mathrm{d}\vec{E}$:

$$\vec{J}\cdot\mathrm{d}\vec{E} = \frac{\sigma^2}{4}\sin\theta\partial_\sigma\varphi\,\mathrm{d}\theta\mathrm{d}\phi. \tag{6.21}$$

Therefore the surface integral in Eq. (6.17) becomes:

$$\begin{aligned} \int_E \vec{J}\cdot\mathrm{d}\vec{E} &= \int_0^{2\pi}\mathrm{d}\phi\int_0^{\pi}\mathrm{d}\theta\frac{\sigma^2}{4}\sin\theta\partial_\sigma\varphi = \pi\sigma^2\partial_\sigma\varphi \\ &= \sqrt{\frac{z_0^3}{r_{V,A}^3}}\frac{\xi}{M_p}M_B. \end{aligned} \tag{6.22}$$

We conclude:

$$\partial_\sigma\varphi = \frac{\xi M_B}{\pi M_p\sigma^2}\sqrt{\frac{z_0^3}{r_{V,A}^3}}. \tag{6.23}$$

Integration in σ gives:

$$\varphi = -\frac{\xi M_B}{\pi M_p\sigma}\sqrt{\frac{z_0^3}{r_{V,A}^3}}. \tag{6.24}$$

We have assumed the boundary condition $\varphi \to 0$ for $\sigma \to \infty$. We observe that the field profile around mass M_B outside of the Vainshtein boundary is ellipsoidal in the sense that surfaces of equal potential are ellipsoids defined through $\sigma^2 = \text{const}$. The ellipsoidal nature of the field originates in the non-linear interactions with the field ϕ_A of mass A. The position of mass A determines the orientation of the ellipsoid, see Figure 6.1.

As one might have expected, outside the Vainshtein boundary, where the equation of motion becomes approximately linear, see Eq. (6.13), the field seems to be almost unscreened in the sense that it scales like $1/\sigma$, i.e. similar to the $1/r$-scaling of the gravitational potential. However, since the factor $\sqrt{z_0^3/r_{V,A}^3}$ appearing in Eq. (6.24) is much smaller than 1 by assumption, the strength of the fifth force is still suppressed compared to gravity. This is a consequence of the mass M_B residing inside the Vainshtein radius $r_{V,A}$ of the larger mass A. We call the factor

$\sqrt{z_0^3/r_{V,A}^3}$ 'screening factor' in the following.

According to our assumptions, the solution in Eq. (6.24) is valid as long as $\partial^2\varphi > M^3\sqrt{r_{V,A}^3/z_0^3}$. By extrapolating the solution outside the Vainshtein boundary up to the boundary, we get an order of magnitude estimate for the location of the boundary, here approximately described by a constant $\sigma_{V,B}$:

$$\left|\partial_\sigma^2\varphi(\sigma_{V,B})\right| = \frac{2\xi M_B}{\pi M_p \sigma_{V,B}^3}\sqrt{\frac{z_0^3}{r_{V,A}^3}} \sim M^3\sqrt{r_{V,A}^3/z_0^3}. \tag{6.25}$$

Solving for $\sigma_{V,B}$ and using the definition of the Vainshtein radius, Eq. (6.5), we get an approximation for the location of the Vainshtein boundary around mass B:

$$\sigma_{V,B} \sim z_0\sqrt[3]{\frac{M_B}{M_A}}. \tag{6.26}$$

Unlike the Vainshtein radius of the isolated mass B ($r_{V,B}^3 = 2\xi M_B/\pi M_p M^3$), the Vainshtein boundary $\sigma_{V,B}$ is independent of the model parameters M^3 and ξ.

It is important to remark that the assumption $z_0 \gg r, |z|$ only holds outside the Vainshtein boundary if the hierarchy between the masses M_A and M_B is large enough such that $\sigma_{V,B} \ll z_0$.

6.4. Test Masses in the Elliptic Galileon Field

The solution in Eq. (6.24) is the main result of this Chapter. The field profile around a spherical mass M_B, which is located inside the Vainshtein radius of a larger spherical mass M_A is ellipsoidal and scales like $1/\sigma$ in a regime outside the Vainshtein boundary of object B, but close enough to mass B such that the assumption $z_0 \gg r, |z|$ holds. In this section we demonstrate explicitly how the elliptic fifth force acts on test masses in the regime outside the Vainshtein boundary.

We consider two test masses C and D at the same distance $l \gtrsim \sigma_{V,B}$ from mass M_B, but C is located at $r = l$, $z = 0$, while D is located at $r = 0$, $z = -l$, see Figure 6.1. In the following we denote by $\vec{a}_{ij}$ the acceleration of object i due to the fifth force sourced by object j. The accelerations of the test masses C and D

sourced by mass M_B are obtained from the solution in Eq. (6.24):

$$\vec{a}_{CB} = -\frac{\xi}{M_p}\vec{\nabla}\varphi(r=l,z=0) = -\frac{\xi^2 M_B}{2\pi M_p^2 l^2}\sqrt{\frac{z_0^3}{r_{V,A}^3}}\hat{e}_r, \tag{6.27}$$

$$\vec{a}_{DB} = -\frac{\xi}{M_p}\vec{\nabla}\varphi(r=0,z=-l) = \frac{\xi^2 M_B}{\pi M_p^2 l^2}\sqrt{\frac{z_0^3}{r_{V,A}^3}}\hat{e}_z. \tag{6.28}$$

We observe that the acceleration of test mass D is twice the acceleration of test mass C, which is a consequence of the elliptic field.

However, there is an important subtlety we have not taken into account yet. The test masses also experience a fifth force sourced by mass M_A which is larger than the elliptic force sourced by mass M_B by assumption of $l \gtrsim \sigma_{V,B} \sim z_0\sqrt[3]{M_B/M_A}$:

$$\begin{aligned}|\vec{a}_{CA}| \approx |\vec{a}_{DA}| \approx |\vec{a}_{BA}| &\sim \frac{\xi}{M_p}\partial_R\phi_A(R=z_0) \approx \frac{\xi^2 M_A}{2\pi M_p^2}\frac{1}{\sqrt{z_0 r_{V,A}^3}} \\ &= \frac{M_A}{M_B}\frac{l^2}{z_0^2}|\vec{a}_{CB}| \gtrsim \sqrt[3]{\frac{M_A}{M_B}}|\vec{a}_{CB}| \gg |\vec{a}_{CB}|.\end{aligned} \tag{6.29}$$

In the first line we made use of the solution in Eq. (6.4) for the field ϕ_A.

The fact that the elliptic force is subdominant compared to the fifth force from mass M_A does not mean that the elliptic force is negligible in all circumstances. For example, if we observe the test masses C and D from the reference frame of mass M_B, only the relative accelerations $\vec{a}_{DA} - \vec{a}_{BA}$ and $\vec{a}_{CA} - \vec{a}_{BA}$ are relevant. At first order in the small quantity $l/z_0 \ll 1$ we obtain $\vec{a}_{DA} - \vec{a}_{BA} \approx -\frac{l}{2z_0}\vec{a}_{BA}$, which is of the same order as $\vec{a}_{DB}$ if $l \sim \sigma_{V,B}$.[3] Therefore, both the elliptic force sourced by mass M_B and the fifth force from mass M_A are equally important in the reference frame of mass M_B. The discovery of the elliptic field profile is essential for testing Vainshtein screened theories in non-linear environments.

6.5. Observable Consequences

In this section we explore how the ellipsoidal nature of the field may be employed for detecting the fifth force on solar-system or intergalactic scales. We are content with rough order of magnitude estimates of the fifth force and leave precise

[3] Similarly, one can show that $\vec{a}_{CA} - \vec{a}_{BA}$ is also of the same order as $\vec{a}_{CB}$ in the reference frame of mass M_B

predictions for realistic experimental and observational set-ups for future work.

For the purpose of estimating the magnitude of the ellipsoidal force, we consider two simplified two-body systems, the sun-earth system, where the sun is mass A and the earth is mass B, and secondly, the neighbourhood of the local group, which we crudely approximate as a two-body system with the Virgo cluster being mass A and the local group being mass B.

We first investigate the sun-earth system. In Appendix A.3 we argue that the Vainshtein radius around mass M_A for a cosmologically relevant cubic galileon model is expected to be of order:

$$r_{V,A}^3 \gtrsim M_A 10^{-39}\,\mathrm{Mpc}^3/\mathrm{kg}. \tag{6.30}$$

Since a smaller Vainshtein radius will typically lead to larger effects from the fifth force, we obtain, in the best case scenario, i.e. the scenario where the Vainshtein radius takes the lower bound given by Eq. (6.30), for the sun-earth system:

$$r_{V,A} \sim 1.3\,\mathrm{kpc} \sim 2.6 \times 10^8\,\mathrm{AU}. \tag{6.31}$$

The screening factor $\sqrt{z_0^3/r_{V,A}^3}$, which determines the strength of the fifth force sourced by object B, i.e. the earth, relative to gravity, is of order:

$$\sqrt{\frac{z_0^3}{r_{V,A}^3}} \sim 2.4 \times 10^{-13}. \tag{6.32}$$

As a next step we consider the magnitude of the Vainshtein boundary around the earth in the sun-earth system. For $M_A = M_\odot \approx 2 \times 10^{30}\,\mathrm{kg}$, $M_B \approx 6 \times 10^{24}\,\mathrm{kg}$ and $z_0 = 1\,\mathrm{AU}$, we obtain:

$$\sigma_{V,B} \approx 0.014\,\mathrm{AU}. \tag{6.33}$$

This is of order 10 times the distance between the earth and the moon. This means that the movement of the moon is not affected by the elliptic field profile and it is safe to treat the earth and the moon as a single matter source for rough order of magnitude estimates. Compared to the Vainshtein radius of the isolated earth ($r_{V,B} \gtrsim 3.7 \times 10^6\,\mathrm{AU}$), the Vainshtein boundary $\sigma_{V,B}$ is significantly smaller.

Surprisingly, the Vainshtein boundary is located in the proximity of the Lagrange points L_1 and L_2 of the sun-earth system, which are located at around $\sim 0.01\,\mathrm{AU}$. These Lagrange points have been used in the past for various space-

missions[4] and will likely be used again in the future. Therefore, it is reasonable to expect that the gravitational forces at the Vainshtein boundary will be put to the test by future space missions.

To precisely compute the effect of the fifth force on the movement of test objects in the regime around the Lagrange points, a numerical analysis of the equation of motion, Eq. (6.13), is necessary since our solution in Eq. (6.24) is not valid at the border of the regime. However, it seems likely that some of the features of the solution outside the Vainshtein boundary will also be found at the boundary. While the ellipticity might be less pronounced, it will still be present.

As we discussed in Chapter 5, lunar laser ranging constrains the evolution of the gravitational constant to an accuracy of $\dot{G}/G \sim 1 \times 10^{-13}\,\mathrm{yr}^{-1}$, see Ref. [134]. This demonstrates that a force of order $\sim 1 \times 10^{-13}$ the strength of gravity, as obtained in Eq. (6.32), is in principle detectable at the distance of the moon. However, the Vainshtein boundary is located at a distance ten times the distance to the moon, where the gravitational force is decreased by a factor of ~ 100, and experiments are much more difficult to perform. We conclude that it will be challenging to detect the elliptic fifth force in the Solar System, but there might be some hope with future technology.

We expect the fifth force on galaxy and galaxy-cluster scales to be much less suppressed than on solar-system scales. As a significantly oversimplified example of an intergalactic two-body system we consider the mass M_A to be the Virgo cluster, which has a mass of $M_A \approx 1.2 \times 10^{15} M_\odot$, see Ref. [156], and the smaller mass M_B to be the local group, $M_B \sim 2 \times 10^{12} M_\odot$. The distance between the two objects is roughly of order $z_0 \sim 16.5\,\mathrm{Mpc}$, see Ref. [157]. We ignore here that the local matter distribution is significantly more complicated than a simple two-body system. Since we are only interested in rough order of magnitude estimates, this simplified scenario seems sufficient.

Using the estimate in Eq. (6.30), we obtain the best-case Vainshtein radius of the Virgo cluster:

$$r_{V,A} \sim 134\,\mathrm{Mpc}. \tag{6.34}$$

The local group is therefore easily inside the Vainshtein radius of the Virgo cluster.

[4] E.g. WMAP, Planck, Gaia and the Herschel observatory at L_2 and the LISA Pathfinder at L_1.

The screening factor becomes:

$$\sqrt{\frac{z_0^3}{r_{V,A}^3}} \sim 0.04. \tag{6.35}$$

An order 4 % effect compared to gravity is small given the large uncertainties on galactic scales,[5] but might be measurable in the foreseeable future.

Using Eq. (6.26), we obtain the Vainshtein boundary around the local group:

$$\sigma_{V,B} \sim 0.1 z_0 \sim 1.65\,\mathrm{Mpc}. \tag{6.36}$$

The Vainshtein boundary thus includes the entire local group[6] and is an order of magnitude smaller than the Vainshtein radius of the isolated local group ($r_{V,B} \sim 16\,\mathrm{Mpc}$).

Galaxies outside the local group but still fairly close, such that the assumption $z_0 \gg r, |z|$ is a decent approximation, will experience the elliptical fifth force. Numerical simulations of the local matter distribution are necessary to compute the precise effects of the elliptic fifth force on nearby galaxies and to formulate useful observables sensitive to the effects of the ellipticity, since accelerations are not directly observable at this scale.

6.6. Summary

In this chapter we calculated the Galileon field in a hierarchical two-body system, where one mass is significantly smaller than the other, in the proximity of the smaller mass. We observed the emergence of two important regimes depicted in Figure 6.1. Inside the elliptic Vainshtein boundary around the small mass, see Eq. (6.26), the solution is equivalent to the screened solution if the small mass was isolated, see Eq. (6.14). Outside the Vainshtein radius but still close to the small mass, the solution is elliptic, see Eq. (6.24), with dependence $\varphi \sim 1/\sigma$. In this regime the solution is suppressed compared to gravity by the screening factor $\sqrt{z_0^3/r_{V,A}^3}$. Test masses in the regime outside the Vainshtein boundary will

[5] For example the distances of nearby galaxies outside the local group are known to roughly $\sim 5\,\%$ accuracy, see Ref. [158].

[6] The distance between the Milky Way and the Andromeda galaxy is $(765 \pm 28)\,\mathrm{kpc}$, see Ref. [159].

experience a force towards mass M_B which depends on their angular position. In the reference frame of mass M_B this elliptic force is comparable to the fifth force from object M_A.

The elliptic nature of the field indicates that there are likely less degeneracies with the radially symmetric gravitational field when testing gravity experimentally or observationally. Potentially, this could make a detection of the fifth force easier.

We have considered two scenarios, where the elliptic nature of the fifth force might play a role. First, we considered the sun-earth system, where we found that the elliptic field profile is approximately valid around the Lagrange points L_1 and L_2. The proximity of the Lagrange points demonstrates the accessibility of the regime to potential future space missions testing the gravitational force in this regime. However, we also found that a realistic value for the screening factor, see Eq. (6.32), is extremely small making a detection of the fifth force unlikely in the near future.

Second, we considered the strongly oversimplified two-body system of the Virgo cluster and the local group. We found that galaxies in the close proximity of the local group experience an elliptical fifth force sourced by the local group. The magnitude of the fifth force acting on those test galaxies could be of order $4\,\%$ of the gravitational force. Since the fifth force is not a direct observable on intergalactic scales, numerical simulations are required to make more realistic predictions for observable consequences in the dynamics of the galaxies around the local group.

7. Summary and Outlook

In this thesis we have explored three approaches to testing screened fifth forces on scales ranging from solar-system scales to cosmological scales.

First, in Chapter 4 we demonstrated how Vainshtein screening affects the cosmic matter bispectrum focussing in particular on the connections to the shape dependence of Vainshtein screening in real space. In real space Vainshtein screening is most effective around spherical objects, less effective for matter sources with cylindrical symmetry and altogether absent for planar symmetry. Analogously, we found that the fifth-force contributions to the bispectrum are maximal for an equilateral configuration of the bispectrum triangle $\vec{k}_1 + \vec{k}_2 + \vec{k}_3 = 0$ and vanish in the flattened limit. Vainshtein screening is thus most effective in scenarios with maximal symmetry in the three cartesian directions of space.

For a conformally coupled cubic Galileon we demonstrated that the non-linear effects of Vainshtein screening in the matter bispectrum scale like $\propto a^{3/2}$ with the scale factor and are thus non-degenerate with the contributions from general relativity. The magnitude of the signal relative to the GR signal in the bispectrum is proportional to the fractional energy density Ω_ϕ of the scalar field. For a realistic cubic Galileon model, which is not excluded at the level of the background and the linear perturbations, the signal on the bispectrum is bound to be at the percent level or lower. A detection of the fifth force through the bispectrum thus seems unlikely since the fifth-force signal on the cosmological background evolution and the linear perturbations will be of a similar magnitude while typically being easier to observe. However, the signal on the bispectrum is very unique to Vainshtein screened fifth forces and may thus be used to differentiate between different fifth force models which have similar signals at the level of the background and linear perturbations.

In our second project, see Chapter 5, we examined the applicability of solar-system constraints on the evolution of the gravitational constant to cosmological scales. Under quite general assumptions we found that the lunar-laser ranging

results put tight constraints on the evolution of the cosmological gravitational constant. This makes self acceleration as an explanation for the accelerated expansion of the late Universe extremely difficult to realise.

The constraints from lunar-laser ranging can be avoided if the screening mechanism leads to violations of the equivalence principle even on the largest cosmological scales, where galaxies are typically used as test objects to trace the gravitational field. For Vainshtein screening this may be achieved if the Vainshtein radius of the tracer galaxies is of order the size of the observable Universe. For Chameleon-type screening mechanisms, the constraints can be avoided if all tracer objects – on any scale, including galactic scales – are screened. This is only possible if the coupling ξ of the Chameleon or Symmetron field to matter is large compared to the inverse Newtonian potential at the boundary of all relevant tracer objects.

The surviving fifth force models with self acceleration are thus extreme in the sense that they are screened even on the largest cosmological scales. It is an open and potentially exciting question how the background evolution of such highly non-linear theories would behave and if they indeed allow a consistent self accelerating solution. A back reaction of the non-linearities on the background evolution seems plausible. We leave a detailed analysis of such extreme models for future work.

Finally, we investigated the behaviour of the Galileon field in a hierarchical two-body system, see Chapter 6. We observed that the Galileon field around the smaller mass is elliptical rather than spherically symmetric at a distance larger than the Vainshtein boundary. While this ellipticity has a very small effect on the dynamics in the sun-earth system, it could be at the percent level compared to gravity on intergalactic scales. The elliptic field leads to an asymmetric fifth force around field galaxies which lie inside the Vainshtein radius of a galaxy cluster. We demonstrated how this asymmetric fifth force arises around the local group which lies inside the Vainshtein radius of the Virgo cluster, but this analysis also applies more generally to any field galaxy.

We conclude that the dynamics of field galaxies may represent a new test for Vainshtein screened fifth forces. However, our analytic calculation in Chapter 6 has to be confirmed by numerical simulations in the context of complicated matter sources like the large-scale structures around the local group or other field galaxies. We are optimistic that our simple two-body model gives a decent order of magnitude estimate, which motivates us to make a detailed numerical analysis in the future.

A. Appendix

A.1. Further Details on the Shape-Dependence of Vainshtein Screening

A.1.1. Formulas and Definitions

The Conservation equations, Einstein equations and the Galileon field equation at linear order are given by:

$$\delta^{(1)\prime} = -\Delta v^{(1)} + 3\Phi^{(1)\prime} + \frac{1}{2(1+\phi)}\left(\phi^{(1)\prime} - \phi'\frac{\phi^{(1)}}{1+\phi}\right), \tag{A.1}$$

$$v^{(1)\prime} + \mathcal{H}v^{(1)} = -\Psi^{(1)} - \frac{1}{2(1+\phi)}\left(\phi' v^{(1)} + \phi^{(1)}\right), \tag{A.2}$$

$$-\frac{a^2 G_0^0}{M_p^2} = 2\Delta\Phi^{(1)} = 3a^2\bar{\rho}\delta^{(1)} + \frac{C_3\phi'^2}{a^2}\Delta\phi^{(1)}, \tag{A.3}$$

$$a^2\partial_i^{-1}\partial_j^{-1}G_j^i = \Phi^{(1)} - \Psi^{(1)} = 0, \tag{A.4}$$

$$\left(C_2 - \frac{2C_3}{a^2}(\phi'' + \mathcal{H}\phi')\right)\Delta\phi^{(1)} - \frac{C_3\phi'^2}{a^2}\Delta\Phi^{(1)} = \frac{3\bar{\rho}a^2}{2(1+\phi)}\left(\delta^{(1)} - \frac{\phi^{(1)}}{1+\phi}\right). \tag{A.5}$$

The functions $\mathcal{A}_{GR}$, $\mathcal{B}_{GR}$, $\mathcal{B}_\phi$ used to describe F_2 in Eq. (4.37) are defined by:

$$\mathcal{A}_{GR}(\tau) \coloneqq 2\int_{\tau_i}^{\tau} \mathrm{d}\tilde{\tau}\, G(\tau,\tilde{\tau})\left(f^2(\tilde{\tau})\mathcal{H}^2(\tilde{\tau}) + \alpha_\delta(\tilde{\tau})\right)\frac{D_+^2(\tilde{\tau})}{D_+^2(\tau)}, \tag{A.6}$$

$$\begin{aligned}\mathcal{B}_{GR}(\tau) &\coloneqq 2\int_{\tau_i}^{\tau} \mathrm{d}\tilde{\tau}\, G(\tau,\tilde{\tau}) f^2(\tilde{\tau})\mathcal{H}^2(\tilde{\tau})\frac{D_+^2(\tilde{\tau})}{D_+^2(\tau)} \\ &= \frac{2}{D_+^2(\tau)}\int_{\tau_i}^{\tau} \mathrm{d}\tilde{\tau}\, G(\tau,\tilde{\tau})\left(D_+'\right)^2,\end{aligned} \tag{A.7}$$

$$\mathcal{B}_\phi(\tau) \coloneqq -\int_{\tau_i}^{\tau} \mathrm{d}\tilde{\tau}\, G(\tau,\tilde{\tau})\frac{9C_3\bar{\rho}^2a^2\alpha_\phi^3}{4A^3(\tau)}\frac{D_+^2(\tilde{\tau})}{D_+^2(\tau)}. \tag{A.8}$$

We now present the Jordan-frame Horndeski functions for the cubic Galileon model defined in Eq. (4.1). These may be computed with the transformation rules in Eq. (3.22) using the conformal factor $\Omega^{-2} = 1 + \phi$. Solving for the non-tilded Jordan-frame quantities gives:

$$\begin{aligned} K(\phi, X) &= -\frac{\Lambda_c}{(1+\phi)^2} - \frac{1}{1+\phi}\left(-C_2 + \frac{3}{2(1+\phi)^2}\right) X \\ &\quad -\frac{2C_3}{(1+\phi)} X^2, \qquad \text{(A.9)} \\ G_3(\phi, X) &= -C_3 X, \qquad \text{(A.10)} \\ G_4(\phi, X) &= \frac{1}{2(1+\phi)}. \qquad \text{(A.11)} \\ G_5(\phi, X) &= 0. \qquad \text{(A.12)} \end{aligned}$$

Further transformation rules between Einstein and Jordan-frame quantities are:

$$\begin{aligned} a &= \sqrt{1+\phi}\tilde{a}, \qquad \text{(A.13)} \\ \mathcal{H} &= \tilde{\mathcal{H}} + \frac{\phi'}{2(1+\phi)}, \qquad \text{(A.14)} \\ \rho_m &= (1+\phi)^{-2}\,\tilde{\rho}_m. \qquad \text{(A.15)} \end{aligned}$$

A.1.2. The Source Term $S^{(\delta)}$

Here we give the full expression for the source term $S^{(\delta)}$ in Eq. (4.29) in terms of the source terms $S^{(1)}$, $S^{(4)}$, $S^{(5)}$, $S^{(6)}$ and $S^{(7)}$ which can be found in the appendix of Ref. [101]. Since we have a Galileon model with a conformal coupling some of the source terms computed in Ref. [101] have to be expanded for our model:

$$\begin{aligned} \tilde{S}^{(5)} &\coloneqq S^{(5)} + \frac{\bar{\rho}}{(1+\phi)^2}\phi^{(1)}\delta^{(1)}, \qquad \text{(A.16)} \\ \tilde{S}^{(6)} &\coloneqq S^{(6)} + \frac{1}{1+\phi}\left(\delta^{(1)}\phi^{(1)\prime} - \frac{\phi'\delta^{(1)}\phi^{(1)} + \phi^{(1)}\phi^{(1)\prime}}{1+\phi}\right), \qquad \text{(A.17)} \\ \tilde{S}^{(7)} &\coloneqq S^{(7)} + \frac{1}{(1+\phi)^2}\left(\left(\partial_i\phi^{(1)}\right)\left(\partial^i\phi^{(1)}\right) + \phi^{(1)}\Delta\phi^{(1)}\right) \\ &\quad -\frac{1}{1+\phi}\left(\left(\partial_i\delta^{(1)}\right)\left(\partial^i\phi^{(1)}\right) + \delta^{(1)}\Delta\phi^{(1)}\right) \\ &\quad -\frac{\phi'}{1+\phi}\left(\partial_i\delta^{(1)}\partial^i v^{(1)} + \delta^{(1)}\Delta v^{(1)}\right). \qquad \text{(A.18)} \end{aligned}$$

The source term $S^{(\delta)}$ can now be defined as:

$$\begin{aligned} S^{(\delta)} &= -\left(1+\frac{C_3\phi'^2\alpha_\phi}{2a^2A(\tau)}\right)\left(\frac{S^{(1)}}{2}-\frac{S^{(4)}}{k^2}\right)+\frac{\alpha_\phi}{2A(\tau)}\tilde{S}^{(5)} \\ &\quad +\tilde{S}^{(6)\prime}+\tilde{S}^{(6)}\left(\mathcal{H}+\frac{\phi'}{2(1+\phi)}\right)-\tilde{S}^{(7)}. \end{aligned} \tag{A.19}$$

A.1.3. Simplification of the Form Factor $\mathbf{F_2}$

In this section we demonstrate that $\mathcal{A}_{GR}+\mathcal{B}_{GR}=2$ which greatly simplifies the form factor F_2 in Eq. (4.37). For this, we firstly note that the following differential equation holds for the Wronskian W defined in Eq. (4.36):

$$W' = -\left(\mathcal{H}+\frac{\phi'}{2(1+\phi)}\right)W. \tag{A.20}$$

Now we can compute $\mathcal{A}_{GR}+\mathcal{B}_{GR}$. For simplicity of notation we will not write all of the dependencies on the integration variable $\tilde{\tau}$ explicitly, however, we will denote dependencies if they differ from $\tilde{\tau}$ or are crucial for the understanding of the equations.

$$\mathcal{A}_{GR}+\mathcal{B}_{GR} = 2\int_{\tau_i}^{\tau}\mathrm{d}\tilde{\tau}\,G(\tau,\tilde{\tau})\left(2f^2\mathcal{H}^2+\alpha_\delta\right)\frac{D_+^2(\tilde{\tau})}{D_+^2(\tau)} \tag{A.21}$$

$$\begin{aligned} &= \frac{2}{D_+^2(\tau)}\int_{\tau_i}^{\tau}\mathrm{d}\tilde{\tau}\,W^{-1}(\tilde{\tau})\left(D_-(\tau)D_+(\tilde{\tau})-D_+(\tau)D_-(\tilde{\tau})\right) \\ &\quad \times\left(2D_+'^2+D_+''D_++\left(\mathcal{H}+\frac{\phi'}{2(1+\phi)}\right)D_+'D_+\right) \end{aligned} \tag{A.22}$$

From Eq. (A.21) to Eq. (A.22) we used that the linear growth equation, Eq. (4.22), holds for the growth function D_+. Now we will integrate parts of this integral by parts:

$$\begin{aligned} \mathcal{A}_{GR}+\mathcal{B}_{GR} &\ni \frac{2}{D_+^2(\tau)}\int_{\tau_i}^{\tau}\mathrm{d}\tilde{\tau}\frac{D_+''D_+}{W}\left(D_-(\tau)D_+(\tilde{\tau})-D_+(\tau)D_-(\tilde{\tau})\right) \\ &= -\frac{2}{D_+^2(\tau)}\int_{\tau_i}^{\tau}\mathrm{d}\tilde{\tau}\left[\left(\frac{D_+'}{W}-\frac{W'D_+}{W^2}\right)\left(D_-(\tau)D_+(\tilde{\tau})-D_+(\tau)D_-(\tilde{\tau})\right)\right. \\ &\quad \left.+\frac{D_+}{W}\left(D_-(\tau)D_+'(\tilde{\tau})-D_+(\tau)D_-'(\tilde{\tau})\right)\right]D_+'. \end{aligned} \tag{A.23}$$

Substituting this result back into the full expression for $\mathcal{A}_{GR}+\mathcal{B}_{GR}$ in Eq. (A.22) and using Eq. (A.20), we arrive at:

$$\begin{aligned}\mathcal{A}_{GR}+\mathcal{B}_{GR} &= \frac{2}{D_+^2(\tau)}\int_{\tau_i}^{\tau}\mathrm{d}\tilde{\tau}\,W^{-1}\left[D_+'^2(\tilde{\tau})\left(D_-(\tau)D_+(\tilde{\tau})-D_+(\tau)D_-(\tilde{\tau})\right)\right.\\ &\qquad\left.-D_+(\tilde{\tau})D_+'(\tilde{\tau})\left(D_-(\tau)D_+'(\tilde{\tau})-D_+(\tau)D_-'(\tilde{\tau})\right)\right]\\ &= \frac{2}{D_+(\tau)}\int_{\tau_i}^{\tau}\mathrm{d}\tilde{\tau}\,D_+'(\tilde{\tau})\frac{D_-'(\tilde{\tau})D_+(\tilde{\tau})-D_+'(\tilde{\tau})D_-(\tilde{\tau})}{W(\tilde{\tau})}\\ &= \frac{2}{D_+(\tau)}\int_{\tau_i}^{\tau}\mathrm{d}\tilde{\tau}\,D_+'(\tilde{\tau})=2. \end{aligned}\tag{A.24}$$

A.2. The Local Conformal Factor of the Cubic Galileon

We will show here how the conservative estimate in Eq. (5.13) can be made far more constraining for a cubic Galileon model. In other words, we will demonstrate that for the cubic Galileon the difference between the local and cosmological conformal factors is even more constrained than the bound in Eq. (5.15), which relied on the estimate in Eq. (5.13). We define our model through the cubic Galileon action in Eq. (3.35) which has the following equation of motion, see Eq. (3.36):

$$\Box\phi+\frac{1}{M^3}\left((\Box\phi)^2-R_{\mu\nu}\nabla^\mu\phi\nabla^\nu\phi-\left(\nabla_\mu\nabla_\nu\phi\right)\left(\nabla^\mu\nabla^\nu\phi\right)\right)=\frac{\xi}{M_p}\rho. \tag{A.25}$$

For brevity, we consider a simple setting with an isolated, spherically symmetric overdensity $\rho_l(r)$ of radius r_0 on top the cosmological background density $\bar{\rho}(\tau)$, where τ is the conformal time. For the metric, we assume a FLRW metric with a small gravitational potential ($|\Phi_N|\ll 1$):

$$\mathrm{d}s^2=a^2\left[-(1+2\Phi_N)\mathrm{d}\tau^2+(1-2\Phi_N)\mathrm{d}\vec{x}^2\right]. \tag{A.26}$$

On the boundary ($r\to\infty$), the solution for ϕ has to approach the cosmological solution $\bar{\phi}$, which fulfils the background equation of motion:

$$\frac{\xi}{M_p}\bar{\rho}(\tau)=-\frac{1}{a^4}\frac{\partial}{\partial\tau}\left(a^2\bar{\phi}'\right)+\frac{3}{M^3a^4}\frac{\partial}{\partial\tau}\left(\mathcal{H}\bar{\phi}'^2\right). \tag{A.27}$$

We now make the ansatz:

$$\phi(r,\tau) = \bar{\phi}(\tau) + \phi_l(r,\tau) \qquad \text{with} \qquad \phi_l(r\to\infty,\tau)\to 0, \tag{A.28}$$

and make the quasi-static approximation, which states that time derivatives of the local solution ϕ_l can be neglected compared to spatial derivatives if we consider sub-horizon scales. Assuming a small gravitational potential $|\Phi_N| \ll 1$, the equation of motion for the scalar field and the (0,0) component of the Einstein equations become:

$$\begin{aligned} a^2r^2\frac{\xi}{M_p}\rho_l(r) &= \frac{\partial}{\partial r}\left[\left(1-\frac{2}{M^3a^3}\frac{\partial}{\partial\tau}\left(a\bar{\phi}'\right)\right)r^2\phi_{l,r} + \frac{2}{a^2M^3}r\phi_{l,r}^2 - \frac{\bar{\phi}'^2}{M^3a^2}r^2\Phi_{N,r}\right], \\ a^2r^2\rho_l(r) &= \frac{\partial}{\partial r}\left[2M_p^2r^2\Phi_{N,r} - \frac{\bar{\phi}'^2}{M^3a^2}r^2\phi_{l,r}\right]. \end{aligned} \tag{A.29}$$

Combining the two equations and eliminating the gravitational potential yields:

$$\frac{\tilde{\xi}}{M_p}\rho_l(r) = \frac{\lambda(\tau)}{a^2r^2}\frac{\partial}{\partial r}\left(r^2\phi_{l,r}\right) + \frac{1}{a^4M^3}\frac{2}{r^2}\frac{\partial}{\partial r}\left(r\phi_{l,r}^2\right), \tag{A.30}$$

where we defined the useful quantities:

$$\begin{aligned} \lambda(\tau) &:= 1-\frac{2}{M^3a^3}\frac{\partial}{\partial\tau}\left(a\bar{\phi}'\right) - \frac{\bar{\phi}'^4}{2M^6M_p^2a^4}, \\ \tilde{\xi} &:= \xi + \frac{\bar{\phi}'^2}{2M^3M_pa^2}. \end{aligned} \tag{A.31}$$

It is now straightforward to solve the equation of motion, Eq. (A.30). Integrating once over r and solving the quadratic equation for $\phi_{l,r}$ gives:[1]

$$\phi_{l,r} = -\frac{\lambda(\tau)a^2M^3}{4}r\left(1-\sqrt{1+\frac{r_V^3}{r^3}\frac{M(r,\tau)}{M_0}}\right), \tag{A.32}$$

where we defined the total mass of the object M_0 and the mass inclosed in the radius r:

$$M(r,\tau) := 4\pi\int_0^r \mathrm{d}r'\, r'^2\rho_l(r',\tau). \tag{A.33}$$

[1] We drop the second branch of the solution, where the sign in front of the square root is reversed, because it doesn't converge for $r\to\infty$.

We also introduced the Vainsthein radius:

$$r_V(\tau) \coloneqq \left(\frac{2\tilde{\xi} M_0}{\pi M_p M^3 \lambda^2(\tau)} \right)^{1/3}. \tag{A.34}$$

On large scales ($r \gg r_V$), the field gradient $\phi_{l,r}$ has a $1/r^2$ dependence , i.e. is unscreened. We use this unscreened solution in the Einstein equation, Eq. (A.29), and obtain:

$$\frac{\partial}{\partial r}\left(r^2 \Phi_{N,r}\right) = \frac{a^2 r^2}{2M_p^2}\rho_l(r)\alpha, \quad \text{where} \quad \alpha \coloneqq 1 + \frac{\bar{\phi}'^2 \tilde{\xi}}{M^3 a^2 \lambda(\tau) M_p}. \tag{A.35}$$

Therefore, the acceleration of a test particle due to the fifth force, $\vec{a}_5$, compared to the acceleration due to gravity, $\vec{a}_N$, becomes for $r \gg r_V$:

$$\frac{|\vec{a}_5|}{|\vec{a}_N|} = \frac{2\xi\tilde{\xi}}{\lambda(\tau)\alpha}. \tag{A.36}$$

Observations of the linear growth of structure in our Universe make it unlikely that this fraction could be significantly larger than 1, see Section 5.3.1, and also imply $\alpha = \mathcal{O}(1)$. Therefore, we assume in the following:

$$\frac{2\xi\tilde{\xi}}{\lambda(\tau)} \lesssim 1. \tag{A.37}$$

In some situations the solution in Eq. (A.32) can be analytically integrated once more in r. For example outside of the boundaries of the overdensity ($r > r_0$) the solution is given in terms of the Hypergeometric function ${}_2F_1$:

$$\phi_l(r,\tau) = -\frac{\lambda(\tau)a^2M^3}{4}r^2\left(\frac{1}{2} - 2\sqrt{1+\left(\frac{r_V(\tau)}{r}\right)^3} + \frac{3}{2}\,{}_2F_1\left[-\frac{2}{3};\frac{1}{2};\frac{1}{3};-\left(\frac{r_V(\tau)}{r}\right)^3\right]\right). \tag{A.38}$$

Deep inside the Vainsthein radius ($r \ll r_V$) this solution is well approximated by:

$$\phi_l(r,\tau) \approx -\frac{\gamma}{2}\lambda(\tau)a^2M^3r_V^2(\tau), \tag{A.39}$$

where we abbreviated:

$$\gamma \coloneqq \frac{3\Gamma\left(\frac{1}{3}\right)\Gamma\left(\frac{7}{6}\right)}{4\sqrt{\pi}} \approx 1.0516\ldots \tag{A.40}$$

If the density profile of the overdensity is well described by a power law $\rho_l \propto r^{-\beta}$, the solution inside the overdensity becomes (for $\beta \neq 4$):

$$\phi_l(r < r_0, \tau) = \phi_l(r_0, \tau) + \frac{\lambda(\tau) a^2 M^3 r_V^2}{4(2-\beta/2)} \left(\frac{r^{2-\beta/2}}{\sqrt{r_V} r_0^{3/2-\beta/2}} - \sqrt{\frac{r_0}{r_V}} \right). \tag{A.41}$$

If $\beta < 4$ and the Vainshtein radius is much larger than the overdensity itself ($r_0 \ll r_V$), i.e. the overdensity is screened, this solution is actually well approximated by just $\phi_l(r_0, \tau)$. $\beta < 4$ is a very reasonable assumption for overdensities like the Milky Way which are typically assumed to have a NFW profile with $\beta = 1$ in the center of the galaxy and $\beta = 3$ on the outskirts of the galaxy.

We summarize, if $r_0 \ll r_V$ and $\beta < 4$, the solution for ϕ_l deep inside the Vainshtein radius is approximately given by:

$$\phi_l(r, \tau) \approx -\frac{\gamma}{2} \lambda(\tau) a^2 M^3 r_V^2(\tau) = 8\gamma \frac{\tilde{\xi} M_p}{\lambda(\tau)} \Phi_N(r_V), \tag{A.42}$$

where the gravitational potential at r_V is $\Phi_N(r_V) = -M_0/8\pi M_p^2 r_V$. Using the conformal factor $\log A^{1/2} = \xi\phi/M_p$, we arrive at the analogue to Eq. (5.14):

$$\frac{1}{2} \log \frac{A(r)}{A_0} = \frac{1}{2} \log \left(1 + \frac{\alpha(r)}{A_0} \right) \approx 8\gamma \frac{\xi\tilde{\xi}}{\lambda(\tau)} \Phi_N(r_V). \tag{A.43}$$

The bound in Eq. (A.37) together with $|\Phi_N(r_V)| \ll 1$ requires the absolute value of the right-hand side of Eq. (A.43) to be small compared to 1. Therefore, we can Taylor expand the left-hand side to find:

$$\alpha(r) \approx 16\gamma \frac{\xi\tilde{\xi}}{\lambda(\tau)} \Phi_N(r_V) A_0. \tag{A.44}$$

We conclude that the relative deviation between the local and the cosmological conformal factor is in this case proportional to the gravitational potential at the Vainshtein radius $\Phi_N(r_V)$, i.e. far outside the object. This is a far tighter constraint than the conservative result in Eq. (5.15), where $\alpha(r)$ is proportional to $\Phi_N(r)$,

the gravitational potential inside the object.

A.3. The Vainshtein Radius of a Cosmologically Relevant Galileon Model

In this section we estimate the magnitude of the Vainshtein radius of a spherically symmetric mass for a cubic Galileon model (defined in Eqs. (3.35) and (3.36)) under the assumption that the cubic Galileon model is cosmologically relevant.

Being defined through Eq. (6.5), the Vainshtein radius around a mass M_A depends on the model parameters ξ and M, which could a priori take any value. However, for the Galileon model to be cosmologically relevant, we expect that its energy density ρ_ϕ on the cosmological background, see Eq. (4.16), is roughly of order $\rho_\phi \lesssim H^2$; we write $\rho_\phi = \Omega_\phi H^2$ with $\Omega_\phi \lesssim 1$. We would like to remind the reader that the Galileon field in Chapter 4 was rescaled by $2\xi\phi/M_p \to \phi$ and that the parameters C_2 and C_3 in Chapter 4 are related to the parameters ξ and M through Eq. (4.3). Assuming furthermore that the non-linear Galileon terms (C_3-terms in Chapter 4) are dominant over the standard kinetic terms (C_2-terms), i.e. we have a meaningful Galileon model, we may estimate the relation $\rho_\phi = \Omega_\phi H^2$ to yield:

$$\phi^3 \sim \alpha \frac{M_p^2 M^3}{H^2} \Omega_\phi. \tag{A.45}$$

We have used here the non-rescaled field and parameters as defined in Chapter 6. Similarly, the Galileon equation of motion on the cosmological background, Eq. (4.18), requires:

$$\phi^2 \sim \frac{M^3 \xi M_p}{H^2}. \tag{A.46}$$

We have used $\rho_m \sim H^2$ here. Combining Eqs. (A.45) and (A.46) we obtain $\phi \sim M_p \Omega_\phi / \xi$ and:

$$\frac{1}{M^3} \sim \frac{\xi^3}{H^2 M_p \Omega_\phi^2}. \tag{A.47}$$

The Vainshtein radius, Eq. (6.5), is thus of order:

$$r_{V,A}^3 \sim \frac{2\xi^4 M_A}{H^2 M_p^2 \Omega_\phi^2} \sim \frac{\xi^4}{\Omega_\phi^2} M_A 10^{-39}\,\mathrm{Mpc}^3/\mathrm{kg}. \tag{A.48}$$

It is now important to note that the parameter ξ is not allowed to take an

arbitrary value anymore. If we would choose $\xi \ll 1$, our assumption that the non-linear Galileon terms are dominant over the standard kinetic terms in Eqs. (4.16) and (4.18) would break down. Careful comparison of the non-linear Galileon terms and the standard kinetic terms shows that $\xi \gtrsim 1$ is required for our estimates to be valid. The minimal Vainshtein radius and thus the largest fifth force effects can be achieved for $\xi \sim \Omega_\phi \sim 1$:

$$r_{V,A}^3 \sim M_A 10^{-39}\,\mathrm{Mpc}^3/\mathrm{kg}. \tag{A.49}$$

Bibliography

[1] I. Newton, *Philosophiae Naturalis Principia Mathematica*. Royal Society, London, 1686.

[2] A. Einstein, *Die grundlage der allgemeinen relativitätstheorie*, *Annalen der Physik* **354** (1916) 769.

[3] C. Burrage, J. Dombrowski and D. Saadeh, *The shape dependence of Vainshtein screening in the cosmic matter bispectrum*, *JCAP* **10** (2019) 023 [1905.06260].

[4] R. Catena, M. Pietroni and L. Scarabello, *Einstein and Jordan reconciled: a frame-invariant approach to scalar-tensor cosmology*, *Phys. Rev. D* **76** (2007) 084039 [astro-ph/0604492].

[5] C. Burrage and J. Dombrowski, *Constraining the cosmological evolution of scalar-tensor theories with local measurements of the time variation of G*, *JCAP* **07** (2020) 060 [2004.14260].

[6] C. M. Will, *The Confrontation between General Relativity and Experiment*, *Living Rev. Rel.* **17** (2014) 4 [1403.7377].

[7] E. G. Adelberger, J. H. Gundlach, B. R. Heckel, S. Hoedl and S. Schlamminger, *Torsion balance experiments: A low-energy frontier of particle physics*, *Prog. Part. Nucl. Phys.* **62** (2009) 102.

[8] R. A. Hulse and J. H. Taylor, *Discovery of a pulsar in a binary system.*, *ApJ* **195** (1975) L51.

[9] LIGO Scientific, Virgo, Fermi-GBM, INTEGRAL collaboration, *Gravitational Waves and Gamma-rays from a Binary Neutron Star Merger: GW170817 and GRB 170817A*, *Astrophys. J.* **848** (2017) L13 [1710.05834].

[10] P. G. Ferreira, *Cosmological Tests of Gravity*, *Ann. Rev. Astron. Astrophys.* **57** (2019) 335 [1902.10503].

[11] N. Straumann, *General Relativity*, Graduate Texts in Physics. Springer, Dordrecht, Heidelberg, New York, London, 2 ed., 2013, https://doi.org/10.1007/978-94-007-5410-2.

[12] D. Lovelock, *The einstein tensor and its generalizations*, *Journal of Mathematical Physics* **12** (1971) 498 [https://doi.org/10.1063/1.1665613].

[13] D. Lovelock, *The fourdimensionality of space and the einstein tensor*, *Journal of Mathematical Physics* **13** (1972) 874 [https://doi.org/10.1063/1.1666069].

[14] T. Clifton, P. G. Ferreira, A. Padilla and C. Skordis, *Modified Gravity and Cosmology*, *Phys. Rept.* **513** (2012) 1 [1106.2476].

[15] D. Saadeh, S. M. Feeney, A. Pontzen, H. V. Peiris and J. D. McEwen, *How isotropic is the universe?*, *Physical Review Letters* **117** (2016) .

[16] Y. Akrami, M. Ashdown, J. Aumont, C. Baccigalupi, M. Ballardini, A. J. Banday et al., *Planck2018 results*, *Astronomy & Astrophysics* **641** (2020) A7.

[17] P. Zhang and A. Stebbins, *Confirmation of the Copernican Principle at Gpc Radial Scale and above from the Kinetic Sunyaev-Zel'dovich Effect Power Spectrum*, *Physical Review Letters* **107** (2011) 041301 [1009.3967].

[18] J. P. Zibin and A. Moss, *Linear kinetic Sunyaev-Zel'dovich effect and void models for acceleration*, *Class. Quant. Grav.* **28** (2011) 164005 [1105.0909].

[19] Q. Ding, T. Nakama and Y. Wang, *A gigaparsec-scale local void and the Hubble tension*, *Sci. China Phys. Mech. Astron.* **63** (2020) 290403 [1912.12600].

[20] T. Buchert, *Dark energy from structure: a status report*, *General Relativity and Gravitation* **40** (2007) 467527.

[21] Planck collaboration, *Planck 2018 results. VI. Cosmological parameters*, *Astron. Astrophys.* **641** (2020) A6 [1807.06209].

[22] M. Milgrom, *A modification of the Newtonian dynamics as a possible alternative to the hidden mass hypothesis.*, *ApJ* **270** (1983) 365.

[23] C. Skordis, *The tensor-vector-scalar theory and its cosmology*, *Classical and Quantum Gravity* **26** (2009) 143001.

[24] C. Burrage, E. J. Copeland and P. Millington, *Radial acceleration relation from symmetron fifth forces*, *Physical Review D* **95** (2017) .

[25] S. Perlmutter, G. Aldering, G. Goldhaber, R. A. Knop, P. Nugent, P. G. Castro et al., *Measurements of and from 42 highredshift supernovae*, *The Astrophysical Journal* **517** (1999) 565586.

[26] A. G. Riess, A. V. Filippenko, P. Challis, A. Clocchiatti, A. Diercks, P. M. Garnavich et al., *Observational evidence from supernovae for an accelerating universe and a cosmological constant*, *The Astronomical Journal* **116** (1998) 10091038.

[27] S. Weinberg, *Cosmology*. Oxford University Press, Oxford, 2019.

[28] I. Sawicki and E. Bellini, *Limits of quasistatic approximation in modified-gravity cosmologies*, *Phys. Rev. D* **92** (2015) 084061 [1503.06831].

[29] M. Lagos, E. Bellini, J. Noller, P. G. Ferreira and T. Baker, *A general theory of linear cosmological perturbations: stability conditions, the quasistatic limit and dynamics*, *JCAP* **03** (2018) 021 [1711.09893].

[30] G. Bertone and D. Hooper, *History of dark matter*, *Rev. Mod. Phys.* **90** (2018) 045002 [1605.04909].

[31] F. Zwicky, *Die Rotverschiebung von extragalaktischen Nebeln*, *Helvetica Physica Acta* **6** (1933) 110.

[32] F. Zwicky, *On the Masses of Nebulae and of Clusters of Nebulae*, *ApJ* **86** (1937) 217.

[33] X.-P. Wu, T. Chiueh, L.-Z. Fang and Y.-J. Xue, *A comparison of different cluster mass estimates: consistency or discrepancy?*, *Monthly Notices of the Royal Astronomical Society* **301** (1998) 861871.

[34] S. W. Allen, A. E. Evrard and A. B. Mantz, *Cosmological parameters from observations of galaxy clusters*, *Annual Review of Astronomy and Astrophysics* **49** (2011) 409470.

[35] D. Clowe, M. Brada, A. H. Gonzalez, M. Markevitch, S. W. Randall, C. Jones et al., *A direct empirical proof of the existence of dark matter*, *The Astrophysical Journal* **648** (2006) L109L113.

[36] M. Viel, J. Lesgourgues, M. G. Haehnelt, S. Matarrese and A. Riotto, *Constraining warm dark matter candidates including sterile neutrinos and light gravitinos with wmap and the lyman-forest*, *Physical Review D* **71** (2005) .

[37] W. J. G. de Blok, *The core-cusp problem*, *Advances in Astronomy* **2010** (2010) 114.

[38] J. S. Bullock, *Notes on the missing satellites problem*, 2010.

[39] S. S. McGaugh, J. M. Schombert, G. D. Bothun and W. J. G. de Blok, *The baryonic tully-fisher relation*, *The Astrophysical Journal* **533** (2000) L99L102.

[40] B. A. Reid, W. J. Percival, D. J. Eisenstein, L. Verde, D. N. Spergel, R. A. Skibba et al., *Cosmological constraints from the clustering of the sloan digital sky survey dr7 luminous red galaxies*, *Monthly Notices of the Royal Astronomical Society* (2010) .

[41] DES collaboration, *Dark Energy Survey Year 1 Results: Constraints on Extended Cosmological Models from Galaxy Clustering and Weak Lensing*, *Phys. Rev.* **D99** (2019) 123505 [1810.02499].

[42] L. Verde, T. Treu and A. G. Riess, *Tensions between the early and late universe*, *Nature Astronomy* **3** (2019) 891895.

[43] J. Martin, *Everything You Always Wanted To Know About The Cosmological Constant Problem (But Were Afraid To Ask)*, *Comptes Rendus Physique* **13** (2012) 566 [1205.3365].

[44] L. Heisenberg, *A systematic approach to generalisations of general relativity and their cosmological implications*, *Physics Reports* **796** (2019) 1113.

[45] LIGO Scientific, Virgo collaboration, *GW170817: Observation of Gravitational Waves from a Binary Neutron Star Inspiral*, *Phys. Rev. Lett.* **119** (2017) 161101 [1710.05832].

[46] C. de Rham and S. Melville, *Gravitational Rainbows: LIGO and Dark Energy at its Cutoff*, *Phys. Rev. Lett.* **121** (2018) 221101 [1806.09417].

[47] K. Krasnov, *Non-Metric Gravity. I. Field Equations*, *Class. Quant. Grav.* **25** (2008) 025001 [gr-qc/0703002].

[48] M. Ostrogradsky, *Mémoires sur les équations différentielles, relatives au problème des isopérimètres*, *Mem. Acad. St. Petersbourg* **6** (1850) 385.

[49] G. W. Horndeski, *Second-order scalar-tensor field equations in a four-dimensional space*, *Int. J. Theor. Phys.* **10** (1974) 363.

[50] C. Deffayet, X. Gao, D. A. Steer and G. Zahariade, *From k-essence to generalised Galileons*, *Phys. Rev.* **D84** (2011) 064039 [1103.3260].

[51] A. Nicolis, R. Rattazzi and E. Trincherini, *The Galileon as a local modification of gravity*, *Phys. Rev.* **D79** (2009) 064036 [0811.2197].

[52] C. Brans and R. H. Dicke, *Mach's principle and a relativistic theory of gravitation*, *Phys. Rev.* **124** (1961) 925.

[53] C. Deffayet, G. Esposito-Farese and A. Vikman, *Covariant Galileon*, *Phys. Rev.* **D79** (2009) 084003 [0901.1314].

[54] C. Deffayet, S. Deser and G. Esposito-Farese, *Generalized Galileons: All scalar models whose curved background extensions maintain second-order field equations and stress-tensors*, *Phys. Rev.* **D80** (2009) 064015 [0906.1967].

[55] J. M. Ezquiaga and M. Zumalacárregui, *Dark Energy After GW170817: Dead Ends and the Road Ahead*, *Phys. Rev. Lett.* **119** (2017) 251304 [1710.05901].

[56] P. Creminelli and F. Vernizzi, *Dark Energy after GW170817 and GRB170817A*, *Phys. Rev. Lett.* **119** (2017) 251302 [1710.05877].

[57] T. Baker, E. Bellini, P. G. Ferreira, M. Lagos, J. Noller and I. Sawicki, *Strong constraints on cosmological gravity from GW170817 and GRB 170817A*, *Phys. Rev. Lett.* **119** (2017) 251301 [1710.06394].

[58] J. Sakstein and B. Jain, *Implications of the Neutron Star Merger GW170817 for Cosmological Scalar-Tensor Theories*, *Phys. Rev. Lett.* **119** (2017) 251303 [1710.05893].

[59] L. Heisenberg, *Generalization of the proca action*, *Journal of Cosmology and Astroparticle Physics* **2014** (2014) 015015.

[60] A. De Felice, L. Heisenberg, R. Kase, S. Mukohyama, S. Tsujikawa and Y.-l. Zhang, *Effective gravitational couplings for cosmological perturbations in generalized Proca theories*, *Phys. Rev. D* **94** (2016) 044024 [1605.05066].

[61] C. de Rham, *Massive Gravity*, *Living Rev. Rel.* **17** (2014) 7 [1401.4173].

[62] J. D. Bekenstein, *Relativistic gravitation theory for the MOND paradigm*, *Phys. Rev. D* **70** (2004) 083509 [astro-ph/0403694].

[63] S. Boran, S. Desai, E. O. Kahya and R. P. Woodard, *GW170817 Falsifies Dark Matter Emulators*, *Phys. Rev. D* **97** (2018) 041501 [1710.06168].

[64] H. A. Buchdahl, *Non-Linear Lagrangians and Cosmological Theory*, *Monthly Notices of the Royal Astronomical Society* **150** (1970) 1.

[65] A. De Felice and S. Tsujikawa, *f(R) theories*, *Living Rev. Rel.* **13** (2010) 3 [1002.4928].

[66] W. Hu and I. Sawicki, *Models of f(R) Cosmic Acceleration that Evade Solar-System Tests*, *Phys. Rev. D* **76** (2007) 064004 [0705.1158].

[67] A. A. Starobinsky, *Disappearing cosmological constant in f(R) gravity*, *JETP Lett.* **86** (2007) 157 [0706.2041].

[68] J. Gleyzes, D. Langlois, F. Piazza and F. Vernizzi, *Healthy theories beyond Horndeski*, *Phys. Rev. Lett.* **114** (2015) 211101 [1404.6495].

[69] D. Langlois and K. Noui, *Degenerate higher derivative theories beyond Horndeski: evading the Ostrogradski instability*, *JCAP* **02** (2016) 034 [1510.06930].

[70] E. P. Verlinde, *On the Origin of Gravity and the Laws of Newton*, *JHEP* **04** (2011) 029 [1001.0785].

[71] T. Padmanabhan, *Thermodynamical Aspects of Gravity: New insights*, *Rept. Prog. Phys.* **73** (2010) 046901 [0911.5004].

[72] E. Belgacem, Y. Dirian, S. Foffa and M. Maggiore, *Nonlocal gravity. Conceptual aspects and cosmological predictions*, *JCAP* **03** (2018) 002 [1712.07066].

[73] T. Kaluza, *Zum Unitätsproblem der Physik*, *Sitzungsberichte der Königlich Preußischen Akademie der Wissenschaften (Berlin* (1921) 966.

[74] O. Klein, *Quantentheorie und fünfdimensionale Relativitätstheorie*, *Zeitschrift fur Physik* **37** (1926) 895.

[75] N. Arkani-Hamed, S. Dimopoulos and G. R. Dvali, *The Hierarchy problem and new dimensions at a millimeter*, *Phys. Lett. B* **429** (1998) 263 [hep-ph/9803315].

[76] R. Maartens and K. Koyama, *Brane-World Gravity*, *Living Rev. Rel.* **13** (2010) 5 [1004.3962].

[77] L. Randall and R. Sundrum, *An Alternative to compactification*, *Phys. Rev. Lett.* **83** (1999) 4690 [hep-th/9906064].

[78] G. R. Dvali, G. Gabadadze and M. Porrati, *4-D gravity on a brane in 5-D Minkowski space*, *Phys. Lett. B* **485** (2000) 208 [hep-th/0005016].

[79] C. Charmousis, R. Gregory, N. Kaloper and A. Padilla, *DGP Specteroscopy*, *JHEP* **10** (2006) 066 [hep-th/0604086].

[80] M. A. Luty, M. Porrati and R. Rattazzi, *Strong interactions and stability in the DGP model*, *JHEP* **09** (2003) 029 [hep-th/0303116].

[81] D. Bettoni and S. Liberati, *Disformal invariance of second order scalar-tensor theories: Framing the Horndeski action*, *Phys. Rev. D* **88** (2013) 084020 [1306.6724].

[82] A. I. Vainshtein, *To the problem of nonvanishing gravitation mass*, *Phys. Lett.* **39B** (1972) 393.

[83] E. Babichev and C. Deffayet, *An introduction to the Vainshtein mechanism*, *Class. Quant. Grav.* **30** (2013) 184001 [1304.7240].

[84] E. Babichev, C. Deffayet and R. Ziour, *k-Mouflage gravity*, *Int. J. Mod. Phys.* **D18** (2009) 2147 [0905.2943].

[85] C. Burrage and J. Khoury, *Screening of scalar fields in Dirac-Born-Infeld theory*, *Phys. Rev. D* **90** (2014) 024001 [1403.6120].

[86] J. Khoury and A. Weltman, *Chameleon fields: Awaiting surprises for tests of gravity in space*, *Phys. Rev. Lett.* **93** (2004) 171104 [astro-ph/0309300].

[87] K. Hinterbichler and J. Khoury, *Symmetron Fields: Screening Long-Range Forces Through Local Symmetry Restoration*, *Phys. Rev. Lett.* **104** (2010) 231301 [1001.4525].

[88] A. Joyce, B. Jain, J. Khoury and M. Trodden, *Beyond the Cosmological Standard Model*, *Phys. Rept.* **568** (2015) 1 [1407.0059].

[89] C. Deffayet, O. Pujolas, I. Sawicki and A. Vikman, *Imperfect Dark Energy from Kinetic Gravity Braiding*, *JCAP* **1010** (2010) 026 [1008.0048].

[90] C. Burrage and J. Sakstein, *Tests of Chameleon Gravity*, *Living Rev. Rel.* **21** (2018) 1 [1709.09071].

[91] C. Burrage, E. J. Copeland and E. A. Hinds, *Probing Dark Energy with Atom Interferometry*, *JCAP* **1503** (2015) 042 [1408.1409].

[92] J. K. Bloomfield, C. Burrage and A.-C. Davis, *Shape dependence of Vainshtein screening*, *Phys. Rev.* **D91** (2015) 083510 [1408.4759].

[93] P. Brax, C. Burrage and A.-C. Davis, *Laboratory Tests of the Galileon*, *JCAP* **1109** (2011) 020 [1106.1573].

[94] B. Falck, K. Koyama, G.-b. Zhao and B. Li, *The Vainshtein Mechanism in the Cosmic Web*, *JCAP* **1407** (2014) 058 [1404.2206].

[95] B. Li, G.-B. Zhao and K. Koyama, *Exploring Vainshtein mechanism on adaptively refined meshes*, *JCAP* **05** (2013) 023 [1303.0008].

[96] A. Barreira, B. Li, W. A. Hellwing, C. M. Baugh and S. Pascoli, *Nonlinear structure formation in the Cubic Galileon gravity model*, *JCAP* **10** (2013) 027 [1306.3219].

[97] A. Lewis, *The real shape of non-Gaussianities*, *JCAP* **1110** (2011) 026 [1107.5431].

[98] J. Renk, M. Zumalacárregui, F. Montanari and A. Barreira, *Galileon gravity in light of ISW, CMB, BAO and H_0 data*, *JCAP* **1710** (2017) 020 [1707.02263].

[99] E. Babichev, C. Deffayet and G. Esposito-Farese, *Constraints on Shift-Symmetric Scalar-Tensor Theories with a Vainshtein Mechanism from Bounds on the Time Variation of G*, *Phys. Rev. Lett.* **107** (2011) 251102 [1107.1569].

[100] C. Burrage, D. Parkinson and D. Seery, *Beyond the growth rate of cosmic structure: Testing modified gravity models with an extra degree of freedom*, *Phys. Rev.* **D96** (2017) 043509 [1502.03710].

[101] N. Bartolo, E. Bellini, D. Bertacca and S. Matarrese, *Matter bispectrum in cubic Galileon cosmologies*, *JCAP* **1303** (2013) 034 [1301.4831].

[102] Y. Takushima, A. Terukina and K. Yamamoto, *Bispectrum of cosmological density perturbations in the most general second-order scalar-tensor theory*, *Phys. Rev.* **D89** (2014) 104007 [1311.0281].

[103] E. Bellini, R. Jimenez and L. Verde, *Signatures of Horndeski gravity on the Dark Matter Bispectrum*, *JCAP* **1505** (2015) 057 [1504.04341].

[104] E. Bellini and M. Zumalacarregui, *Nonlinear evolution of the baryon acoustic oscillation scale in alternative theories of gravity*, *Phys. Rev.* **D92** (2015) 063522 [1505.03839].

[105] D. Yamauchi, S. Yokoyama and H. Tashiro, *Constraining modified theories of gravity with the galaxy bispectrum*, *Phys. Rev.* **D96** (2017) 123516 [1709.03243].

[106] N. Chow and J. Khoury, *Galileon Cosmology*, *Phys. Rev.* **D80** (2009) 024037 [0905.1325].

[107] H. A. Winther and P. G. Ferreira, *Vainshtein mechanism beyond the quasistatic approximation*, *Phys. Rev.* **D92** (2015) 064005 [1505.03539].

[108] K. Koyama, A. Taruya and T. Hiramatsu, *Non-linear Evolution of Matter Power Spectrum in Modified Theory of Gravity*, *Phys. Rev. D* **79** (2009) 123512 [0902.0618].

[109] T. Matsubara, *Nonlinear perturbation theory integrated with nonlocal bias, redshift-space distortions, and primordial non-gaussianity*, *Physical Review D* **83** (2011) [1102.4619].

[110] F. Bernardeau, S. Colombi, E. Gaztanaga and R. Scoccimarro, *Large scale structure of the universe and cosmological perturbation theory*, *Phys. Rept.* **367** (2002) 1 [astro-ph/0112551].

[111] D. Blas, J. Lesgourgues and T. Tram, *The Cosmic Linear Anisotropy Solving System (CLASS) II: Approximation schemes*, *JCAP* **1107** (2011) 034 [1104.2933].

[112] M. Zumalacàrregui, E. Bellini, I. Sawicki, J. Lesgourgues and P. G. Ferreira, ***hi_class**: Horndeski in the Cosmic Linear Anisotropy Solving System*, *JCAP* **1708** (2017) 019 [1605.06102].

[113] E. Bellini, I. Sawicki and M. Zumalacárregui, *hi_class: Background Evolution, Initial Conditions and Approximation Schemes*, 1909.01828.

[114] E. Bellini and I. Sawicki, *Maximal freedom at minimum cost: linear large-scale structure in general modifications of gravity*, *JCAP* **1407** (2014) 050 [1404.3713].

[115] F. Rondeau and B. Li, *Equivalence of cosmological observables in conformally related scalar tensor theories*, *Phys. Rev.* **D96** (2017) 124009 [1709.07087].

[116] J. Francfort, B. Ghosh and R. Durrer, *Cosmological Number Counts in Einstein and Jordan frames*, 1907.03606.

[117] P. Meszaros, *The behaviour of point masses in an expanding cosmological substratum*, *Astron. Astrophys.* **37** (1974) 225.

[118] E. J. Groth and P. J. E. Peebles, *Closed-form solutions for the evolution of density perturbations in some cosmological models*, *Astron. Astrophys.* **41** (1975) 143.

[119] S. Nesseris, G. Pantazis and L. Perivolaropoulos, *Tension and constraints on modified gravity parametrizations of $G_{eff}(z)$ from growth rate and Planck data*, *Phys. Rev.* **D96** (2017) 023542 [1703.10538].

[120] G.-B. Zhao et al., *The clustering of the SDSS-IV extended Baryon Oscillation Spectroscopic Survey DR14 quasar sample: a tomographic measurement of cosmic structure growth and expansion rate based on optimal redshift weights*, *Mon. Not. Roy. Astron. Soc.* **482** (2019) 3497 [1801.03043].

[121] F. G. Mohammad et al., *The VIMOS Public Extragalactic Redshift Survey (VIPERS): Unbiased clustering estimate with VIPERS slit assignment*, *Astron. Astrophys.* **619** (2018) A17 [1807.05999].

[122] BOSS collaboration, *The clustering of galaxies in the completed SDSS-III Baryon Oscillation Spectroscopic Survey: cosmological analysis of the DR12 galaxy sample*, *Mon. Not. Roy. Astron. Soc.* **470** (2017) 2617 [1607.03155].

[123] F. Shi et al., *Mapping the Real Space Distributions of Galaxies in SDSS DR7: II. Measuring the growth rate, clustering amplitude of matter and biases of galaxies at redshift* 0.1, *Astrophys. J.* **861** (2018) 137 [1712.04163].

[124] J. Carrick, S. J. Turnbull, G. Lavaux and M. J. Hudson, *Cosmological parameters from the comparison of peculiar velocities with predictions from the 2M++ density field*, *Mon. Not. Roy. Astron. Soc.* **450** (2015) 317 [1504.04627].

[125] D. Huterer, D. Shafer, D. Scolnic and F. Schmidt, *Testing ΛCDM at the lowest redshifts with SN Ia and galaxy velocities*, *JCAP* **1705** (2017) 015 [1611.09862].

[126] H. Gil-Marín, W. J. Percival, L. Verde, J. R. Brownstein, C.-H. Chuang, F.-S. Kitaura et al., *The clustering of galaxies in the SDSS-III Baryon Oscillation Spectroscopic Survey: RSD measurement from the power spectrum and bispectrum of the DR12 BOSS galaxies*, *Mon. Not. Roy. Astron. Soc.* **465** (2017) 1757 [1606.00439].

[127] V. Yankelevich and C. Porciani, *Cosmological information in the redshift-space bispectrum*, *Mon. Not. Roy. Astron. Soc.* **483** (2019) 2078 [1807.07076].

[128] J. Wang, L. Hui and J. Khoury, *No-Go Theorems for Generalized Chameleon Field Theories*, *Phys. Rev. Lett.* **109** (2012) 241301 [1208.4612].

[129] R. Kimura, T. Kobayashi and K. Yamamoto, *Vainshtein screening in a cosmological background in the most general second-order scalar-tensor theory*, *Phys. Rev.* **D85** (2012) 024023 [1111.6749].

[130] A. Barreira, B. Li, C. M. Baugh and S. Pascoli, *Spherical collapse in Galileon gravity: fifth force solutions, halo mass function and halo bias*, *JCAP* **1311** (2013) 056 [1308.3699].

[131] P. Brax and P. Valageas, *Nonscreening of the cosmological background in K-mouflage modified gravity*, *Phys. Rev. D* **98** (2018) 083509 [1806.09414].

[132] P. Creminelli, G. Tambalo, F. Vernizzi and V. Yingcharoenrat, *Dark-Energy Instabilities induced by Gravitational Waves*, 1910.14035.

[133] J. Noller, *Cosmological constraints on dark energy in light of gravitational wave bounds*, 2001.05469.

[134] F. Hofmann and J. Müller, *Relativistic tests with lunar laser ranging*, *Class. Quant. Grav.* **35** (2018) 035015.

[135] J. D. Barrow, *Varying G and other constants*, *NATO Sci. Ser. C* **511** (1998) 269 [gr-qc/9711084].

[136] M. Braglia, M. Ballardini, W. T. Emond, F. Finelli, A. E. Gumrukcuoglu, K. Koyama et al., *A larger value for H_0 by an evolving gravitational constant*, 2004.11161.

[137] G. Ballesteros, A. Notari and F. Rompineve, *The H_0 tension: ΔG_N vs. ΔN_{eff}*, 2004.05049.

[138] J. Alvey, N. Sabti, M. Escudero and M. Fairbairn, *Improved BBN Constraints on the Variation of the Gravitational Constant*, *Eur. Phys. J. C* **80** (2020) 148 [1910.10730].

[139] J. Ooba, K. Ichiki, T. Chiba and N. Sugiyama, *Cosmological constraints on scalar–tensor gravity and the variation of the gravitational constant*, *PTEP* **2017** (2017) 043E03 [1702.00742].

[140] L. Amendola, *Phantom energy mediates a long-range repulsive force*, *Phys. Rev. Lett.* **93** (2004) 181102 [hep-th/0409224].

[141] M. Wittner, G. Laverda, O. F. Piattella and L. Amendola, *Transient weak gravity in scalar-tensor theories*, 2003.08950.

[142] L. Amendola, M. Kunz, I. D. Saltas and I. Sawicki, *Fate of Large-Scale Structure in Modified Gravity After GW170817 and GRB170817A*, *Phys. Rev. Lett.* **120** (2018) 131101 [1711.04825].

[143] H. Desmond, P. G. Ferreira, G. Lavaux and J. Jasche, *Fifth force constraints from the separation of galaxy mass components*, *Phys. Rev.* **D98** (2018) 064015 [1807.01482].

[144] H. Desmond and P. G. Ferreira, *Galaxy morphology rules out astrophysically relevant Hu-Sawicki $f(R)$ gravity*, *Phys. Rev. D* **102** (2020) 104060 [2009.08743].

[145] E.-M. Mueller, W. Percival, E. Linder, S. Alam, G.-B. Zhao, A. G. Sánchez et al., *The clustering of galaxies in the completed SDSS-III Baryon Oscillation Spectroscopic Survey: constraining modified gravity*, *Mon. Not. Roy. Astron. Soc.* **475** (2018) 2122 [1612.00812].

[146] A. Barreira, A. G. Sánchez and F. Schmidt, *Validating estimates of the growth rate of structure with modified gravity simulations*, *Phys. Rev.* **D94** (2016) 084022 [1605.03965].

[147] B. Bose, K. Koyama, W. A. Hellwing, G.-B. Zhao and H. A. Winther, *Theoretical accuracy in cosmological growth estimation*, *Phys. Rev.* **D96** (2017) 023519 [1702.02348].

[148] L. Hui, A. Nicolis and C. Stubbs, *Equivalence Principle Implications of Modified Gravity Models*, *Phys. Rev. D* **80** (2009) 104002 [0905.2966].

[149] T. Hiramatsu, W. Hu, K. Koyama and F. Schmidt, *Equivalence Principle Violation in Vainshtein Screened Two-Body Systems*, *Phys. Rev. D* **87** (2013) 063525 [1209.3364].

[150] L. Perenon, J. Bel, R. Maartens and A. de la Cruz-Dombriz, *Optimising growth of structure constraints on modified gravity*, *JCAP* **06** (2019) 020 [1901.11063].

[151] W. J. Wolf and M. Lagos, *Standard Sirens as a Novel Probe of Dark Energy*, *Phys. Rev. Lett.* **124** (2020) 061101 [1910.10580].

[152] M. Lagos and H. Zhu, *Gravitational couplings in Chameleon models*, 2003.01038.

[153] A. Kuntz, *Two-body potential of Vainshtein screened theories*, *Phys. Rev. D* **100** (2019) 024024 [1905.07340].

[154] P. Brax, L. Heisenberg and A. Kuntz, *Unveiling the Galileon in a three-body system : scalar and gravitational wave production*, *JCAP* **05** (2020) 012 [2002.12590].

[155] N. C. White, S. M. Troian, J. B. Jewell, C. J. Cutler, S.-w. Chiow and N. Yu, *Robust numerical computation of the 3D scalar potential field of the cubic Galileon gravity model at solar system scales*, *Phys. Rev. D* **102** (2020) 024033 [2003.02648].

[156] P. Fouque, J. M. Solanes, T. Sanchis and C. Balkowski, *Structure, mass and distance of the virgo cluster from a tolman-bondi model*, *Astron. Astrophys.* **375** (2001) 770 [astro-ph/0106261].

[157] S. Mei, J. Blakeslee, P. Cote, J. Tonry, M. J. West, L. Ferrarese et al., *The ACS Virgo Cluster Survey. 13. SBF Distance Catalog and the Three-Dimensional Structure of the Virgo Cluster*, *Astrophys. J.* **655** (2007) 144 [astro-ph/0702510].

[158] O. Müller, M. Rejkuba and H. Jerjen, *Distances from the tip of the red giant branch to the dwarf galaxies dw1335-29 and dw1340-30 in the centaurus group*, *Astronomy & Astrophysics* **615** (2018) A96.

[159] A. G. Riess, J. Fliri and D. Valls-Gabaud, *Cepheid Period-Luminosity Relations in the Near-infrared and the Distance to M31 from the Hubble Space Telescope Wide Field Camera 3*, *ApJ* **745** (2012) 156 [1110.3769].